

ISSN 0280-5316
ISRN LUTFD2/TFRT--5773--SE

Model-based Friction Compensation for the the Furuta Pendulum using the LuGre Model

Thomas Dietz

Department of Automatic Control
Lund University
July 2006

Department of Automatic Control Lund Institute of Technology Box 118 SE-221 00 Lund Sweden		<i>Document name</i> MASTER THESIS	
		<i>Date of issue</i> July 2006	
		<i>Document Number</i> ISRN LUTFD2/TFRT--5773--SE	
<i>Author(s)</i> Thomas Dietz		<i>Supervisor</i> Rolf Johansson at Automatic Control in Lund, Sweden Hans Peter Geering at Control Laboratory ETH in Zürich, Switzerland.	
		<i>Sponsoring organization</i>	
<i>Title and subtitle</i> Model-based Friction Compensation for the Furuta Pendulum using the LuGre Model. (Modellbaserad friktionskompensering för Furuta-pendel med hjälp av LuGre-modellen)			
<i>Abstract</i> <p>Friction is present in all mechanical systems and causes a wide range of problems for control. The development of friction models and methods to account for friction in control has been an active research area for many years. A promising friction model that is capable of describing a wide array of observed friction phenomena is the LuGre model. This thesis deals with the application of friction compensation based on the LuGre model for the unstable Furuta pendulum. LuGre friction compensation schemes and a model of the plant are implemented quasi-continuous and tested in simulation. An identification of LuGre friction parameters for the Furuta pendulum is carried out, showing the limitations due to the sensor equipment of the device.</p> <p>The LuGre friction compensation schemes are tested with hardware in the loop, evaluated and compared with friction compensation schemes based on the Dahl and Coulomb model. Further the influence of velocity observation on the control and friction compensation performance is elucidated. Friction compensation based on the LuGre model, discretized as proposed by Freidovich [2], is a suitable method to compensate for friction offering several advantages in comparison to other tested friction compensation schemes. Due to the used sensor equipment the full potential of the LuGre model cannot be tapped and the proposed friction observers require further modification before being applicable for the Furuta pendulum.</p>			
<i>Keywords</i> LuGre Model, Dahl Model, Colomb Model, Friction Compensation, Friction Observation, Furuta Pendulum, Limit Cycle.			
<i>Classification system and/or index terms (if any)</i>			
<i>Supplementary bibliographical information</i>			
<i>ISSN and key title</i> 0280-5316			<i>ISBN</i>
<i>Language</i> English	<i>Number of pages</i> 119	<i>Recipient's notes</i>	
<i>Security classification</i>			

Preface

This thesis is the final thesis (Diplomarbeit) of my university course at the Department of Mechanical and Process Engineering at the Swiss Federal Institute of Technology (ETH) Zürich. It was carried out within the Erasmus framework at the Department of Automatic Control of the Lund Institute of Technology (LTH) at Lund University.

I would like to thank Prof. Dr. Rolf Johansson at LTH for his supervision of and the important impulses for my thesis. His commitment to supervising my thesis and criticism for my work were a great help and indispensable for my thesis. I am indebted to Dr. Anders Robertsson for his help, advice and inspiration for my thesis.

I would like to thank the people at the control systems department at LTH for providing the framework for my work. Especially I want to thank Lic. Tech. Johan Åkesson for his help with and tips for the Furuta pendulum, Rolf Braun for his practical advice and help and Britt-Marie Mårtensson, Eva Schildt and Agneta Tuszyński for their administrative help and support during my time here in Lund. I would like to thank Prof. Dr. Anton Shiriaev, Dr. Leonid Freidovich and MSc. Uwe Mettin from Umeå University for their impulses for my work and especially for their introduction for the dSPACE system whose use was essential for my thesis. Special thanks go to Prof. Hans Peter Geering for the supervision of my thesis at ETH and for the help while organizing my stay here in Lund.

I also want to thank the employees at the international departments at LTH and ETH for their support and help while organizing my stay here in Lund.

Thanks go to my friends here in Lund for their help in times off work to obtain the distance from work that is needed to feel well and to work efficiently. Above all I would like to thank Joachim Widberg for the mind clearing runs, the interesting discussions and joyful evenings. I want to express my gratitude to Matthieu Gerard, Simone Del Favero, Francesco Pierri and Chiang Ming Yin, for making my stay and work here in Lund such a positive and joyful experience.

I want to thank my friends Sukanya (Lin) Prayoonpanich, Cornelia Hirsch, Johannes Boniolo, Marc Bickel, Sebastian Rihm and Robin Böhringer for their support. Your backing, also from afar, means much to me and you all play an indispensable role in my life.

Finally and most importantly I want to thank my parents for their care, inspiration and support - material and personal - that provide the absolutely indispensable foundation for my education at university and any other achievement in my life.

Thomas Dietz,
Lund, July 21, 2006

Contents

Abstract	7
List of Abbreviations	9
1 Introduction	11
1.1 Problem Description	11
1.2 Motivation	11
1.3 Typical Friction Behavior and the LuGre Model	15
1.4 Outline of this Thesis	19
2 Control Plant and Modeling	21
2.1 Hardware	21
2.2 Model of the Furuta Pendulum	21
2.2.1 Mechanic Part	21
2.2.2 Motor of Furuta Pendulum	28
3 Methods for Implementation and Evaluation	29
3.1 Implementation of the Friction Compensation	29
3.1.1 Controller Hardware	29
3.1.2 Framework for Friction Compensation	30
3.1.3 Control System	31
3.1.4 Implementation of the LuGre Model	36
3.1.5 Other Friction Models	37
3.1.6 Dahl Friction Model	39
3.1.7 Leuven Friction Model	41
3.2 Evaluation Criteria for Friction Compensation	41
3.2.1 Experimental Conditions	41
3.2.2 Benchmark	42
3.2.3 Evaluation Method	44
4 Friction Parameters	45
4.1 Estimation of the Voltage Constant	45
4.2 Estimation of Friction Parameters	47
4.2.1 Estimation of the Friction Forces	48
4.2.2 Estimation of the Viscous Friction Coefficients	50
4.2.3 Estimation of the Stiffness σ_0	54
4.2.4 Estimation of Static Parameters	54
4.2.5 Chosen Parameter Values	56
4.3 Origins of Friction and Influence on Parameter Estimation	58

5	Simulation of Friction Compensation	61
5.1	Friction Compensation with the LuGre Model	61
5.1.1	Simulation Setup	61
5.1.2	Compensation Using LuGre Friction Model	62
5.1.3	Closed-Loop LuGre Friction Observers	64
5.1.4	Quantitative Evaluation	67
5.2	Influence of Velocity Dependent Damping	68
6	Experiments with Friction Compensation	75
6.1	Influence of LuGre Friction Parameters on the Friction Compensation	75
6.1.1	Influence of the Friction Forces	75
6.1.2	Influence of the Viscous Friction Coefficients	76
6.1.3	Influence of the Stribeck Velocity v_s	79
6.1.4	Influence of the Stiffness σ_0	79
6.1.5	Influence of the Damping $\sigma_1(\dot{\varphi})$	79
6.2	Experimental Evaluation of Friction Compensation	81
6.2.1	Performance Improvement through Friction Compensation	81
6.2.2	Closed-Loop Friction Observers	86
6.2.3	Interplay of Velocity Estimation and Friction Compensation	89
6.2.4	Qualitative Assessment of Friction Compensation Schemes	92
6.2.5	Comparison of Simulation and Experiment	95
7	Conclusions and Outlook	99
7.1	Conclusions	99
7.1.1	Friction Compensation	99
7.1.2	Friction Parameters	100
7.1.3	LuGre Friction Model	100
7.2	Outlook and Recommendations	101
A	Task Description	103
B	Setup and Operation of the dSPACE System	105
B.1	Instructions for the Use of the dSPACE System	105
B.1.1	General Setup and Nomenclature	105
B.1.2	Important Instructions	105
B.1.3	Getting Started	106
B.1.4	Brief Overview of the Used Connectors and how to Access them in Simulink	106
B.1.5	General Tips for Working with the dSPACE System	107
B.2	Manual for Running the Friction Compensation Experiment	107
B.2.1	Setting Up the Experiment	107
B.2.2	Shutting Down the Experiment	108
B.2.3	Using the Experiment	108
B.2.4	Additional Information	111
C	Parameter Values	115
C.1	Explanation of Parameters	115
C.2	Basic Parameter Setup	116
C.3	Gain values for Estimation of Voltage Constant	118
	Bibliography	119

List of Abbreviations

Symbols and Notation

\bullet^T	Transposed matrix	[–]
\mathbf{x}	Vector with name x	[–]
${}_R\mathbf{x}$	Vector \mathbf{x} , expressed in the coordinate system R	[–]
${}_R\dot{\mathbf{x}}$	Derivative of the representation of the vector \mathbf{x} in the coordinate system R (${}_R\dot{\mathbf{x}} = \frac{d}{dt}({}_R\mathbf{x})$); this is in general not equal to the derivative of the vector \mathbf{x})	[–]
${}_R(\dot{\mathbf{x}})$	Derivative of the vector \mathbf{x} , expressed in the coordinate system R (${}_R(\dot{\mathbf{x}}) = {}_R(\frac{d}{dt}\mathbf{x})$)	[–]
\mathbf{A}	Matrix with Name A	[–]
\mathbf{A}_{RD}	Transformation matrix from coordinate system D to R	[–]
$\bar{\Theta}$	Tensor with name Θ	[–]
$ \bullet $	Absolute value	[–]
$max(\bullet)$	Maximal value of a function, signal or array	[X]
$sgn(\bullet)$	The sign function: $sgn(x) = \begin{cases} 0 & \text{if } x = 0 \\ \frac{x}{ x } & \text{if } x \neq 0 \end{cases}$	[–]
$o(\bullet)$	Order of magnitude	[X]
F_c	Coulomb friction moment	[Nm]
F_s	Stiction friction moment	[Nm]
σ_0	Stiffness of the friction model	[Nm/m]
σ_1	Damping of the friction model	[$Nm/(m/s)$]
v_s	Stribeck velocity	[m/s]
v_d	Analogon to Stribeck velocity for damping σ_1	[m/s]
F_v	Viscous friction coefficient	[$Nm/(m/s)$]
u	Control signal	[Nm]
F_{est}	Friction estimate	[Nm]
F_F	Friction force/ moment; either estimated, real or simulated	[N] or [Nm]
K_M	Constant transferring the voltage delivered to the socket of the pendulum into the moment produced by the motor	[Nm/V]
$\lim_{\dot{\varphi} \rightarrow 0^+}(\bullet)$	Right sided limit value: $\lim_{\substack{\dot{\varphi} \rightarrow 0 \\ \dot{\varphi} > 0}}(\bullet)$	[–]
$\lim_{\dot{\varphi} \rightarrow 0^-}(\bullet)$	Left sided limit value: $\lim_{\substack{\dot{\varphi} \rightarrow 0 \\ \dot{\varphi} < 0}}(\bullet)$	[–]

Indices

<i>ov</i>	Overall.
<i>dec</i>	Decline.
<i>pos</i>	For rotation in positive direction.
<i>neg</i>	For rotation in negative direction.

Acronyms and Abbreviations

CPU	Central Processing Unit
cog	Center of gravity
iid	Independent identically distributed
fft	Fast Fourier transformation
LTH	Lunds Tekniska Högskola
ETH	Eidgenössische Technische Hochschule

Chapter 1

Introduction

1.1 Problem Description

The topic of this thesis is the implementation of LuGre friction compensation for the arm of the inverted Furuta pendulum in simulation and experiment.

The Furuta pendulum consists of an arm, that is actuated by an electric motor and can rotate in the horizontal plane. A pendulum rod with a weight attached to its end is joined to the end of the arm in a way that it can rotate freely around the axis of the arm (see figure1.1).

The task is to stabilize the pendulum in the unstable upright position, while controlling the position of the arm along or to a desired reference by delivering appropriate control signals to the electric drive.

Further the LuGre friction parameters of the Furuta pendulum have to be estimated within the framework of the thesis.

Experiments are to be carried out evaluating the performance of the implemented friction compensation schemes and comparing it to alternative approaches, namely friction compensation based on the Dahl and Coulomb model.

For a more detailed task description please refer to appendix A.

1.2 Motivation

Various control approaches for linear and nonlinear systems were developed. However only few approaches are capable to take into account friction, that is immanent in any mechanical system. Since friction is often a crucial factor for the behavior of a mechanical system the control performance deteriorates significantly if the controller does not account for appropriate compensation. Phenomena like hunting, slip-stick motion and limit cycles can occur because of uncompensated friction effects.

Figure 1.3 shows an example of the hunting behavior that can result for a block on a surface (see figure 1.2), that is controlled with a constant reference by an PI-controller $F = K_p(x_{ref} - x) + K_i \int (x_{ref} - x)dt$ (see e.g. Geering [9]) when uncompensated friction is present. As friction model to compute the friction force F_F , the LuGre model was used.

The block never reaches the desired reference, since the integrator in the controller



Figure 1.1: Furuta pendulum

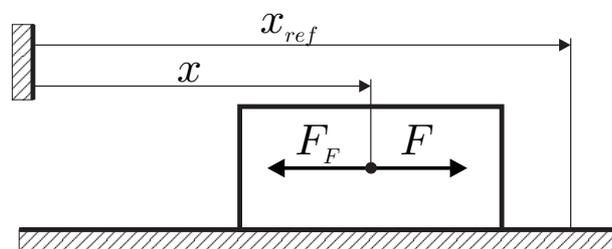


Figure 1.2: Picture of setup for block on surface.

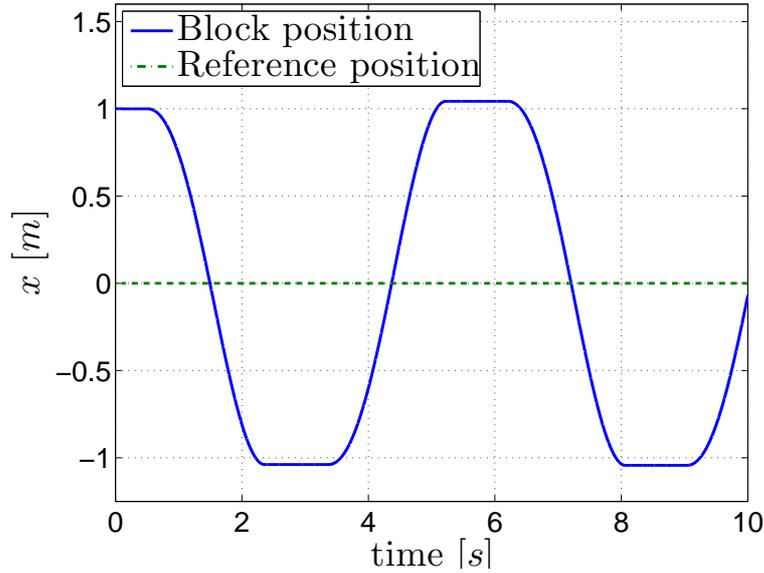


Figure 1.3: Hunting for block on surface (see figure 1.2) controlled with PI-controller to constant reference.

integrates to high values to overcome the stiction. This causes the block to overshoot the desired reference and to stick in a position on the other side of the desired reference.

An example of slip-stick motion is shown in figure 1.4 where the block from figure 1.2 is controlled with a P-controller $F = K_p(x_{ref} - x)$ and a ramp signal as reference. Again friction prevents the block from following the reference accurately, since the control forces near the desired reference do not suffice to maintain the movement of the block.

Figure 1.6 shows a limit cycle resulting from simulation for the Furuta pendulum with LuGre friction model (see figure 1.5). Due to the friction an oscillation around the desired reference occurs. This is caused by sticking of the actuator of the pendulum. In the time the actuator sticks the pendulum is not stabilized in the upright position and therefore falls. Movement and thus stabilization of the pendulum resume when the control error in the states of the pendulum demand a control signal that is sufficiently high to overcome the static friction.

Due to the highly nonlinear behavior of friction forces¹, especially at low relative speed between the contact surfaces, the mathematical description of friction is difficult. Additionally, for low relative velocities, the friction force exhibits very fast and highly velocity dependent dynamics. However in most applications it is hard to obtain reliable and precise velocity measurements for low speeds.

Due to the high importance of friction compensation in mechanical systems and the increased technical possibilities to implement dynamic systems for friction compensation, the field of friction modeling and friction compensation has become an active area of research.

¹The device considered in this thesis only possesses rotational joints. Thus the term friction force always also refers to friction moment, just as the notation F_F for friction forces will also be used for friction moments throughout the thesis.

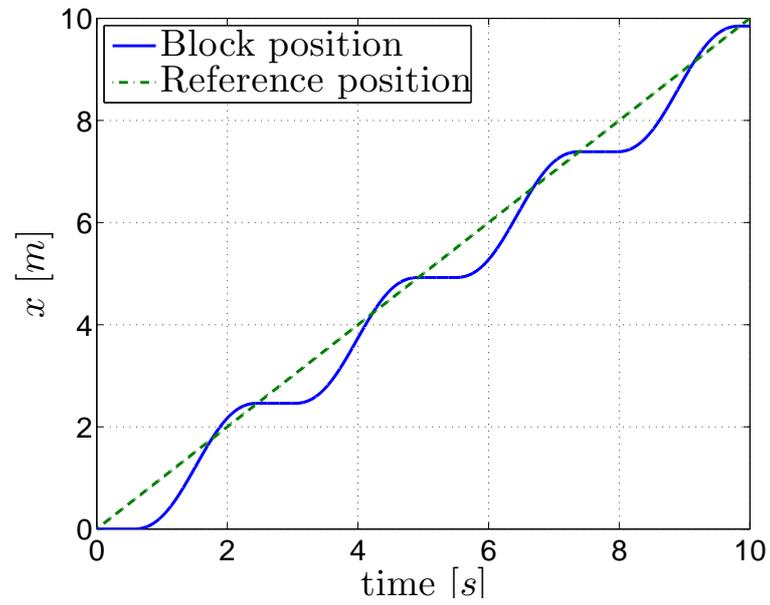


Figure 1.4: Stick-slip behavior for block on surface (see figure 1.2) controlled with P-controller along ramp reference.

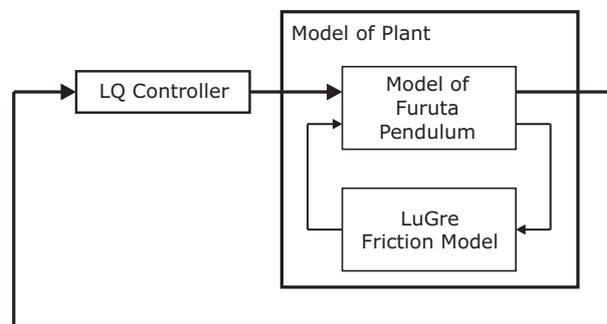


Figure 1.5: Picture of setup for simulation of limit cycles with Furuta pendulum.

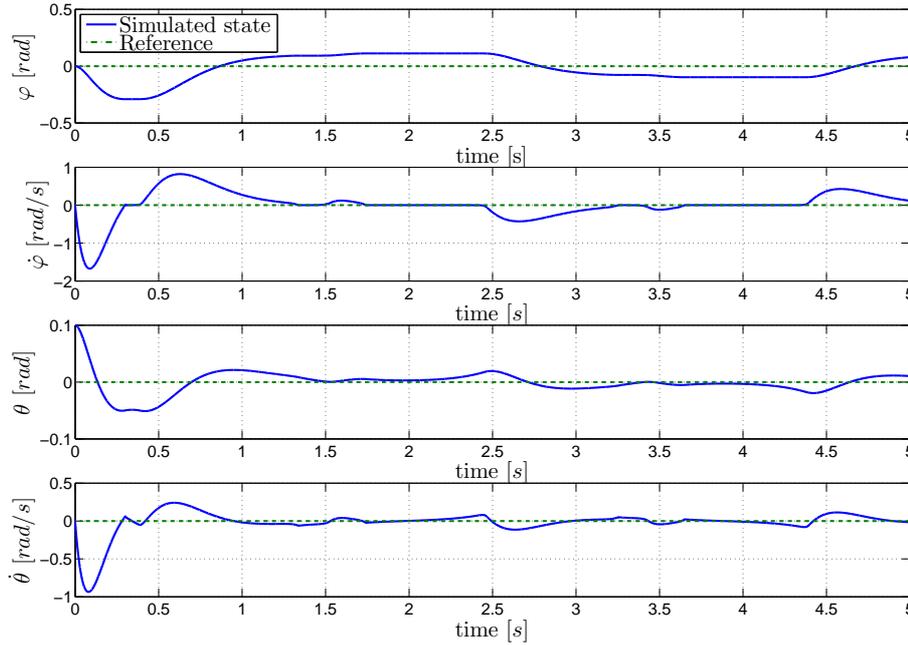


Figure 1.6: Resulting limit cycle for the Furuta pendulum for the setup as in figure 1.5, depicting the angle φ and angular velocity $\dot{\varphi}$ of the arm as well as the angle θ and angular velocity $\dot{\theta}$ of the pendulum.

Many models for the description of the behavior of the friction force were developed. Numerous simulations have been conducted to evaluate the theoretical advantages and shortcomings of the different approaches.

However the number of implementations of friction compensation based on dynamic friction models using real hardware is still limited. One reason for this may be difficulties that arise during the discretization of some of the friction models, that is necessary for the implementation on microcontrollers in real time.

1.3 Typical Friction Behavior and the LuGre Model

Friction contacts occur in one of the two following states.

Either the friction contact is in the state of sticking, i.e. there is no or more precise only microscopic motion between the contact surfaces. The state of sticking is also called presliding.

Or the friction contact is in the state of sliding, i.e. there is macroscopic relative movement between contact surfaces. The transition between presliding and sliding is continuous.

A particular friction model that received a lot of attention recently is the so called LuGre model².

It is capable of capturing a wide range of behavior that is observed while studying the friction behavior of real systems. This section intends to give a short introduction of the LuGre model and some of the characteristic phenomena that are observed while studying friction behavior. Further annotations and expressions concerning the description of friction that will be used throughout this thesis are

²LuGre for Lund Grenoble friction model.

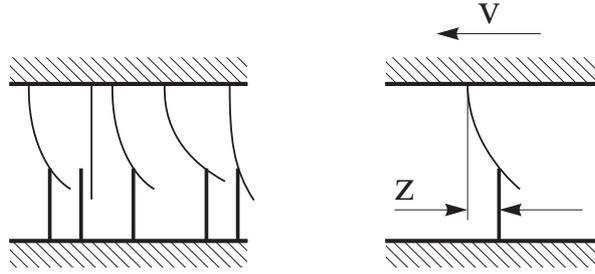


Figure 1.7: Left: Schematic picture of model of the contact between the surfaces with contact asperities being modeled as bristles; Right: Contact asperities accumulated to one bristle as in the LuGre model.

introduced. This section does not claim to be a complete listing of the corresponding properties and phenomena. For more information on these topics the reader may want to refer for example to Canudas de Wit et al. [3] and Shiriaev [4]. Further Olsson [1] gives a very good introduction into the topic of friction modeling, since it also describes friction models that were developed prior to the LuGre model.

The LuGre model is a dynamic model for the description of the behavior of the friction force. It has a physical analogy in the description of the friction behavior as the result of the bending of surface asperities between the contact surfaces. The asperities are modeled as bristles that bend under load (see Olsson [1] and Canudas de Wit et al. [3]). The LuGre model collects the behavior of all these surface asperities in contact and describes their accumulated behavior through one asperity (see figure 1.7).

Referring to Olsson [1] the LuGre model is described by the following equations:

$$\frac{dz}{dt} = v - \sigma_0 \frac{|v|}{g(v)} z \quad (1.1)$$

$$F_F = \sigma_0 z + \sigma_1(v) \frac{dz}{dt} + F_v v \quad (1.2)$$

$$g(v) = \left(F_C + (F_S - F_C) e^{-(v/v_S)^2} \right) \quad (1.3)$$

$$\sigma_1(v) = \sigma_1 e^{-(v/v_d)^2} \quad (1.4)$$

where v denotes the relative velocity of the contact surfaces and F_F is the LuGre friction force.

Again referring to Olsson [1] these equation can be interpreted as follows.

Equation (1.1) describes the behavior of the internal state of the friction model, i.e. the deflection of the above mentioned bristles. The first term on the right hand side causes a deflection of the bristles that is proportional to the integral of the relative velocity between the contact surfaces. The second term ensures that the deflection of the bristles reaches a final value $z_{SS} = g(v) \cdot \text{sgn}(v)$, i.e. it introduces a steady-state friction state z for nonzero velocity v and therefore accounts for the continuous breaking and new formation of contact points between the contact surfaces.

Equation (1.2) describes the dependence of the friction force upon the internal friction state and its derivative. The first term corresponds to the friction force due

to the stiffness of the bristles, while the second term adds damping to the friction model³, to counteract unwanted oscillations of the bristle deflection. The third term accounts for viscous friction that is predominant at high relative speeds of the contact surfaces. In this situation the contact surfaces are usually not in contact anymore, because they are separated by a lubricant layer.

Equation (1.3) describes the velocity dependence of the bristle deflection for steady state. As seen before for nonzero velocities v the bristle deflection approaches the steady state value $z_{SS} = g(v) \cdot \text{sgn}(v)$. Thus $g(v)$ can be used to account for the Stribeck effect, that will be described later in this chapter. Further $g(v)$ can also be seen as a time constant, defining how quick the steady state value z_{SS} is reached. It should be noted here that different parameters for $g(v)$ can be used for positive and negative velocities, i.e. the function $g(v)$ is not required to be symmetric with respect to v and may have a discontinuity for zero velocity.

Equation (1.4) describes a common parametrization of the damping coefficient $\sigma_1(v)$. This parametrization yields a damping coefficient that declines with increasing velocity. The parameters controlling this decline allow to influence possible unwanted effects in the breakaway behavior that can occur due to high damping and ensure passivity of the state equation for arbitrary high relative velocities. However a simplified version of the friction model above where the damping coefficient $\sigma_1(v)$ is assumed to be constant, i.e. $\sigma_1(v) = \sigma_1 = \text{const.}$ is also used frequently.

Some of the typical friction phenomena that are covered by the LuGre model are listed below. For more information on the various phenomena the reader is again referred to Olsson [1].

- *Stribeck effect*
The experimentally observed decrease of the friction force at low relative velocities from the usually higher value at stiction to a lower value when sliding occurs is known as Stribeck effect (see figure 1.8). The Stribeck effect is captured in the LuGre model through the function $g(v)$, governing the steady state value of the friction state and thus the friction force for nonzero velocities.
- *Static friction and breakaway*
The static friction and breakaway forces depend on the rate of increase of the external force and thus velocity. This shows that friction is a dynamic process and not only a static phenomenon only dependent on the relative velocity of the contact.
- *Presliding displacement*
Before macroscopic sliding between two friction surfaces occurs the so called presliding displacement can be observed. This means that the two friction surfaces move relative to each other even when the applied force is smaller than the breakaway force. The friction surfaces can be imagined to be connected by springs, allowing a relative movement between the friction surfaces. These springs break when the breakaway force is reached and formate new, when the relative velocity between the friction surfaces occurs to be zero. However experiments suggest that the presliding behavior is highly nonlinear and exhibits for example hysteresis (see e.g. Swevers et al. [6]).

³Since σ_1 does not directly affect the friction state the term damping is not completely accurate. However the term damping of the LuGre model will be used to refer to σ_1 throughout this thesis since this term is widespread in literature about the LuGre model.

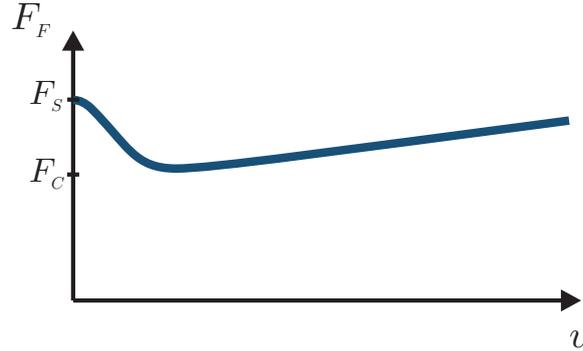


Figure 1.8: Typical behavior of the friction force F_F in the sliding regime in dependence of the velocity. For low velocities the Stribeck effect, governing the transition of the friction force from the stiction force F_s to the Coulomb friction force F_c becomes evident. For high velocities the viscous friction and the Coulomb friction dominate the behavior.

- *Frictional lag*

Experiments indicate dynamic and nonlinear friction behavior also in the sliding regime. Prominent is in particular the so called frictional lag, i.e. a time delay between velocity and steady state friction force. This causes hysteretic behavior of the friction force for velocity changes, i.e. the Friction force is usually lower for decreasing than for increasing velocities. This hysteretic behavior strongly depends on the rate of the velocity change. This implies that the shape of the curve depicted in figure 1.8 depends on the rate of increase of the velocity.

Also shortcomings of the LuGre model are pointed out by several authors (see e.g. Swevers et al. [6] and Lampaert et al. [7]). According to Swevers et al. [6] one of the mayor shortcomings of the LuGre model is its inability to account for hysteresis with nonlocal memory. Further the LuGre model does not offer the opportunity to shape the relation between position and force in presliding, since this relations is given implicitly in the structure of the model.

As proven by Barabanov and Ortega [5] the map from the relative velocity v to the friction estimate F_F defined by the LuGre model is only passive for parameter choices that fulfill the condition:

$$\frac{1}{F_c} \leq \frac{1}{F_c} \left(1 + \frac{F_v}{\sigma_1} \right). \quad (1.5)$$

It is further mentioned that this condition is violated for the parameters of some real systems. This poses an theoretical shortcoming of the LuGre model, even though the LuGre model still produces good estimates for the measured friction data even when the passivity condition is violated.

1.4 Outline of this Thesis

Chapter 2 introduces the hardware of the Furuta pendulum and presents the derivation of the model of the plant.

In chapter 3 the used control system and the different friction compensation schemes are introduced and their implementation is discussed. Further conditions for the evaluation of the friction compensation schemes are addressed.

Methods for and results of the estimation of the friction parameters of the Furuta pendulum are documented in chapter 4.

Chapter 5 presents the evaluation of the different friction compensation schemes based on simulation.

In chapter 6 the evaluation of the different friction compensation schemes is continued based on experimental data.

Concluding the thesis chapter 7 summarizes the most important results and conclusions from the analysis presented in the thesis. Additionally the chapter comprises an outlook and recommendations for further research.

Chapter 2

Control Plant and Modeling

2.1 Hardware

As mentioned in chapter 1.1 the friction compensation is implemented for the inverted Furuta pendulum.

For stabilizing the pendulum in the upright position the angles of the arm φ and the pendulum rod θ are measured (see also figure 2.1).

For the measurement of the angle θ two potentiometers are used. The first one is used to measure the angle θ in a range of 360° , while the second one can only be used to measure angle deviations of about 60° from the upright position, but therefore with higher accuracy. The signals from the potentiometers are transferred to the base of the pendulum via slip rings enabling endless rotation of the arm of the pendulum.

The angle of the arm φ is measured by an encoder attached to the motor. The impulses of the encoder are integrated by built-in analog electronics and the position of the arm is indicated by a voltage on the connection panel of the pendulum.

Further the device possesses a built-in analog filter for the reconstruction of the joint velocities $\dot{\varphi}$ and $\dot{\theta}$ ¹.

The Furuta pendulum at LTH further possesses an internal analog current controller that controls the current of the motor to a value proportional to the control voltage delivered to the pendulum (see section 2.2.2 for more information).

2.2 Model of the Furuta Pendulum

2.2.1 Mechanic Part

In this section a model of the mechanical part of the Furuta pendulum is derived.

The following assumptions were made while modeling the Furuta pendulum:

- All bodies are perfect rigid bodies. In particular oscillations due to flexibility of the bodies are neglected.
- All connections between bodies are perfect, except for friction. In particular flexibility and backlash in the joints are neglected.

¹These velocity reconstructions are for convenience sometimes denoted as velocity measurements throughout this thesis, even though this term is not completely accurate.

- The friction in the bearings is not influenced by the forces and moments that are acting on the joints, i.e. tilting and wedging in the joints are neglected.
- Parameters of the system are assumed to be constant in time and not dependent on environmental parameters, e.g. dependency of spatial dimensions of bodies on temperature is neglected.

Figure 2.1 shows the schematic picture that is used for modeling the Furuta pendulum. The system parameters that are used for the model are²:

- R : The length of the arm of the pendulum.
- J : The combined moment of inertia of arm and motor with reference to the center of rotation.
- L : The length of the pendulum rod, i.e. the distance of the pendulum mass, that is marked as point M , from the joint that connects pendulum and arm.
- m : The mass of the pendulum
- L_2 : The distance of point M_2 , that marks the center of gravity of the pendulum rod, from the joint that connects the pendulum with the arm.
- m_2 : The mass of the pendulum rod.
- J_p : The moment of inertia of the pendulum rod with reference to point M_2 .

Lagrange's second equation is used in order to obtain the equations of motion³:

$$\frac{d}{dt} \left(\frac{\delta L}{\delta \dot{\mathbf{q}}} \right)^T - \left(\frac{\delta L}{\delta \mathbf{q}} \right)^T = \mathbf{f}_{NP} \quad (2.1)$$

where:

- L : Lagrangian of the system given by $L = T - V$.
- T : Kinetic energy of the system.
- V : Potential energy of the system.
- \mathbf{f}_{NP} : Generalized form of the external, non-potential forces acting on the system.
- \mathbf{q} : Vector of minimal coordinates of the system.

²The set of parameters presented here is not the minimal set of parameters that is required to describe the dynamics of the pendulum. However the current set of parameters was chosen since many of the used parameters are available through measurements and because the use of quantities with respect to the center of gravity of the pendulum seems to be more intuitive in the eyes of the author.

³Please see the annotations on page 9 for more information on the used conventions concerning vectors, matrices and coordinate systems.

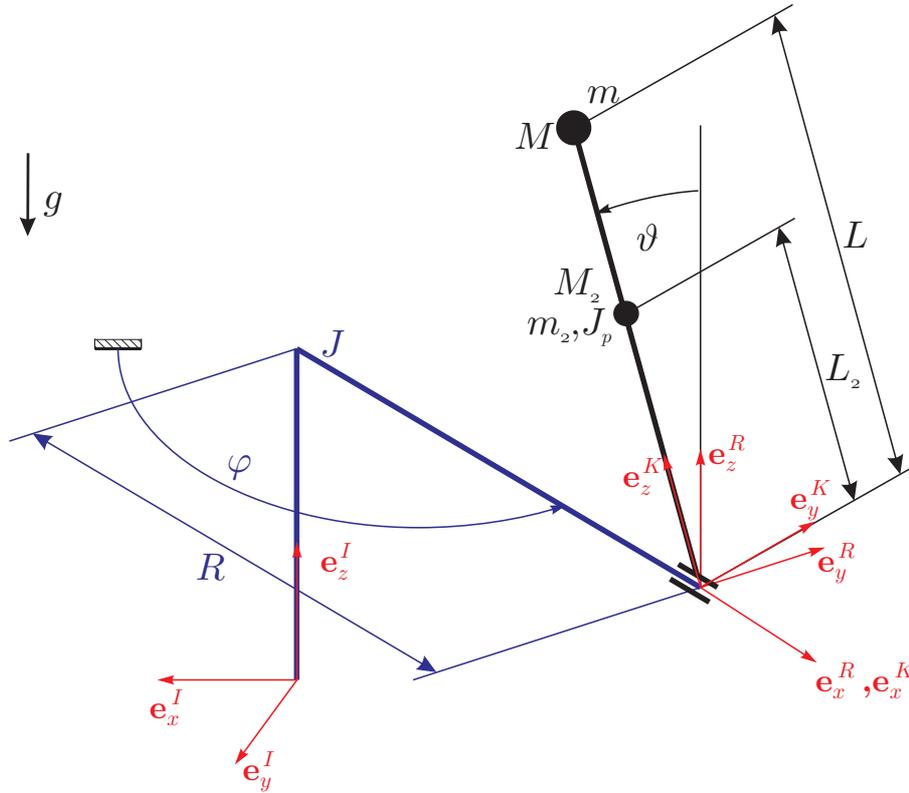


Figure 2.1: Schematic picture of the Furuta pendulum

The system has two degrees of freedom and the posture of the system can be described by the two angles φ and θ . Therefore the following vector of minimal coordinates is chosen:

$$\mathbf{q} = \begin{pmatrix} \varphi \\ \theta \end{pmatrix},$$

where:

- φ : The angle of the arm of the pendulum in positive direction of rotation around e_z^I .
- θ : The angle of the pendulum in positive direction of rotation around e_x^R , measured from the upright position of the pendulum.

Throughout this thesis the term upright position of the pendulum will be used for configurations of the pendulum where $\theta = 0$, while the term hanging position will be used for referring to configurations with $\theta = \pi$.⁴

⁴And in both cases the corresponding configurations that are only distinct by an offset of $\Delta\theta = 2n\pi$ where n is an integer.

The kinetic energy of a rigid body is given by:

$$T = \frac{1}{2}m\mathbf{v}_P^T \mathbf{v}_P + m\mathbf{v}_P^T(\boldsymbol{\Omega} \times \mathbf{r}_{PS}) + \frac{1}{2}\boldsymbol{\Omega}^T \bar{\boldsymbol{\Theta}}_P \boldsymbol{\Omega} \quad (2.2)$$

where:

- P : A chosen reference point on the rigid body.
- S : Center of gravity (cog) of the rigid body.
- \mathbf{v}_P : Velocity at point P .
- \mathbf{r}_{PS} : Vector from point P to point S .
- $\boldsymbol{\Omega}$: Angular velocity of the rigid body.
- $\bar{\boldsymbol{\Theta}}_P$: Tensor of the momenta of inertia in the point P .

Choosing a point on the axis of the arm as reference point P and considering that the arm can only rotate around one single axis the kinetic energy of the arm can be computed using equation (2.2) as:

$$T_{arm} = \frac{1}{2}J\dot{\theta}^2. \quad (2.3)$$

Since at no time a point on the arm has a velocity component in vertical direction (e_z^I) the potential energy of the arm is given by a constant:

$$V_{arm} = V_{arm0} = const. \quad (2.4)$$

For the calculation of the kinetic energy of the pendulum the center of gravity for the rod of the pendulum and the center of gravity of the pendulum mass are chosen as reference points.

This yields for the rod of the pendulum:

$$T_{pendulum,rod} = \frac{1}{2}m\mathbf{v}_{M_2}^T \mathbf{v}_{M_2} + \frac{1}{2}\boldsymbol{\Omega}^T \bar{\boldsymbol{\Theta}}_{rod} \boldsymbol{\Omega} \quad (2.5)$$

where:

- $\boldsymbol{\Omega}$: Rotational velocity of the pendulum.
- $\bar{\boldsymbol{\Theta}}_{rod}$: Inertia tensor of the rod of the pendulum with respect to its cog.

And for the mass of the pendulum:

$$T_{pendulum,mass} = \frac{1}{2}m\mathbf{v}_M^T \mathbf{v}_M \quad (2.6)$$

To be able to evaluate this expression the velocity of the mass of the pendulum and the velocity of the center of gravity of the pendulum rod are needed.

The location of a point R on the rod of the pendulum can be described as:

$${}^R\mathbf{r}_{OR} = \begin{pmatrix} R \\ -L_R \sin(\theta) \\ L_R \cos(\theta) + C_z \end{pmatrix} \quad (2.7)$$

where L_R denotes the the distance of the point R from the joint between the rod of the pendulum and the arm and C_z is a constant depending on the vertical position of the point of origin coordinate system I .

Now \mathbf{r}_{OR} can be differentiated using Euler's derivation rule to obtain the velocity of point R :

$$\begin{aligned}
{}^R\mathbf{v}_R &= R\dot{\mathbf{r}}_{OR} + {}^B\boldsymbol{\omega}_{IR} \times R\mathbf{r}_{OR} \\
&= \begin{pmatrix} 0 \\ -L_R\dot{\theta}\cos(\theta) \\ -L_R\dot{\theta}\sin(\theta) \end{pmatrix} + \begin{pmatrix} 0 \\ 0 \\ \dot{\varphi} \end{pmatrix} \times \begin{pmatrix} R \\ -L_R\sin(\theta) \\ L_R\cos(\theta) + C_z \end{pmatrix} \\
&= \begin{pmatrix} L_R\dot{\varphi}\sin(\theta) \\ R\dot{\varphi} - L_R\dot{\theta}\cos(\theta) \\ -L_R\dot{\theta}\sin(\theta) \end{pmatrix} \tag{2.8}
\end{aligned}$$

The rotational velocity of the rod of the pendulum is given by:

$${}^R\boldsymbol{\Omega}_{pendulum} = \begin{pmatrix} \dot{\theta} \\ 0 \\ \dot{\varphi} \end{pmatrix} \tag{2.9}$$

The transformation matrix A_{KR} from the coordinate system R to the coordinate system K that is attached to the rod of the pendulum is given by:

$$A_{KR} = \begin{pmatrix} 1 & 0 & 0 \\ 0 & \cos(\theta) & \sin(\theta) \\ 0 & -\sin(\theta) & \cos(\theta) \end{pmatrix} \tag{2.10}$$

Hence the rotational velocity of the rod in the coordinate system K is:

$${}^K\boldsymbol{\Omega}_{pendulum} = A_{KRR}\boldsymbol{\Omega}_{pendulum} = \begin{pmatrix} \dot{\theta} \\ \dot{\varphi}\sin(\theta) \\ \dot{\varphi}\cos(\theta) \end{pmatrix} \tag{2.11}$$

The inertial tensor $\boldsymbol{\Theta}_{rod}$ of the rod of the pendulum expressed in the coordinate system K is due to symmetry reasons:

$${}^K\boldsymbol{\Theta}_{rod} = \begin{pmatrix} J_P & 0 & 0 \\ 0 & J_P & 0 \\ 0 & 0 & 0 \end{pmatrix} \tag{2.12}$$

Now the kinetic energy of the pendulum can be computed by using equations (2.5), (2.6), (2.8), (2.11) and (2.12):

$$\begin{aligned}
T_{pendulum} &= T_{pendulum,rod} + T_{pendulum,mass} \\
&= \frac{1}{2}(mL^2 + m_2L_2^2)\dot{\varphi}^2\sin^2(\theta) + \frac{1}{2}(m + m_2)R^2\dot{\varphi}^2 \dots \\
&\quad - (mL + m_2L_2)R\dot{\varphi}\dot{\theta}\cos(\theta) + \frac{1}{2}(mL^2 + m_2L_2^2)\dot{\theta}^2 \dots \\
&\quad + \frac{1}{2}J_P\dot{\theta}^2 + \frac{1}{2}J_P\dot{\varphi}^2\sin^2(\theta) \tag{2.13}
\end{aligned}$$

The potential energy of the mass and the rod of the pendulum can be obtained by using:

$$dV = F \cdot dh = mg \cdot dh \tag{2.14}$$

and hence:

$$V_{pendulum} = g(mL + m_2L_2)\cos(\theta) + V_{pendulum_0} \tag{2.15}$$

where $V_{pendulum_0}$ is a constant depending on the zero level chosen for the potential energy.

Using equations (2.3), (2.4), (2.13) and (2.15) the Lagrangian Function of the system can now be computed to:

$$\begin{aligned}
L &= T_{arm} + T_{pendulum} - V_{arm} - V_{pendulum} \\
&= \frac{1}{2}(mL^2 + m_2L_2^2 + J_P)\dot{\varphi}^2 \sin^2(\theta) + \frac{1}{2}((m + m_2)R^2 + J)\dot{\varphi}^2 \dots \\
&\quad - (mL + m_2L_2)R\dot{\varphi}\dot{\theta} \cos(\theta) + \frac{1}{2}(mL^2 + m_2L_2^2 + J_P)\dot{\theta}^2 \dots \\
&\quad - g(mL + m_2L_2) \cos(\theta) - V_{pendulum_0} - V_{arm_0}
\end{aligned} \tag{2.16}$$

In order to be able to evaluate equation (2.1) the following derivatives of the Lagrangian function have to be calculated:

$$\frac{\partial L}{\partial \varphi} = 0 \tag{2.17}$$

$$\begin{aligned}
\frac{\partial L}{\partial \theta} &= (mL^2 + m_2L_2^2 + J_P)\dot{\varphi}^2 \sin(\theta) \cos(\theta) \dots \\
&\quad + (mL + m_2L_2)R\dot{\varphi}\dot{\theta} \sin(\theta) + g(mL + m_2L_2) \sin(\theta)
\end{aligned} \tag{2.18}$$

$$\begin{aligned}
\frac{d}{dt} \left(\frac{\partial L}{\partial \dot{\varphi}} \right) &= (mL^2 + m_2L_2^2 + J_P)\ddot{\varphi} \sin^2(\theta) + 2(mL^2 + m_2L_2^2 + J_P)\dot{\varphi}\dot{\theta} \sin(\theta) \cos(\theta) \dots \\
&\quad + ((m + m_2)R^2 + J)\ddot{\varphi} - (mL + m_2L_2)R\ddot{\theta} \cos(\theta) \dots \\
&\quad + (mL + m_2L_2)R\dot{\theta}^2 \sin(\theta)
\end{aligned} \tag{2.19}$$

$$\begin{aligned}
\frac{d}{dt} \left(\frac{\partial L}{\partial \dot{\theta}} \right) &= -(mL + m_2L_2)R\ddot{\varphi} \cos(\theta) + (mL + m_2L_2)R\dot{\varphi}\dot{\theta} \sin(\theta) \dots \\
&\quad + (mL^2 + m_2L_2^2 + J_P)\ddot{\theta}
\end{aligned} \tag{2.20}$$

The external, non-conservative moments acting on the system are the moment M_M of the motor, the friction moment M_F of the motor and the friction moment M_{FP} of the joint of the pendulum. No external, non-conservative forces are acting on the system.

The external, non-conservative generalized forces f_{NP} are determined using Jacobi Matrices. The Jacobi Matrices of rotation ${}_I\mathbf{J}_{Rarm}$ and ${}_R\mathbf{J}_{Rpendulum}$ of the two bodies can be obtained via the rotational velocities of the bodies of the system as follows:

$$\begin{aligned}
{}_I\boldsymbol{\Omega}_{arm} &= \begin{pmatrix} \dot{\varphi} \\ 0 \\ 0 \end{pmatrix} = \begin{bmatrix} 1 & 0 \\ 0 & 0 \\ 0 & 0 \end{bmatrix} \begin{pmatrix} \dot{\varphi} \\ \dot{\theta} \end{pmatrix} \\
\text{thus: } {}_I\mathbf{J}_{Rarm} &= \begin{bmatrix} 1 & 0 \\ 0 & 0 \\ 0 & 0 \end{bmatrix}
\end{aligned} \tag{2.21}$$

$$\begin{aligned}
{}_R\boldsymbol{\Omega}_{pendulum} &= \begin{pmatrix} \dot{\varphi} \\ 0 \\ \dot{\theta} \end{pmatrix} = \begin{bmatrix} 1 & 0 \\ 0 & 0 \\ 0 & 1 \end{bmatrix} \begin{pmatrix} \dot{\varphi} \\ \dot{\theta} \end{pmatrix} \\
\text{thus: } {}_R\mathbf{J}_{Rpendulum} &= \begin{bmatrix} 1 & 0 \\ 0 & 0 \\ 0 & 1 \end{bmatrix}
\end{aligned} \tag{2.22}$$

Therefore the external, non-conservative generalized forces \mathbf{f}_{NP} are:

$$\begin{aligned}\mathbf{f}_{NP} &= {}_I\mathbf{J}_{R_{arm}}^T {}_I\mathbf{M}_{arm}^a + {}_R\mathbf{J}_{R_{pendulum}}^T {}_R\mathbf{M}_{pendulum}^a \\ &= {}_I\mathbf{J}_{R_{arm}}^T \begin{pmatrix} 0 \\ 0 \\ M_M - M_F \end{pmatrix} + {}_R\mathbf{J}_{R_{pendulum}}^T \begin{pmatrix} -M_{FP} \\ 0 \\ 0 \end{pmatrix} \\ &= \begin{pmatrix} M_M - M_F \\ -M_{FP} \end{pmatrix}\end{aligned}\quad (2.23)$$

Now the equation of motion can be obtained by inserting equations (2.17) to (2.20) and (2.23) into equation (2.1):

$$\mathbf{M}(\mathbf{q}) \begin{pmatrix} \ddot{\varphi} \\ \ddot{\theta} \end{pmatrix} - \mathbf{h}(\mathbf{q}) - \mathbf{G}(\mathbf{q}) = \mathbf{f}\quad (2.24)$$

with:

$$\begin{aligned}\mathbf{M}(\mathbf{q}) &= \begin{bmatrix} (mL^2 + m_2L_2^2 + J_P)\sin^2(\theta) + (m + m_2)R^2 + J & -(mL + m_2L_2)R\cos(\theta) \\ -(mL + m_2L_2)R\cos(\theta) & (mL^2 + m_2L_2^2 + J_P) \end{bmatrix} \\ \mathbf{h}(\mathbf{q}) &= \begin{pmatrix} -2(mL^2 + m_2L_2^2 + J_P)\dot{\varphi}\dot{\theta}\sin(\theta)\cos(\theta) - (mL + m_2L_2)R\dot{\theta}^2\sin(\theta) \\ (mL^2 + m_2L_2^2 + J_P)\dot{\varphi}^2\sin(\theta)\cos(\theta) \end{pmatrix} \\ \mathbf{G}(\mathbf{q}) &= \begin{pmatrix} 0 \\ g(mL + m_2L_2)\sin(\theta) \end{pmatrix} \\ \mathbf{f} &= \begin{pmatrix} M_M - M_F \\ -M_{FP} \end{pmatrix}\end{aligned}$$

It can easily be proven that the upright and hanging pendulum position are equilibrium points of the system by inserting $\dot{\varphi} = \dot{\theta} = 0$ and $\varphi = \theta = 0$ and $\varphi = \dot{\theta} = 0, \theta = \pi$, respectively, together with $M_M = M_F = M_{FP} = 0$.

The two equations can be decoupled with respect to the second derivatives of the minimal coordinates by applying basic arithmetic operations, yielding:

$$\begin{aligned}\ddot{\varphi} &= \frac{1}{C_1(C_1\sin^2(\theta) + C_3 + J) - C_2^2R^2\cos^2(\theta)} \cdots \\ &\quad \left[C_1(-2C_1\dot{\varphi}\dot{\theta}\sin(\theta)\cos(\theta) - C_2R\dot{\theta}^2\sin(\theta) + M_M - M_F) \dots \right. \\ &\quad \left. C_2R\cos(\theta)(C_1\dot{\varphi}^2\sin(\theta)\cos(\theta) + gC_2\sin(\theta) - M_{FP}) \right]\end{aligned}\quad (2.25)$$

$$\begin{aligned}\ddot{\theta} &= \frac{1}{C_1(C_1\sin^2(\theta) + C_3 + J) - C_2^2R^2\cos^2(\theta)} \cdots \\ &\quad \left[(C_1\sin^2(\theta) + C_3 + J)(C_1\dot{\varphi}^2\sin(\theta)\cos(\theta) + gC_2\sin(\theta) - M_{FP}) \dots \right. \\ &\quad \left. C_2R\cos(\theta)(-2C_1\dot{\varphi}\dot{\theta}\sin(\theta)\cos(\theta) - C_2R\dot{\theta}^2\sin(\theta) + M_M - M_F) \right]\end{aligned}\quad (2.26)$$

where the constants $C_1 = mL^2 + m_2L_2^2 + J_P$, $C_2 = mL + m_2L_2$ and $C_3 = (m + m_2)R^2$ were introduced⁵.

⁵By introducing these constants a simpler parametrization for the parameters of the pendulum was introduced, since the constants collect the parameters of the rod and the mass of the pendulum, thus combining them in the equations to one rigid body. C_1 is the moment of inertia of this body with respect to the joint between pendulum and arm, while C_2 is a constant that is related to the impulse of the pendulum. C_3 is the moment of inertia of the pendulum in the upright or hanging position with respect to the axis of rotation of the motor.

The linearization of the system around the upright position of the pendulum ($\varphi = \varphi_0$, $\dot{\varphi} = \theta = \dot{\theta} = 0$, $M_M = M_F = M_{FP} = 0$) yields the following linearized system:

$$\dot{\mathbf{x}} = \mathbf{A}_{lin}\mathbf{x} + \mathbf{B}_{lin}\mathbf{u} \quad (2.27)$$

with:

$$\mathbf{x} = \begin{pmatrix} x_1 \\ x_2 \\ x_3 \\ x_4 \end{pmatrix} = \begin{pmatrix} \varphi \\ \dot{\varphi} \\ \theta \\ \dot{\theta} \end{pmatrix} \quad (2.28)$$

$$\mathbf{A}_{lin} = \begin{pmatrix} 0 & 1 & 0 & 0 \\ 0 & 0 & \frac{C_2^2 R g}{C_1(C_3+J) - C_2^2 R^2} & 0 \\ 0 & 0 & 0 & 1 \\ 0 & 0 & \frac{g C_2(C_3+J)}{C_1(C_3+J) - C_2^2 R^2} & 0 \end{pmatrix} \quad (2.29)$$

$$\mathbf{u} = \begin{pmatrix} M_M + M_F \\ -M_{FP} \end{pmatrix} \quad (2.30)$$

$$\mathbf{B}_{lin} = \frac{1}{C_1(C_3+J) - C_2^2 R^2} \begin{pmatrix} 0 & 0 \\ C_1 & C_2 R \\ 0 & 0 \\ C_2 R & C_3 + J \end{pmatrix} \quad (2.31)$$

2.2.2 Motor of Furuta Pendulum

The Furuta pendulum device at LTH is equipped with an internal voltage controller. It is assumed that the motor behaves like an ideal DC motor and thus the moment produced by the motor is proportional to the motor current. Further it is assumed that the internal, analog voltage controller is fast in comparison to the time constants of the mechanical part of the system. Thus it is assumed that applied moment is proportional to the voltage delivered to the input sockets of the pendulum:

$$M_M = K_M u_c,$$

where M_M is the output moment of the motor, while u_c is the voltage delivered to the socket of the device. The factor K_M is the conversion factor between applied voltage and resulting moment.

Chapter 3

Methods for Implementation and Evaluation

This chapter aims to provide an overview of the general framework that was used for the implementation of the friction compensation. Further the conditions and criteria that were used for the evaluation of simulations and experiments are discussed.

3.1 Implementation of the Friction Compensation

3.1.1 Controller Hardware

For the implementation of the controller and the friction compensation for the pendulum a dSPACE¹ system was used. A dSPACE system is combination of soft- and hardware for real time control. dSPACE systems possess the possibility to generate real time executable code for control directly from Matlab Simulink² models and use this code for the control of a real plant.

After successful simulation the model of the plant in the Simulink simulation can be replaced by corresponding input and output blocks contained in the dSPACE Simulink library. The Simulink model can then be used for automatically generating code to test the control system with real hardware.

The dSPACE system used is a DS1103 with a Power PC PPC 750GX CPU with 1GHz CPU clock. The Board is equipped with 32MB application memory where the real time programs to be executed are stored.

The Board is mounted in a so called extension box (see figure 3.1) making it easy to connect the board to different devices and host PC's with different versions of the dSPACE software and Matlab.

The board can be connected to the host PC on which the code generation with Matlab is performed via a bus connection either by using a bus card or a special PCMCIA card delivered with the system.

Further the connection panel to which the out- and inputs of the plant are connected is connected to the dSPACE board contained in the extension box (see figure 3.1).

For the experiments the dSPACE system was assembled and the corresponding hardware and software components were set up appropriately³.

¹dSPACE is a trademark of dSPACE GmbH

²Matlab and Simulink are registered trademarks of The MathWorks, Inc..

³The used Matlab release is Matlab 7.1 (R14) SP3 with Simulink 6.3 (R14SP3). The release of the used dSPACE software is release 5.0.

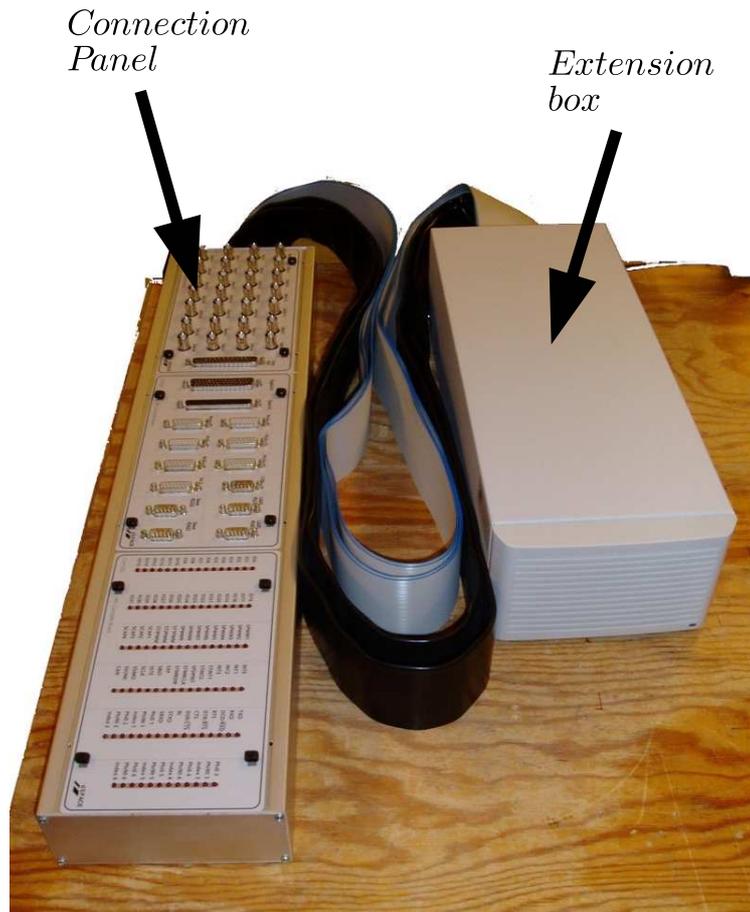


Figure 3.1: dSPACE extension box and connection panel.

For a collection of remarks and instruction for the setup and operation of the dSPACE system please refer to corresponding document that is contained in appendix B.1. A manual for the use of the experiment is contained in appendix B.2. For further information on the dSPACE system and software please refer to the dSPACE documentation.

3.1.2 Framework for Friction Compensation

For the implementation of the friction compensation a Simulink model was built. This model contains input and output blocks to read and write signals from and to the Furuta pendulum. These blocks can easily be replaced by a model of the plant for simulating the behavior of the system without hardware in the loop.

For experiments with the real hardware, a discrete time model with Euler solver (“ode1”) was used.

For simulations a hybrid system approach was used where the propagation of the states of the pendulum⁴ was computed with a variable step solver (“ode23s (Stiff/Mod. Rosenbrock)”), while the controller and the friction compensation were

⁴Including the model of the friction acting on the device.

executed with the same fixed step size as in the experiments.

The implementation was carried out quasi-continuous with a fixed step sampling time of $0.1 \cdot 10^{-3}$ s was chosen.

3.1.3 Control System

Controller for Stabilizing the Pendulum

For the stabilization of the pendulum a linear-quadratic (LQ) controller was applied. Continuous time, as well as discrete time LQ control was used. Due to the short sampling time the achieved performances are similar.

The design parameters of the LQ-controller were chosen so that state errors concerning the pendulum ($\theta, \dot{\theta}$) are punished harder than errors concerning the arm ($\varphi, \dot{\varphi}$). Thus the controller focuses on keeping the pendulum in the upright position in order to assure stability.

Friction compensation

In order to compensate for the friction effects the friction estimates obtained from one of the friction models whose implementations are described in sections 3.1.4 and 3.1.5 is added to the control signal computed by the controller:

$$M_M = M_{controller} + F_F,$$

where:

- M_M : Applied control signal.
- $M_{controller}$: Control momentum demanded by the controller without friction compensation.
- F_F : Estimate of the friction momentum used for friction compensation.

This approach assumes that the friction acting in the real plant acts like an additional external forces on the bodies of the system. Thus an accurate friction estimate would cancel out the influence of friction in the equations of motion.

Velocity estimation

To have an alternative to the built-in velocity reconstruction and to examine the interplay of velocity observation and friction compensation a high-gain observer was implemented (see Khalil [10] chapter 14.5) to reconstruct the full system state from the measurements of the angles φ and θ .

The equations for the high-gain observer are:

$$\dot{\hat{\mathbf{x}}} = \dot{\mathbf{x}}_0(\hat{\mathbf{x}}, u) + \mathbf{H}(\mathbf{y} - \mathbf{C}\hat{\mathbf{x}})$$

where:

- $\hat{\mathbf{x}}$: The estimated state.
- $\dot{\mathbf{x}}_0(\hat{\mathbf{x}}, u)$: The derivative of the state when calculated with the model of the plant (see equations (2.25) and (2.26)) by inserting the estimated state $\hat{\mathbf{x}}$ and the applied control signal u .
- \mathbf{H} : Observer gain matrix.

- u : Control signal applied to the plant
- \mathbf{C} : Output matrix of the system model (conversion of system state to system output).
- \mathbf{y} : Measured output of the real plant.

Further the observer gain matrix is chosen to (again see Khalil [10] chapter 14.5):

$$H = \begin{bmatrix} \alpha_1/\epsilon_1 \\ \alpha_2/\epsilon_1^2 \\ \beta_1/\epsilon_2 \\ \beta_2/\epsilon_2^2 \end{bmatrix}$$

Where ϵ_1 and ϵ_2 are positive constants and $\alpha_1 > 0$, $\alpha_2 > 0$, $\beta_1 > 0$ and $\beta_2 > 0$ are chosen such that the real part of the roots of the polynomials

$$\begin{aligned} s^2 + \alpha_1 s + \alpha_2 &= 0 \\ s^2 + \beta_1 s + \beta_2 &= 0 \end{aligned}$$

are negative.

To obtain an observer whose behavior is not explicitly dependent on the friction estimation method the friction estimation is not used in the model $\dot{\mathbf{x}}_0(\hat{\mathbf{x}}, u)$ of the plant implemented in the observer. Thus also the control signal u feed to the observer is the control signal without applied friction compensation.

Further efforts for discretization of the high gain observed were not necessary, since integration of the observer equations using forward Euler approximation proved to be stable with the used sample time. However experiments show that for sampling times of $o(10^{-2} \text{ s})$ or larger, additional effort would have to be done in order to assure stability.

Signal Filtering

A issue worth noting here is that resonance with the mechanical Structure of the Furuta pendulum is observed, if the measurements of the velocities supplied by the pendulum are used for the stabilization of the pendulum. This is due to the excitation of unmodeled high-frequency dynamics of the plant, e.g. due the finite stiffness of the parts of the pendulum.

Without applied countermeasures the resonance may lead to the situation where the controller loses the ability to stabilize the pendulum in the upright position. This Problem can be eluded by filtering the control signal applied to the plant with a first-order low-pass filter. An example of the resonance behavior is shown in figure 3.2 when the low-pass filter is turned off a $t = 10\text{s}$. Figure 3.3 shows a close-up of figure 3.2.

As expected, the tendency to show this resonance behavior increases with faster controllers. It is likely that the noise in the velocity measurement is responsible for the excitation of the high-frequency dynamics, since the resonance behavior does not occur when angular velocities calculated with the help of state observers are used⁵.

⁵Even though noise is removed from the measurements by the observer there is no improvement in the control behavior since the gains of the observer have to be tuned in order not to transfer excessive noise into the observed quantities. Therefore delays between the measured and the observed quantities are introduced and thus the use of fast controllers (fast in relation to the observer) does not yield big performance improvements.

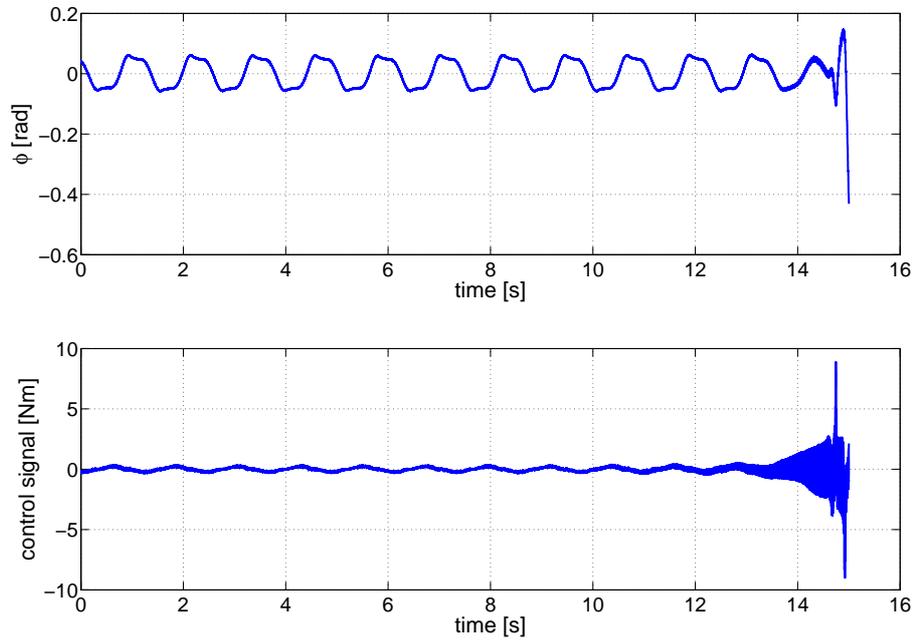


Figure 3.2: Resonance with mechanical structure in the measurement of the pendulum angle (top) and the control signal (bottom), when the low-pass filter is switched off at $t = 10$ s.

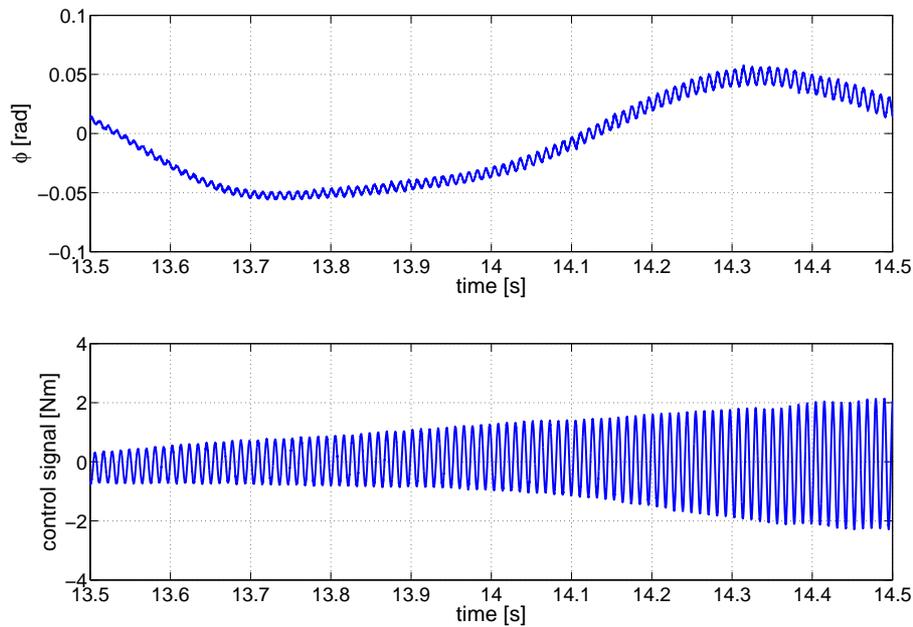


Figure 3.3: Close-up of resonance with mechanical structure in the measurement of the pendulum angle (top) and the control signal (bottom), when the low-pass filter is switched off at $t = 10$ s.

Namely the measurement of $\dot{\theta}$ seems to introduce noise that leads to the resonance with the mechanical structure, since as an alternative to filtering the control signal also a filtering of $\dot{\theta}$ with an first-order low-pass filter works to elude the problem. Not depending on whether the control signal or $\dot{\theta}$ are filtered a low-pass filter with static gain one and cut-off frequency around $250Hz$ suffices to suppress the resonance behavior. With increasing operation time the cut-off frequency that is sufficient for suppressing the resonance increases. After long operation even a cut-off frequency above $1000Hz$ may suffice to hinder the resonance from occurring.

Swinging Up the Pendulum

For swinging up the pendulum the concept presented in Åström et al. [8] was adapted for the Furuta pendulum. During the development of the controller for swing-up perfect parameter knowledge is assumed. Further analysis of the properties of the resulting controller was not carried out since swinging up the pendulum is not part of the main focus of this thesis.

The task of swinging up the pendulum can be interpreted as the task of increasing the sum of potential and rotational energy of the pendulum. The sum of rotational and potential energy of the pendulum rod and the mass attached to it can be expressed as:

$$E = \frac{1}{2}C_1\dot{\theta}^2 + C_2g(1 + \cos(\theta)), \quad (3.1)$$

where the parameters introduced in chapter 2.2 for modeling the pendulum were used. The potential energy in equation (3.1) was chosen so it is zero in the hanging position (i.e. $\theta = \pi$) of the pendulum.

Note that equation (3.1) is not the energy content of the Furuta pendulum, since the kinetic energy due to the rotation of the arm of the Furuta pendulum was not considered.

Derivation of equation (3.1) with respect to time yields:

$$\dot{E} = C_1\dot{\theta}\ddot{\theta} - C_2g\dot{\theta}\sin(\theta) \quad (3.2)$$

First a controller is designed that compensates for the influence of the movement of the pendulum rod on the arm. Setting the equation for the acceleration of the arm $\ddot{\varphi}$ (equation (2.25)) to zero and solving for the moment applied by the Motor results in:

$$M_{M,comp} = 2C_1\dot{\varphi}\dot{\theta}\sin(\theta)\cos(\theta) + C_2R\dot{\theta}^2\sin(\theta) - C_2R\dot{\varphi}^2\sin(\theta)\cos^2(\theta) - g\frac{C_2^2}{C_1}R\sin(\theta)\cos(\theta) \quad (3.3)$$

Inserting $M_M = M_{M,comp} + M_{M,add}$ into the equation for the acceleration of the pendulum $\ddot{\theta}$ (equation (2.26)), where $M_{M,comp}$ is given by equation (3.3) and $M_{M,add}$ is an additional control input for pumping energy into the system, produces:

$$\ddot{\theta} = \dot{\varphi}^2\sin(\theta)\cos(\theta) + g\frac{C_2}{C_1}\sin(\theta) + \frac{C_2R\cos(\theta)}{C_1(C_1\sin^2(\theta) + (m + m_2)R^2 + J) - C_2^2R^2\cos^2(\theta)}M_{M,add} \quad (3.4)$$

Hence inserting equation 3.4 into equation 3.2 the derivative of the energy of the pendulum is:

$$\dot{E} = C_1 \dot{\theta}^2 \sin(\theta) \cos(\theta) + \frac{C_1 C_2 R \dot{\theta} \cos(\theta)}{C_1 (C_1 \sin^2(\theta) + (m + m_2) R^2 + J) - C_2^2 R^2 \cos^2(\theta)} M_{M,add} \quad (3.5)$$

The first term of equation (3.5) does not appear in the case of a pendulum with fixed or linearly moving joint. Considering equation (3.4) it becomes obvious why this term arises for the Furuta pendulum. The inertia forces in the pendulum due to the rotation of the arm of the pendulum have, for constant rotational velocity of the arm, the same influence on the dynamics of the pendulum as a gravity component that is acting radially to the arm of the pendulum. If the pendulum would be located in an environment without gravity ($g = 0$), only $M_{M,comp}$ is applied and the rotational velocity of the arm is nonzero ($\dot{\varphi} \neq 0$) then the additional term would cause the creation of two additional stable equilibrium points of θ at $\theta = \pm\pi/2$, while the equilibrium points at $\theta = 0$ and $\theta = \pi$ are then unstable.

Again assuming perfect parameter knowledge the influence of the additional term caused by the rotation of the pendulum is eliminated by choosing:

$$M_{M,add} = -\frac{C_1 (C_1 \sin^2(\theta) + (m + m_2) R^2 + J) - C_2^2 R^2 \cos^2(\theta)}{C_2 R} \dot{\varphi}^2 \sin(\theta) + M_{M,pump} \quad (3.6)$$

As in Åström et al. [8] the Lyapunov function:

$$V = \frac{1}{2} (E - E_0)^2 \quad (3.7)$$

is chosen to develop a control input $M_{M,pump}$ that brings the energy level E to the value E_0 . Derivation of equation (3.7) yields:

$$\dot{V} = (E - E_0) \dot{E} \quad (3.8)$$

and by choosing:

$$M_{M,pump} = -k_{lya} (E - E_0) \frac{\dot{\theta} \cos(\theta)}{C_1 (C_1 \sin^2(\theta) + (m + m_2) R^2 + J) - C_2^2 R^2 \cos^2(\theta)}, \quad (3.9)$$

with design constant $k_{lya} > 0$, the derivative of the Lyapunov function becomes:

$$\dot{V} = -k_{lya} (E - E_0)^2 C_1 C_2 R \left(\frac{\dot{\theta} \cos(\theta)}{C_1 (C_1 \sin^2(\theta) + (m + m_2) R^2 + J) - C_2^2 R^2 \cos^2(\theta)} \right)^2. \quad (3.10)$$

Thus the Lyapunov function tends to zero as $t \rightarrow \infty$ and the pendulum reaches the desired energy level. The speed of convergence can be influenced by the design parameter k_{lya} .

A proportional controller was added to the control signal, to keep the arm of the pendulum during the swing-up process near the desired reference value. Since this controller destroys the structure of the energy based controller presented above a

dead-zone φ_{dead} around the reference position for the arm of the Furuta pendulum was defined in which the proportional controller is not active, i.e.:

$$M_{prop} = \begin{cases} k_{prop}(\varphi_{ref} - \varphi - \varphi_{dead}) & , \text{ for } (\varphi_{ref} - \varphi) > \varphi_{dead} \\ k_{prop}(\varphi_{ref} - \varphi + \varphi_{dead}) & , \text{ for } (\varphi_{ref} - \varphi) < -\varphi_{dead} \\ 0 & , \text{ for } |(\varphi_{ref} - \varphi)| \leq \varphi_{dead} \end{cases} \quad (3.11)$$

where:

- k_{prop} : Proportional factor of the controller.
- φ_{dead} : Half of the width of the dead-zone in that the controller is not active.
- φ_{ref} : Reference value for the angle of the arm.
- φ : Measure for the actual position of the arm.

The controller was implemented for the Furuta pendulum in the laboratory. The swinging of the pendulum worked as expected for small values of θ (i.e. small values of E_0). For higher values two problems arise:

1. The measurement of θ from the potentiometer switches when the amplitude of the oscillation of the pendulum is about $\pi/2$. This discontinuity is difficult to remove from the signal, since the time that is needed for the switching is considerably long ($o(1e - 2 \text{ s})$) and varies depending on the speed of the pendulum.
2. At higher oscillation amplitudes ($\Delta\theta > \pi/2$) of the pendulum the excitation of unmodeled high-frequency dynamics increases. Especially oscillations of the pendulum rod with amplitude radial to the rotation axis of the arm are significant. This is due to the flexibility of the parts of the pendulum.

3.1.4 Implementation of the LuGre Model

Additionally to the continuous time representation as in equations (1.1)-(1.4) the following representation as in Freidovich [2] was also implemented:

$$\frac{1}{\sigma_0} \frac{dz}{dt} = \dot{\varphi} - \frac{|\dot{\varphi}|}{g(\dot{\varphi})} z \quad (3.12)$$

$$F = z + \sigma_1(v) \frac{1}{\sigma_0} \frac{dz}{dt} + F_v v \quad (3.13)$$

$$g(\dot{\varphi}) = \begin{cases} F_{c+} + (F_{s+} - F_{c+})e^{-(\dot{\varphi}/v_s)^2} & \text{for } \dot{\varphi} > 0 \\ F_{c-} + (F_{s-} - F_{c-})e^{-(\dot{\varphi}/v_s)^2} & \text{for } \dot{\varphi} < 0 \\ \frac{1}{2} \left(\lim_{\dot{\varphi} \rightarrow 0^+} g(\dot{\varphi}) + \lim_{\dot{\varphi} \rightarrow 0^-} g(\dot{\varphi}) \right) & \text{for } \dot{\varphi} = 0 \end{cases} \quad (3.14)$$

$$\sigma_1(\dot{\varphi}) = \sigma_1 e^{-(\dot{\varphi}/v_d)^2} \quad (3.15)$$

This representation is distinct from the representation presented in equations (1.1)-(1.4) only in the chosen state variable. It is $z_{(3.12)-(3.15)} = \sigma_0 z_{(1.1)-(1.4)}$. Therefore the state of the friction model in equations (3.12)-(3.15) is in a order of magnitude that is numerically more favorable, since it reduces the numerical error.

Further equation (3.14) shows the implementation of a function $g(\dot{\varphi})$ that uses distinct parameters for positive and negative velocities.

The LuGre model was discretized as suggested in Freidovich [2] in order to overcome the discretization problems discussed in this paper. Therefore the state equation of the LuGre model is written as:

$$\frac{dz}{dt} = b(\dot{\varphi}) - a(\dot{\varphi})z,$$

with:

- $a(\dot{\varphi}) = \sigma_0 \frac{|\dot{\varphi}|}{g(\dot{\varphi})}$.
- $b(\dot{\varphi}) = \dot{\varphi}$.

Assuming as in Freidovich [2] that the coefficients $a(\dot{\varphi})$ and $b(\dot{\varphi})$ are constant during one sampling period an analytic solution for the propagation of the friction state can be found.

With this method the resulting equations for the the discretized LuGre model are:

For $a \neq 0$:

$$z_{k+1} = e^{-a_k T} z_k + \frac{b_k}{a_k} (1 - e^{-a_k T}) \quad (3.16)$$

and for $a = 0$:

$$z_{k+1} = b_k T + z_k \quad (3.17)$$

with:

- $a_k = \sigma_0 \frac{|\dot{\varphi}_k|}{g(\dot{\varphi}_k)}$.
- $b_k = \dot{\varphi}_k$.
- T : Sampling time.

This discretization scheme was chosen since a discretization of the LuGre model using Euler approximation leads to instability for abrupt changing reference signals and the resulting high angular velocities $\dot{\varphi}$ (see Freidovich [2]). Further this discretization allows tests with different parameter setups without causing instability.

The discretization scheme works for the tested sampling time of $0.1 \cdot 10^{-3}$ s without problems. The absolute errors in simulations compared to a continuous LuGre model solved with variable step size are of order of magnitude $o(10^{-7} \text{ Nm})$ and thus small, while the average relative errors are of $o(10^{-4})$ and thus only one order of magnitude larger than the relative tolerance used for the simulation.

3.1.5 Other Friction Models

For comparison of the performance achieved with the LuGre model the Dahl and the Coulomb friction model were also implemented.

Static Coulomb Friction

The friction compensation via a static Coulomb map is widely used for friction compensation. The concept can be extended easily so that also the Stribeck effect, stiction and viscous friction can be considered (see figure 3.4).

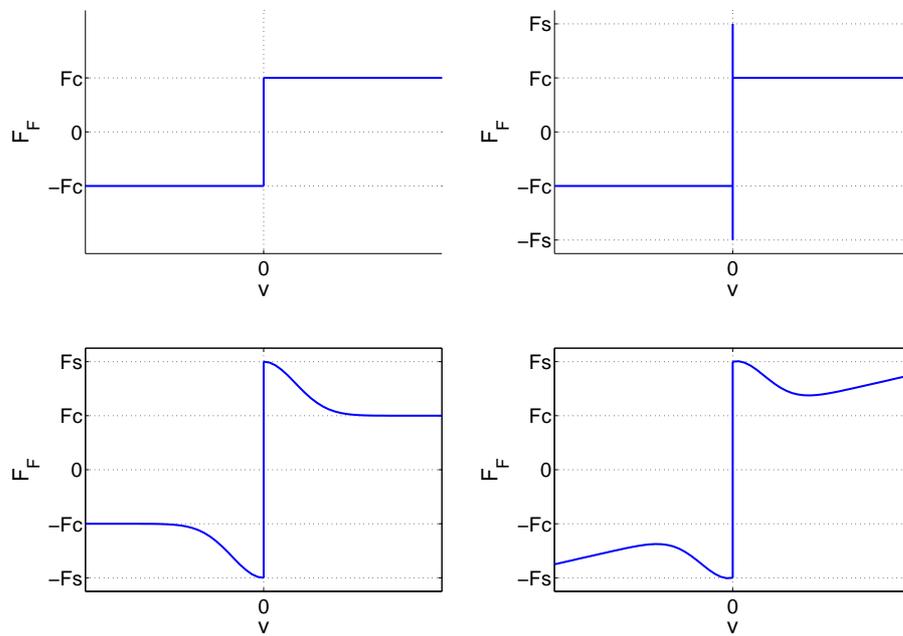


Figure 3.4: Coulomb friction map mapping nonzero velocities v to the corresponding friction force F_F . Shown are the original Coulomb friction map (upper left) and coulomb friction maps including stiction (upper right), Stribeck effect (lower left) and viscous friction (lower right).

The coulomb friction map is not continuous at zero velocity. This is due to that the Friction force for zero velocity equals the force that is applied to the system. This shows that, contrary to what can sometimes be found in literature, Coulomb friction is not only a function of velocity.

Often a regularized Coulomb model is used where the infinite derivative at zero velocity is replaced by a high, but finite derivative. However this modification allows drift for infinitely small external forces. This contradicts observed friction behavior.

Two different approaches of the Coulomb model were implemented:

1. For zero velocities the stiction force F_s multiplied by the sign of the applied control force is used for friction compensation if the control signal without friction compensation is nonzero. The friction compensation uses always the stiction value F_s at zero velocity if a nonzero control signal is applied, since a nonzero control signal indicates that the controller is trying to force the arm of the Furuta pendulum to move, i.e. the control error is nonzero. Thus it is reasonable to use the stiction force for friction compensation and not the actual friction estimate given by the demanded control force. The use of the magnitude of the control signal itself which would be the accurate friction estimate resulting from the Coulomb map is not useful, since the Coulomb map is static, i.e. an increase in the control signal results in an instantaneous increase of the friction force as long as it does not exceed the stiction force F_s and would result in an algebraic loop.
Further to avoid excessive switching of the friction force two dead-zones, around zero values for velocity and around zero values for the control signal, are applied. For absolute values smaller than the threshold of the corresponding dead-zone the velocity or the control signal are assumed to be zero respectively (see also figure 3.5).
2. The Coulomb model is regularized, i.e. the switching of the friction force at zero velocity is replaced by a transition of the friction force following a linear function (see also figure 3.6).

Both of these modifications cause drift for infinitely small velocities. However since the models are used for friction compensation and the coulomb model is also not capable of describing dynamic friction behavior (see Olsson [1]) this shortcoming appears to be of minor importance here.

3.1.6 Dahl Friction Model

The so called Dahl friction model can be viewed as a predecessor of the LuGre model. It is a simple dynamic friction model described by the equations:

$$\begin{aligned} \frac{dz}{dt} &= v \left(1 - \frac{\sigma_0}{F_c} \operatorname{sgn}(v)z \right)^i \\ F &= \sigma_0 z \end{aligned}$$

Thus the Dahl model for the commonly used value $i = 1$ is a special case of the LuGre model for the following choices $g(v) = F_c$ and $\sigma_1 = 0$ in the LuGre model. The Dahl model is not capable of capturing the Stribeck effect. It can be augmented with viscous friction analog to the LuGre model.

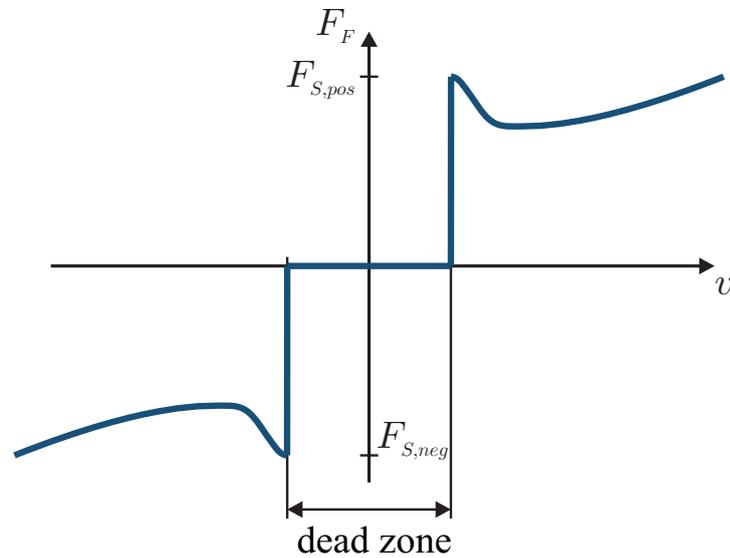


Figure 3.5: Definition of dead zone around zero velocity, in order to prevent excessive switching. The friction force is set to $F_s * \text{sgn}(v)$ if the velocity takes values smaller than the threshold of the dead zone and the control signal exceeds the threshold for the control signal.

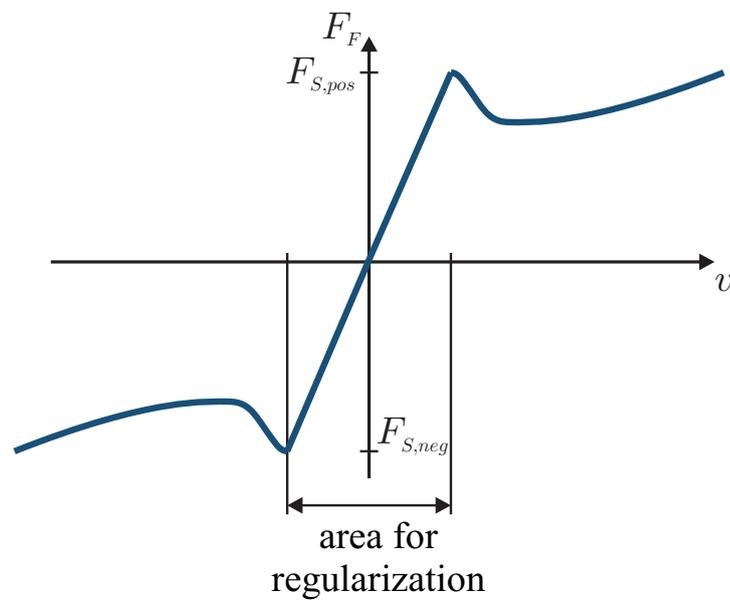


Figure 3.6: Regularization of the coulomb model for velocities around zero.

For the Simulation the Dahl friction model was discretized in the same way as the LuGre model (see section 3.1.4). This yields the same equations as equations (3.16) and (3.17), but instead with the coefficients:

- $a_k = \sigma_0 \frac{|\dot{\varphi}_k|}{F_c}$.
- $b_k = \dot{\varphi}_k$.

3.1.7 Leuven Friction Model

In Swevers et al. [6] and Lampaert et al. [7] the so called Leuven friction model is described. In the form as in Lampaert et al. [7] the Leuven friction model is a generalization of the LuGre model.

The Leuven model offers two major improvements to the LuGre model:

1. The Leuven model is able to exhibit hysteresis with non-local memory.
2. The Leuven model offers the possibility to shape the form of the relation between force and displacement in the presliding regime explicitly.

The Leuven model was not implemented, since the differences of the Leuven model in comparison with the LuGre model are in the presliding regime. The parameter identification showed that presliding parameters are hardly measurable with the sensor equipment of the device and that, judging from the measurement data, no statements about the shape of the relation between friction force and displacement in the presliding regime can be made (see chapter 4).

3.2 Evaluation Criteria for Friction Compensation

To be able to assess the performance of different friction compensation approaches general procedures and experimental conditions are defined in this section.

3.2.1 Experimental Conditions

The following conditions were met during the different experiments:

- *Operation State*
Since the friction behavior of the system changes significantly with the operation time⁶ similar conditions were used for the different tests. Therefore the pendulum was used for a time interval of at least five minutes before the begin of the first measurement in order to ensure that the pendulum was close to a steady state operation condition.
- *Controller*
The same controller was used for obtaining measurements with different friction compensation approaches that are to be compared.
- *Measurements and Velocity Reconstruction*
The same measurements and/or observers for velocity reconstruction were used for obtaining data with different friction compensation schemes that are compared. The friction estimates were not used in the dynamics of the observer, if an observer was applied.
- *Begin and End of Evaluation Measurement*
The begin of end of the measurements to be used for the evaluation were triggered in dependence to the reference signal.

⁶A possible reason for this are e.g. temperature changes in motor and bearings.

- *Angular Position of the Arm for the Measurements*

Since the friction behavior of the pendulum varies in dependence of the position of the arm⁷, it was assured that the measurement cycles for the different compensation schemes started always at similar angular position of the arm. It had to be taken care of this since the zero position of the arm moves depending on the initialization position.

3.2.2 Benchmark

To be able to compare the different approaches for friction compensation the following reference signals were used:

1. *Assessment of positioning accuracy with constant reference*

The behavior of the pendulum is recorded for 20 seconds with a constant zero reference for all angles and angular velocities. This experiment is used to assess the improvement through the friction compensation scheme in holding a constant reference. The reduction of limit cycles due to friction can be evaluated using this reference.

2. *Assessment of transient response with step signals*

To be able to assess the speed of the control system comprising different friction compensation schemes, the angular position reference for the arm is changed in one step by 45 degrees and back with a period time of 10 seconds (see figure 3.7). The references for the angular velocities and the pendulum position remain zero.

3. *Assessment of reference tracking using chirp signal*

To evaluate the improvement of reference tracking with the approach a sinus signal with linearly increasing frequency (chirp signal) is used as reference for the arm of the pendulum. The corresponding derivative is used as reference signal for the angular velocity, while the references for the pendulum remain zero. The references for the angle of the pendulum arm and the corresponding velocity are thus, as depicted in figure 3.8, expressed by the equations:

$$\varphi_{ref}(t) = A \sin(2\pi f(t_c)t_c) = A \sin(2\pi(c_1 t_c + c_2)t_c) \quad (3.18)$$

$$\dot{\varphi}_{ref}(t_c) = (4\pi c_1 t_c + 2\pi c_2)A \cos(2\pi(c_1 t_c + c_2)t_c) \quad (3.19)$$

where:

- $A = \pi/4$: Amplitude of sinus for the angular position reference signal.
- t_c : Cycle time, i.e. the time since the start of the test cycle.
- $f(t_c)$: Frequency of the chirp signal that is modified as $f(t_c) = c_1 t_c + c_2$. Where $c_1 = 0.0075$ and $c_2 = 0$.

Test runs without friction compensation but the same controller and combination of measurements and observations were used as benchmarks for the friction compensation schemes.

It should be noted that it is not possible for the pendulum to follow the reference signals as in 2. and 3. perfectly. The controller has to compromise in these cases between following the reference signal with the arm and holding the pendulum upright. However it is assumed that these signals are useful to assess the performance improvement due to friction compensation since the same reference signals are used for all friction compensation schemes to be compared.

⁷Possible reasons for this are e.g. inaccuracies in the bearings of the pendulum and effects that occur because of the motor winding.

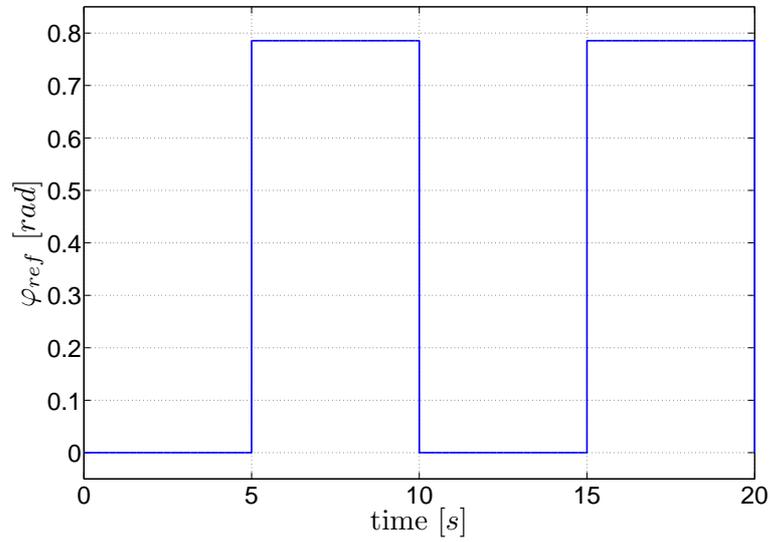


Figure 3.7: Reference used for the angular position in second test run.

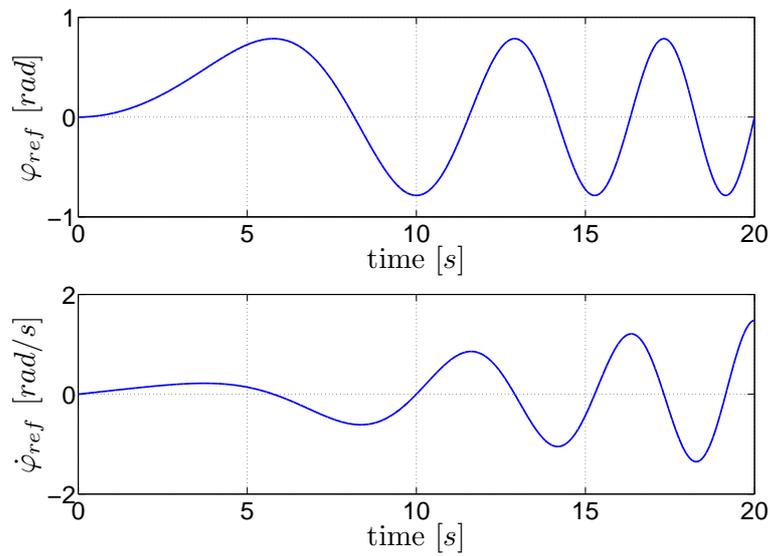


Figure 3.8: Reference used for the angular position (top) and angular velocity (below) in third test run.

3.2.3 Evaluation Method

For the evaluation of the experiments the following error measure was applied:

$$Q = \frac{1}{n} \sum_{i=1}^n \Delta x_i^T \Delta x_i, \text{ with: } \Delta x_i = \begin{bmatrix} (\varphi - \varphi_{ref}) \\ (\dot{\varphi} - \dot{\varphi}_{ref}) \\ (\theta - \theta_{ref}) \\ (\dot{\theta} - \dot{\theta}_{ref}) \end{bmatrix}_i, \quad (3.20)$$

where:

- n : Number of measurement points.
- $\varphi, \dot{\varphi}, \theta, \dot{\theta}$: Values of the state variables of the pendulum as delivered by the Furuta pendulum (velocity reconstruction via built-in analog filter).
- $\varphi_{ref}, \dot{\varphi}_{ref}, \theta_{ref}, \dot{\theta}_{ref}$: Reference values for the state variables of the pendulum.

The matrix Q is an estimate of the covariance matrix. It contains the least squares errors of the state variables on the main diagonal and an estimate of the covariance between the errors in the states in the remaining fields.

Since only the friction in the joint belonging to φ is compensated and the LQ-controller focuses on controlling the angle θ for stabilizing the pendulum, the effect of the friction compensation can be best observed in φ . Therefore for evaluation the least squares error in φ ($Q_{1,1}$ -component) is considered to be the most important error measure.

The errors in the velocity reconstructions are of minor importance for the evaluation since the obtained velocities are less reliable than the angle measurements. Further the true velocity errors are connected to the position errors through a pure differentiator as long corresponding references are used for positions and velocities.

For more than one measurement for the evaluation of the experiment the mean values of the components of the error measure as in equation (3.20) was used to assess the performance and the root mean square error:

$$\sigma_{u,v}^2 = \frac{1}{m-1} \sum_{k=1}^m ({}^k Q_{u,v} - \bar{Q}_{u,v})^2 \quad (3.21)$$

with:

- $\sigma_{u,v}$: Sample standard deviation of the $Q_{u,v}$ -component of the error measure
- ${}^k Q_{u,v}$: $Q_{u,v}$ -component of the error measure from the k^{th} measurement
- m : Number of measurements
- $\bar{Q}_{u,v} = \frac{1}{m} \sum_{k=1}^m {}^k Q_{u,v}$: Mean value of the $Q_{u,v}$ -component of the error measure as in equation (3.20) for all measurements

was used to evaluate the scattering of the determined performance indices⁸ and thus to give a measure of the significance of differences in the performance indices.

⁸Since the number of values used to calculate the standard deviation $\sigma_{u,v}$ is not high it cannot be used to estimate the parameters of a probability distribution. However it can be used to obtain a measure of the order of magnitude of the variation of the performance indices from different measurements and thus give an idea of the significance of differences in the error measures.

Chapter 4

Friction Parameters

This chapter documents the estimation of the LuGre friction parameters and the voltage constant of the Furuta pendulum.

4.1 Estimation of the Voltage Constant

As mentioned above the Furuta pendulum is equipped with a current controller. Assuming that the dynamics of this internal control loop are fast compared to the time constants of the process and that the used motor behaves like an ideal DC motor it can be assumed that the moment applied to the mechanical part of the Furuta pendulum is proportional to the control voltage supplied to the device. Thus the control moment can be applied to the plant by scaling the calculated control momentum with the inverse of the constant that describes the transfer from applied voltage to applied momentum and delivering the resulting voltage to the socket of the device.

Considering the mechanical part of the Furuta pendulum device with detached pendulum the following equation of motion is obtained:

$$J_{arm}\ddot{\varphi} = M_M - M_F, \quad (4.1)$$

where:

- J_{arm} : Moment of inertia of the arm assembly with respect to its center of rotation.
- M_M : Moment produced by the motor.
- M_F : Friction moment.

Applying feedback position control with an proportional controller and assuming that the friction moment can be modeled by Coulomb friction, equation (4.1) can be transformed to:

$$J_{arm}\ddot{\varphi} = K_M K_p (\varphi_{ref} - \varphi) - F_c \operatorname{sgn}(\dot{\varphi}), \quad (4.2)$$

with:

- K_M : Constant transforming the voltage supplied to the pendulum into the moment M_M applied to the mechanical part of the pendulum.
- F_c : Coulomb friction force.

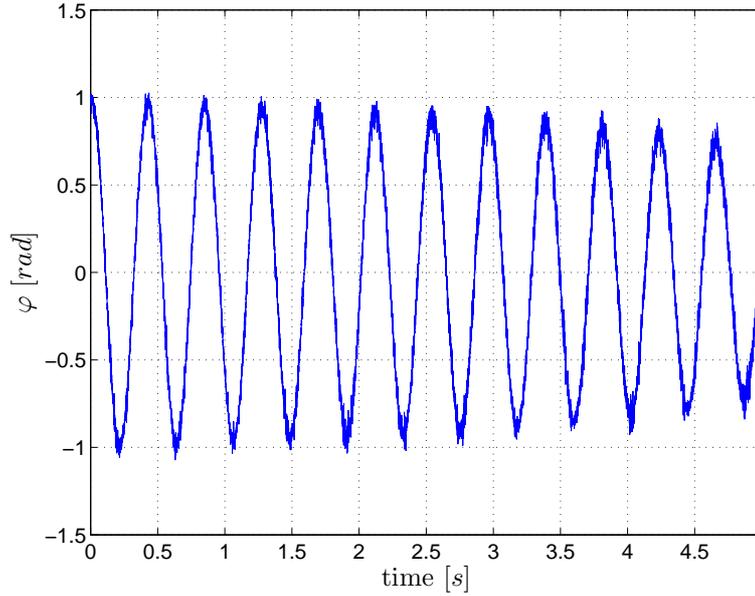


Figure 4.1: Measurement of the first 5 sec of the step response (step height 1 rad) for $K_p = 0.35$ V/rad.

Neglecting the coulomb part F_c of the equation for a moment equation (4.2) results in the equation of a harmonic oscillator with natural frequency:

$$\omega_0 = \sqrt{\frac{K_M K_P}{J_{arm}}}.$$

To consider the effect of the coulomb friction force a half of a period of the motion is considered since the Coulomb friction force only changes at velocity reversals. Since equation (4.2) is linear in the half period of the motion where $\dot{\varphi}$ does not change its sign, the constant term F_c only adds an offset to the solution of the system. At velocity reversals the value of the Coulomb friction force and thus also the offset of the solution jumps. Since the natural frequency of a harmonic oscillator does not depend on the amplitude of the oscillation the frequency is the same on before and after the velocity reversal.

Thus on the above mentioned assumptions the voltage constant can be estimated by measuring the natural frequency of the arm of the Furuta pendulum when proportional control is used.

Figure 4.1 shows an example of a measurement that was made to determine the natural frequency. The effects of friction are relatively small in the first seconds of the measurement. For evaluation the dominant frequency in the spectrum of the measurements was determined via fft (see figure 4.2 for an example). The power spectra have a pronounced peak making it possible to determine the predominant frequency component in the measurements.

According to the model of the Furuta pendulum used at the department the moment of inertia of the arm assembly is $J_{arm} \approx 0.0014$ kg m². The setup is like in the upper picture in figure 4.3. The voltage constant to be calculated has to serve the purpose to cancel the influence of K_M as depicted in the picture as the bottom of figure 4.3.

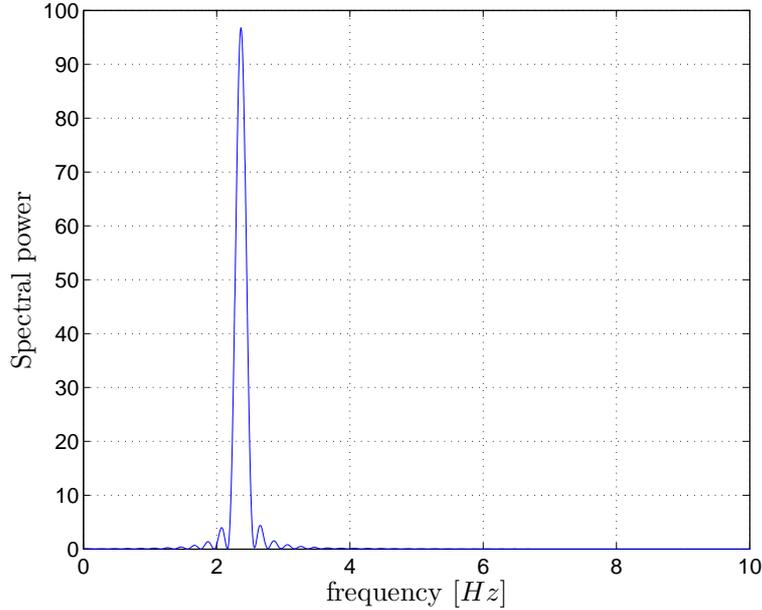


Figure 4.2: Power spectrum of the signal from figure 4.1.

Hence the voltage constant K_{uov} can be computed as:

$$K_{uov} = \frac{1}{K_M} = \frac{K_p}{J_{arm}\omega_0^2}$$

Since signals delivered to the dSPACE output blocks are normalized and the maximal output voltage is $10V$ the voltage constant is multiplied by this factor to make it platform independent¹:

$$K_u = 10 \cdot K_{uov}.$$

Overall nine measurements with different controller gains and initial amplitudes were taken. The resulting mean for the voltage constant is $K_u = 10.96 V/(Nm)$ with an estimated variance of $6.2 \cdot 10^{-3} (V/Nm)^2$. For a complete listing of the used controller parameters please refer to appendix C.3.

The estimated value is thus in good correspondence with value $K_{u,data} = 9.43 V/Nm$ from data sheets that is valid for a new motor.

4.2 Estimation of Friction Parameters

This section aims to document the estimation of the LuGre friction parameters of the arm of the Furuta pendulum. An estimation of the fundamental system parameters like the masses and moments of inertia of the different bodies was not carried out again, since reliable estimates of these parameters are available at the department.

In order to perform measurements to determine the friction parameters the pendulum was detached from the Furuta pendulum. Without the pendulum the device resembles a motor with an inertia attached to its shaft.

¹Of course this factor has also to be recognized while calculating the gain K_p since it contributes to the gain of the P-controller as depicted in figure 4.3, i.e. it is in series connection with the “real” compensator gain $K_{p,model}$ that is defined in the model. Thus $K_p = K_{p,model} \cdot K_{u,est} / 10V$, where $K_{u,est}$ is the estimate of the voltage constant used for the measurements.

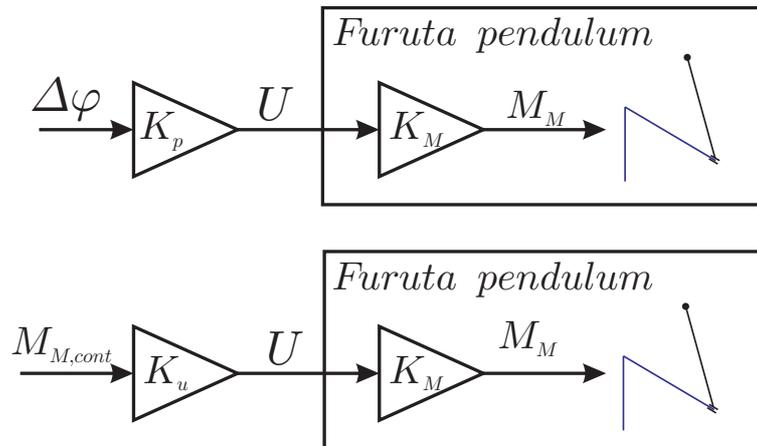


Figure 4.3: Arrangement of the gains for the measurement of the natural frequency (top) and for the implementation of controllers computing the desired torque (bottom). $\Delta\varphi$ denotes the control error, U the voltage delivered to the socket of the Furuta pendulum, $M_{M,cont}$ the desired moment and M_M the actual moment delivered to the mechanical part of the Furuta pendulum.

4.2.1 Estimation of the Friction Forces

To obtain an estimate of the stiction force F_s and the coulomb friction force F_c the moment of the motor was slowly ramped up and down (see figure 4.4).

The amplitude of the signal was chosen high enough, so macroscopic movement of the arm starts before the peak moment is reached. The φ -positions at which sticking and breakaway occurs vary, because the friction parameters are distinct depending on the sign of M_M .

The values of F_c and F_s and their variation for the different cycles can be obtained graphically from the plots if the recorded estimate of the angular velocity as supplied by the Furuta pendulum and the applied moment M_M are plotted against each other (see figures 4.5, 4.6 and 4.7). For each of the three used input signals six measurements with a length of 120 sec or 240 sec (for period length 40 sec) at a sampling rate of $0.1 \cdot 10^{-3}$ s were performed. Table 4.1 lists the ranges of the friction forces that were obtained from the plots² and the corresponding parameters of the input signal.

The higher absolute values for the Coulomb force F_c for the smaller amplitude of the moment is due to the fact that the rate of decrease of the moment is smaller in this case. With amplitude 0.2 Nm the pendulum reaches a relatively high speed of rotation and due to the higher rate of decrease of the motor moment the state of the device is farther apart from the stationary state where the friction and motor moment equal each other, i.e. where the acceleration $\ddot{\varphi}$ is zero, thus allowing the applied moment to decrease further until the friction force can dissipate the kinetic energy contained in the arm. Thus the absolute values for F_c with higher period time are in most cases higher than the values for smaller period times.

²The values were determined manually by observation of the figures and estimating when the measurements leave zero velocity. The applied method seems appropriate to the author, since the measured forces for breakaway and sticking vary for different measurements and the determined forces can anyway only be an indicator of the approximate magnitude of the friction forces.

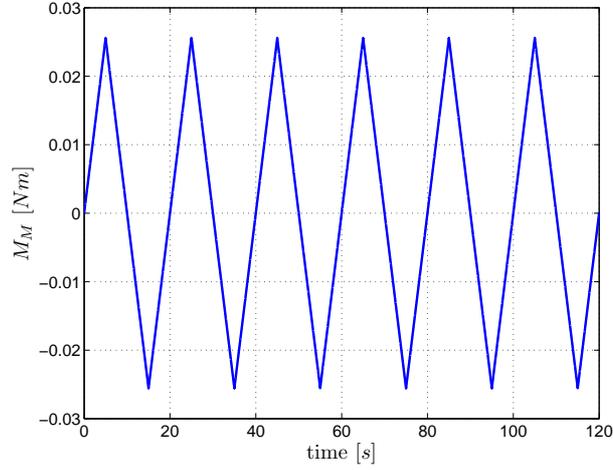


Figure 4.4: Input signal used for determining the friction forces F_c and F_s .

Table 4.1: Ranges for the friction forces F_c and F_s that were obtained from figures 4.5, 4.6 and 4.7 respectively.

<i>Period time</i>	$\max(M_M)$ [Nm]	$\text{sgn}(M_M)$	<i>Friction force</i>	<i>Lower bound</i> [Nm]	<i>Upper bound</i> [Nm]
20 s	≈ 0.026	1	F_s	0.0153	0.0211
			F_c	0.0109	0.0141
		-1	F_s	-0.0192	-0.0134
			F_c	-0.0111	-0.0089
	≈ 0.023	1	F_s	0.0156	0.0217
			F_c	0.0134	0.0153
		-1	F_s	-0.0192	-0.0143
			F_c	-0.0128	-0.0105
40 s	≈ 0.023	1	F_s	0.0153	0.0224
			F_c	0.0134	0.0160
		-1	F_s	-0.0211	-0.0141
			F_c	-0.0141	-0.0121

Remark: The exact values of M_M are known, but due to the subsequent estimation of the voltage constant not round.

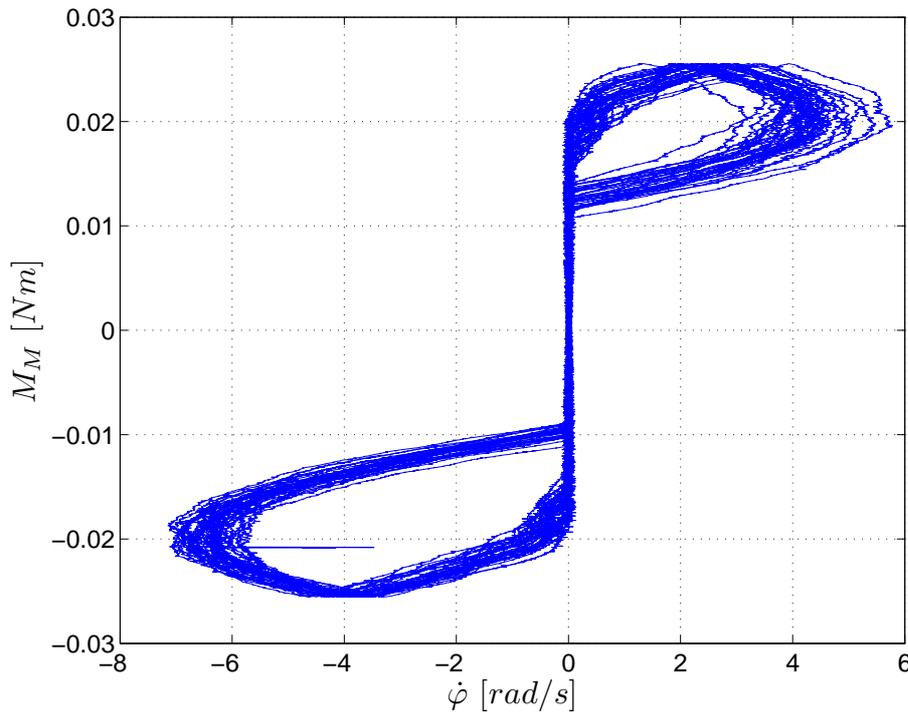


Figure 4.5: Plot of applied motor moment versus rotational speed of the arm for an input signal as in figure 4.4 with amplitude 0.2 Nm and period time 20 s (The data was downsampled with a factor of 25 to keep the file size acceptable).

Further the measurements show the dependency of the breakaway force on the rate of increase of the motor moment. The minimal breakaway force is lower if the rate of increase of the Motor moment is higher.

Further it becomes obvious from figures 4.5 to 4.7 that the friction forces vary depending on the position of the arm φ and/or the operation conditions. The figures show that the break away force is not clearly defined, but rather break away occurs in an interval for the applied force (see table 4.1). For forces within this interval it can occur that the arm breaks away temporarily, then reaches an area with higher friction force and sticks again.

No systematic variation of the friction forces depending on the angle φ could be determined. Thus the estimated friction forces can only be mean values of the actual forces for different arm positions.

4.2.2 Estimation of the Viscous Friction Coefficients

For the estimation of the viscous friction coefficient F_v constant motor moments were applied to the device. The angular velocity $\dot{\varphi}$ of the arm at steady-state and the applied motor moment M_M are recorded over several turns of the arm around its axis of rotation with a sampling rate of $0.1 \cdot 10^{-3} \text{ s}$. A straight line is fit to the data points made up by the mean values of $\dot{\varphi}$ for the individual measurement series and the applied torques. For this purpose the built-in Matlab function “fminsearch” is used.

The used performance index $L_{ls, \hat{\sigma}_{\dot{\varphi}}}$ is a least squares error measure that is obtained by weighting the errors at the data points with the inverse of the root mean error

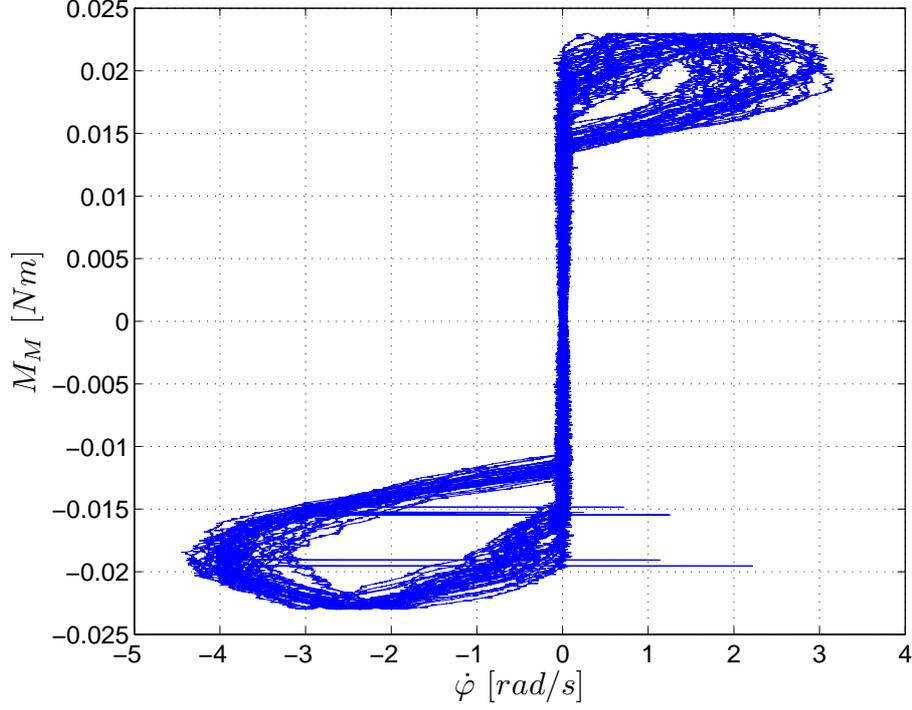


Figure 4.6: Plot of applied motor moment versus rotational speed of the arm for an input signal as in figure 4.4 with amplitude 0.18 Nm and period time 20 s (The data was downsampled with a factor of 25 to keep the file size acceptable).

of the arm angle φ :

$$L_{ls, \hat{\sigma}_{\dot{\varphi}}} = \sum_{i=0}^n \frac{1}{i \hat{\sigma}_{\dot{\varphi}}^2} ({}^i M_M - (a_1 + a_2 {}^i \mu_{\dot{\varphi}}))^2, \quad (4.3)$$

with:

$${}^i \hat{\sigma}_{\dot{\varphi}}^2 = \frac{1}{m-1} \sum_{k=1}^m ({}^{i,k} \dot{\varphi} - {}^i \mu_{\dot{\varphi}})^2, \quad (4.4)$$

$${}^i \mu_{\dot{\varphi}} = \frac{1}{k} \sum_{k=1}^m {}^{i,k} \dot{\varphi}, \quad (4.5)$$

where:

- n : Number of data points (${}^i M_{Mi}, {}^i \mu_{\dot{\varphi}}^i$) for optimization.
- ${}^i M_M$: Moment of the motor applied in the i^{th} measurement.
- a_1, a_2 : Parameters to be optimized. a_1 resembles the Coulomb friction force F_c , while a_2 resembles the viscous friction coefficient F_v .
- ${}^i \mu_{\dot{\varphi}}$: Mean value of the measured arm velocity $\dot{\varphi}$ for the i^{th} measurement.
- ${}^i \hat{\sigma}_{\dot{\varphi}}$: Sample standard deviation (root mean error).
- ${}^{i,k} \dot{\varphi}$: k^{th} data point of the i^{th} measurement.
- m : Number of data points per measurement, i.e. measured values of $\dot{\varphi}$.

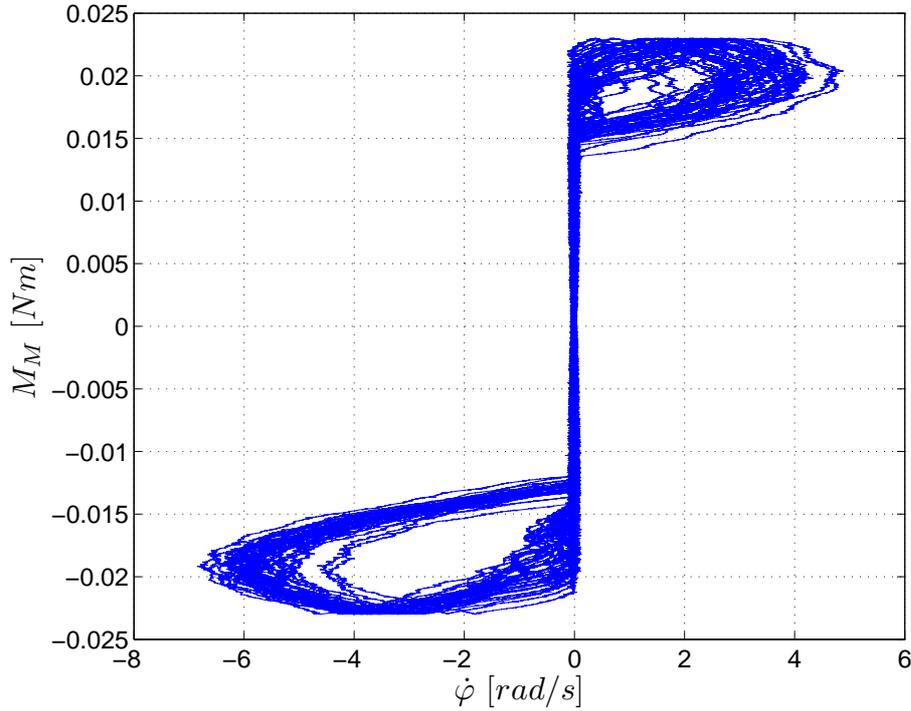


Figure 4.7: Plot of applied motor moment versus rotational speed of the arm for an input signal as in figure 4.4 with amplitude 0.18 Nm and period time 40 s (The data was downsampled with a factor of 25 to keep the file size acceptable).

Table 4.2: Resulting parameter values from the optimization of F_v as described in section 4.2.2.

$\text{sgn}(M_M)$	$F_c \text{ [Nm]}$	$F_v \text{ [Nm/(m/s)]}$
1	0.0218	0.00023
-1	-0.0202	0.00022

The weighting with the sample standard deviation favors measurements where the rotational speed stays closer to the mean value. Assuming a correct model structure (e.g. assuming that F_s , F_c and F_v are constants) these measurements appear to be more accurate. However in the present case the differences to an optimization with an traditional least squares performance index are negligible given the used accuracy. This indicates similar sample standard deviations for the different measurements.

As start values for the optimization the mean values of the friction forces F_c that were determined in section 4.2.1 were used for a_1 , whereas the guess 0.01 was used as initial value for a_2 .

Figure 4.8 show the data points and the resulting fit for positive velocities, while figure 4.9 is the corresponding plot for negative velocities. The parameter values that result from the optimization are listed in table 4.2.

The estimated viscous friction is negligible small. Note that considering the viscous friction coefficients of $F_v \approx 0.0002 \text{ Nm/(m/s)}$ an angular velocity of $\dot{\varphi} \approx 75 \text{ rad/s}$

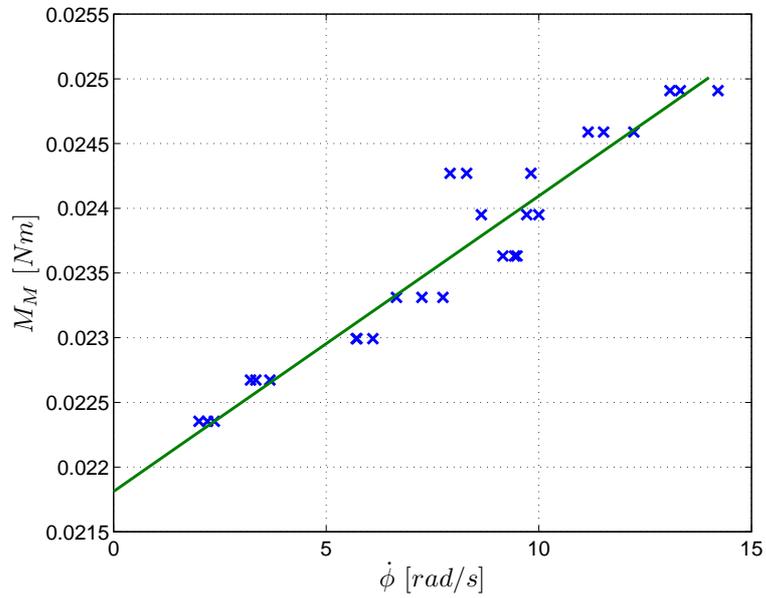


Figure 4.8: Data points and corresponding fit for positive values of the motor moment M_M with performance index as in equation (4.3).

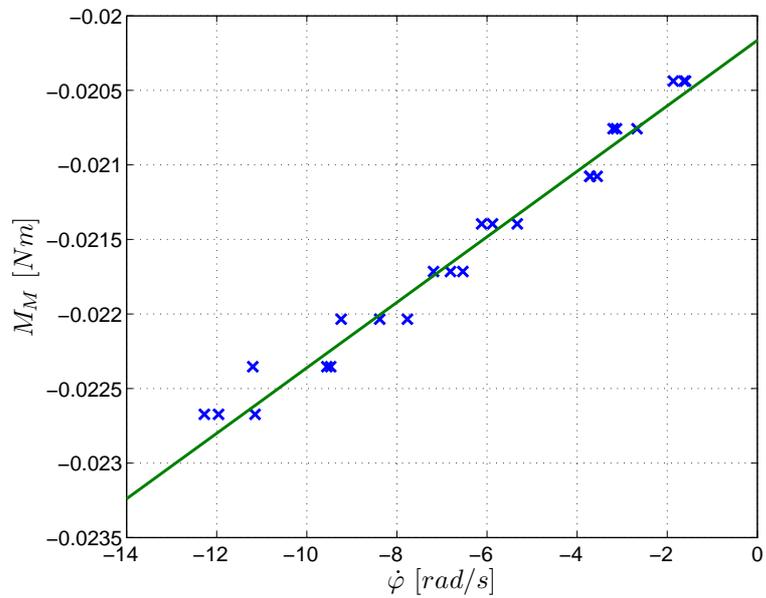


Figure 4.9: Data points and corresponding fit for negative values of the motor moment M_M with performance index as in equation (4.3).

would be needed to produce a viscous friction force that is approximately of the same value as the coulomb friction ($F_c \approx 0.015 Nm$).

Note that the values for F_c as in table 4.2 are much higher than the values estimated in section 4.2.1. When increasing the applied motor momentum manually the values as estimated in chapter 4.2.1 appear to be more realistic. However the values of the friction forces vary depending on the position of the arm and operation conditions like operation time, wear, temperature, etc.. Another reason for the disagreement are structural differences between the LuGre model and the friction behavior of the plant.

4.2.3 Estimation of the Stiffness σ_0

For the estimation of the stiffness σ_0 of the LuGre model the motor moment M_M was ramped up slowly to a value lower than the stiction force F_s , so that no large scale movement of the arm occurs. The input signal is ramped up from zero to a maximum value³ of $M_M \approx 0.018 Nm$ in 20 sec. Measurements are performed in different positions of the arm and for positive and negative values of the moment M_M .

Again using the built-in Matlab function “fminsearch” the least squares error between the measurements of φ and a straight line is minimized. The results that are obtained for the different measurements are displayed in figure 4.10.

The mean of the inverse of all estimated stiffnesses that were depicted in figure 4.10 is $1/\bar{\sigma}_0 = 2.98 \cdot 10^{-3} N$ what corresponds to $\bar{\sigma}_0 = 3.36 \cdot 10^2 N$. The corresponding sample standard deviation (see equation (4.4)), is $\hat{\sigma}_{1/\sigma_0} = 4.23 \cdot 10^{-3} N$. Thus the root mean error is one size of magnitude larger than the absolute value. This indicates that due to the proposed method, the measurement equipment or the unsuitability of the model structure a clear determination of σ_0 is not possible.

However the analysis presented can be used to give a lower bound on the stiffness σ_0 . Examining figure 4.10 it is likely that $1/\sigma_0 < 1 \cdot 10^{-3} m/Nm$ and therefore $\sigma_0 > 1000 Nm/m$.

The big variance of the estimate of the stiffness of the LuGre model becomes more clear if the measurements from the Furuta pendulum are examined more closely. The quantization of the signals from the encoder is of order of magnitude $o(10^{-4})$. Since the friction moments are $o(10^{-2})$ and the LuGre model has a spring like behavior in the presliding regime only stiffnesses smaller than $o(10^2)$ are measurable with the used encoder. This is exactly the order of magnitude of the lower bound obtained above.

The lower bound for σ_0 as determined above is used since it seems not useful to use values for this parameter that are significantly higher than what is observable from measurements.

4.2.4 Estimation of Static Parameters

Further an attempt was made to estimate all parameters that determine the static behavior of the LuGre model in the sliding regime, i.e. F_s , F_c , v_s and F_v , at once.

A fast PI-Controller was used to control the angular velocity $\dot{\varphi}$ of the arm to a constant reference.

³The exact maximum value of M_M is known but due to subsequent estimation of the voltage constant not round.

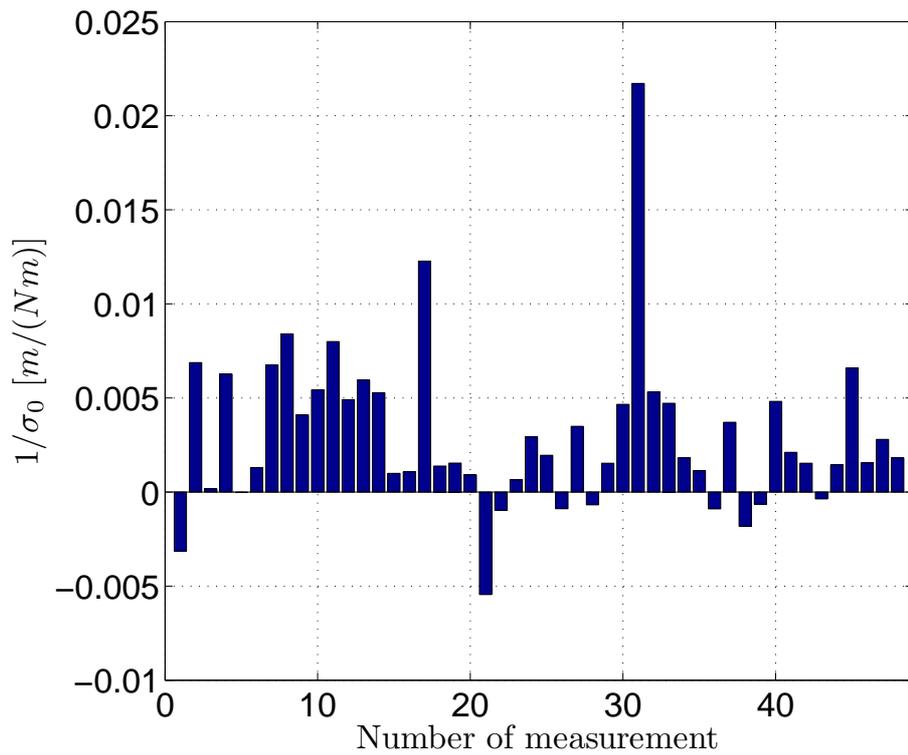


Figure 4.10: Resulting inverse of the Stiffness $1/\sigma_0$ from the optimization. The first 24 values were obtained with measurements with a positive ramp for M_M , while the second 24 values originate from optimization using measurements with a negative ramp for M_M . In each of these groups the first six measurements were performed near the back position of the arm (arm toward wall). The second six measurements were taken near the front position of the arm (arm toward glass wall), near the left position of the arm and right position of the arm (displayed in the figure in this order).

After giving the controller time to control the system near the desired velocity reference the velocity estimated and applied control moment are recorded.

For small reference velocities ($v_{ref} < 0.1 \text{ m/s}$) six measurements with a length of 20 s and a sampling time of $0.1 \cdot 10^{-3} \text{ s}$ in different positions of the arm were taken for each velocity. For bigger reference velocities ($v_{ref} \geq 0.1 \text{ m/s}$) three measurements were taken for every velocity while the length of the measurement was chosen so the arm makes at least one full turn of 360° .

For a constant velocity the LuGre model reaches the following steady-state⁴:

$$\begin{aligned} \dot{z} &= \dot{\varphi} - \sigma_0 \frac{|\dot{\varphi}|}{g(\dot{\varphi})} z \equiv 0 \text{ with } \dot{\varphi} \neq 0 \\ \Rightarrow z &= \frac{g(\dot{\varphi})}{\sigma_0} \text{sgn}(\dot{\varphi}) \end{aligned} \quad (4.6)$$

$$(4.7)$$

By using equation (1.3) this yields the following expression for the steady-state friction force:

$$F = g(\dot{\varphi}) \text{sgn}(\dot{\varphi}) + F_v \dot{\varphi} \quad (4.8)$$

where:

$$g(\dot{\varphi}) = F_c + (F_s - F_c) e^{-(\dot{\varphi}/v_s)^2}$$

Thus the parameters F_s , F_c , v_s and F_v can theoretically be estimated with the help of measurements of the steady state velocity $\dot{\varphi}$ and friction moment F . For this purpose the Matlab function “fminsearch” with the same performance index as in equation (4.3) is used.

To obtain data points for the estimation of the parameters the mean of the measured values for $\dot{\varphi}$ and F is calculated for every measurement.

Figure 4.11 shows the measurements for positive angular velocities of the arm while figure 4.12 is the corresponding plot for negative arm velocities. The values scatter for small velocity values and no distinct Stribeck effect can be observed in the measurements. While some measurements suggest an increase in the friction moment for small velocities as suggested by the Stribeck effect others suggest a decrease.

The scattering of the obtained values for small velocities may have several reasons. The limited resolution of the encoder prohibits accurate measurements and control for very small velocities. The controller could also be too slow to compensate for the fast friction dynamics and thus lead to stick-slip motion. Further the variation of the friction parameters in dependence of the arm position φ is a possible reason. Local maxima in the friction forces could cause the strong variance of the measurements for slow velocities, where the measurements only cover a small angle range $\Delta\varphi$.

4.2.5 Chosen Parameter Values

The parameters that could not be determined through parameter estimation were tuned by hand. Table 4.3 lists the parameters of the LuGre model, the chosen values and a brief explanation how and why these values were chosen.

⁴Since the original LuGre model is continuous this state is theoretically reached after infinite time. However it is assumed that the velocity remained constant for a sufficiently long time so the state of the LuGre model is sufficiently close to the steady-state value.

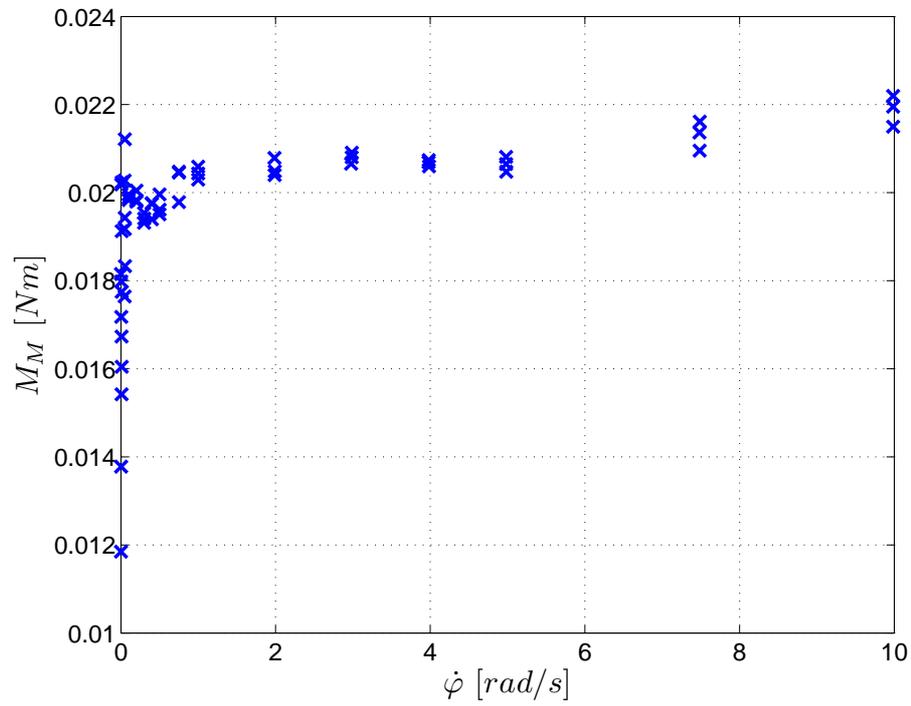


Figure 4.11: Example of data points resulting from measurements as described in section 4.2.4 for positive reference velocities.

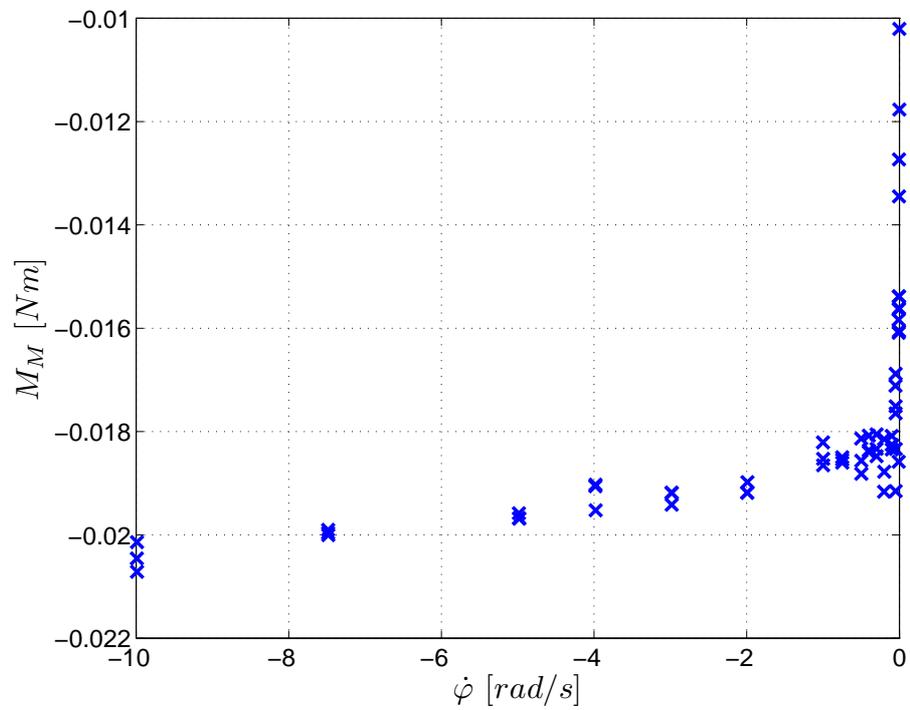


Figure 4.12: Example of data points resulting from measurements as described in section 4.2.4 for negative reference velocities.

Table 4.3: Chosen parameter values

<i>Parameter</i>	<i>Value</i>	<i>Explanation</i>
$F_{c_{pos}}$	$1.4 \cdot 10^{-2} \text{ Nm}$	Average of the values from parameter estimation (see table 4.1).
$F_{s_{pos}}$	$1.9 \cdot 10^{-2} \text{ Nm}$	Average of the values from parameter estimation (see table 4.1).
$F_{c_{neg}}$	$1.2 \cdot 10^{-2} \text{ Nm}$	Average of the values from parameter estimation (see table 4.1).
$F_{s_{neg}}$	$1.7 \cdot 10^{-2} \text{ Nm}$	Average of the values from parameter estimation (see table 4.1).
$F_{v_{pos}}$	$2.3 \cdot 10^{-4} \text{ Nm/(m/s)}$	As determined in section 4.2.2 (see table 4.2.2).
$F_{s_{neg}}$	$2.2 \cdot 10^{-4} \text{ Nm/(m/s)}$	As determined in section 4.2.2 (see table 4.2.2).
v_s	0.04 m/s	Tuned by hand (see also chapter 6.1.3).
σ_0	$3.4 \cdot 10^2 \text{ Nm/m}$	Value from section 4.2.3. See also chapter 6.1.4.
σ_1	1 Nm/(m/s)	Tuned by hand (see also chapter 6.1.5).
v_d	0.006 m/s	Tuned by hand (see also chapter 6.1.5).

Note that these parameters result in a violation of the passivity condition for the LuGre model as derived by Barabanov and Ortega [5] (see equation (1.5)) for small velocities.

4.3 Origins of Friction and Influence on Parameter Estimation

The friction of the pendulum seems to depend on the position φ of the motor arm. This is due to inaccuracies in the elements causing the friction. For example a major part of the friction is caused by the slip rings that transmit the measurements of the pendulum angle θ to the base of the pendulum (see figure 4.13). The friction reduces significantly when the cantilevers resting on the slip rings are lifted. When examining the slip rings more closely the surface seems to be rather rough and pitted. Further the rings are dirty due to dust resulting from the wear between slip rings and cantilever. Thus these rings cannot be kept in a state where the friction parameters are constant in φ and time, since the macroscopic variations in the surface properties over time and space cause the friction parameters to change.

This illustrates the problems arising when trying to identify the parameters of the LuGre model, since some parameters are hardly - if at all - measurable and in addition dependent on time, wear, position, temperature and other environmental factors.

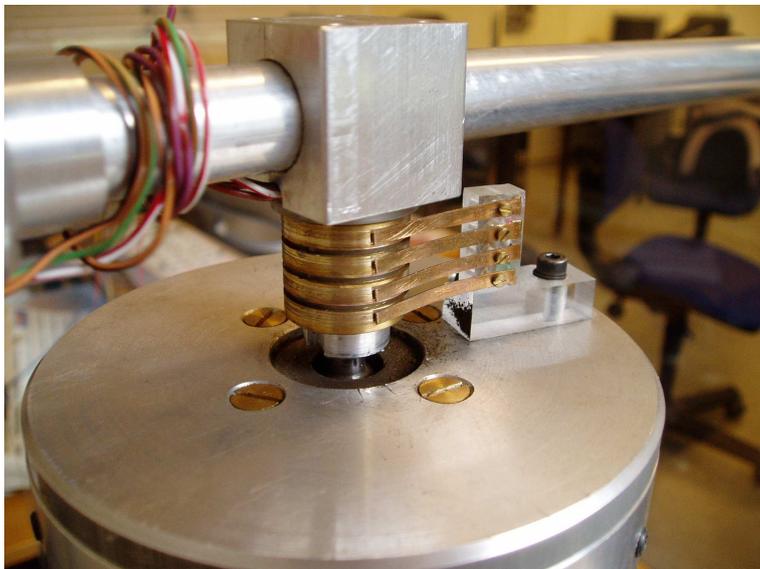


Figure 4.13: Slip rings for the transmission of the measurements of θ .

Chapter 5

Simulation of Friction Compensation

This chapter intends to document the observations concerning the friction compensation that were made while running simulations in Matlab Simulink.

When running simulations with friction compensation a friction model for the plant has to be chosen. Therefore it is not possible to compare different schemes for friction compensation since the model that is also used in the plant for the simulation of the friction effects will outperform other models for friction compensation. However simulations can be used to explore problems that can occur with the tested friction models and to evaluate the theoretical performance of the friction compensation.

5.1 Friction Compensation with the LuGre Model

5.1.1 Simulation Setup

For the following examination the friction of the plant was assumed to have a structure of the LuGre friction model as in equations (1.1)-(1.4). The friction model in the plant is a continuous LuGre model and is solved with variable step size.

The choice of the solver has critical influence on the quality of the solution, since numerical problems arise with some of the built-in Simulink solvers. Due to the fast friction dynamics the use of solvers for stiff systems is reasonable. The best results concerning numerical accuracy and execution speed are achieved with the Simulink solver “ode23s (Stiff/Mod. Rosenbrock)” and therefore this solver was chosen. For simulations it is advantageous to specify the minimum step size and tolerance manually to prevent the solver from getting stuck at zero velocity crossings.

For friction compensation the discretization as in equations (3.16) and (3.17) was used on the assumption of perfect knowledge of the friction parameters.

The used simulation setup thus forms a hybrid system with the model of the plant and the friction model of the plant being solved with variable step size, while the control signal and friction compensation being computed at discrete time with a sampling time of $0.1 \cdot 10^{-3} \text{ s}$.

For the simulation an initial control error of 0.1 rad for θ is used in order to excite limit cycles and to show transient behavior.

For the experiments where velocity reconstructions from the high-gain observer (see chapter 3.1.3) are used the gains of the observer have to be tuned in a way that the delay of the state estimates is sufficiently small to ensure that the friction compensation can work.

As mentioned before the LuGre model exhibits strong elements of spring like behavior in the presliding regime. The period time of a linear spring with the stiffness of the LuGre model and the inertia of the pendulum including pendulum rod in the upright position is:

$$T_{spring,lin} = \frac{2\pi}{\omega} = 2\pi \sqrt{\frac{J_{pmot}}{\sigma_0}} = o(10^{-2} \text{ s})$$

where:

- $J_{pmot} = o(10^{-3}) \text{ kg m}^2$: Moment of inertia of the arm assembly and the pendulum in the upright position with respect to the axis of rotation of the arm.
- $\sigma_0 = o(10^2) \text{ Nm/m}$: Stiffness of the LuGre model.

Justified by the spring like behavior of the LuGre model in the stiction regime this period time can be used to obtain an estimation of an acceptable order of magnitude of the observer delays. In simulation and experiments good results were obtained when choosing $\epsilon_1 = \epsilon_2 = 1 \cdot 10^{-2}$ and pole location -1 for the polynomials for the observer design (see chapter 3.1.3). The resulting delays are two orders of magnitude smaller than $T_{spring,lin}$ and therefore also for experiments with increased stiffness σ_0 sufficiently small.

These design parameter for the observer were tuned manually in experiments with the real plant. Slower observers yield worse control performance in experiments, while faster observers propagate too much of the measurement noise into the observed states and therefore also reduce the control performance. No improvement could be obtained by variation of the location of the poles.

To test the convergence and the influence of the peaking behavior of the observer (see Khalil [10] chapter 14.5) the initial values of the observer are chosen resulting in an initial observation error of -0.1 rad for θ .

For a complete listing of the used parameters please refer to appendix C.2.

5.1.2 Compensation Using LuGre Friction Model

State Feedback

Figure 5.1 shows the resulting limit cycle for constant zero reference when state feedback is used in the controller without friction compensation. Figure 5.2 shows the same setup, but with friction estimate added to the control signal. As expected the limit cycle due to friction is eliminated when the LuGre friction estimate is added to the control signal. The remaining control errors lie in the order of magnitude of the tolerance of the simulation. Also for other reference signals the performance of the control system controlling a plant without friction can be recovered.

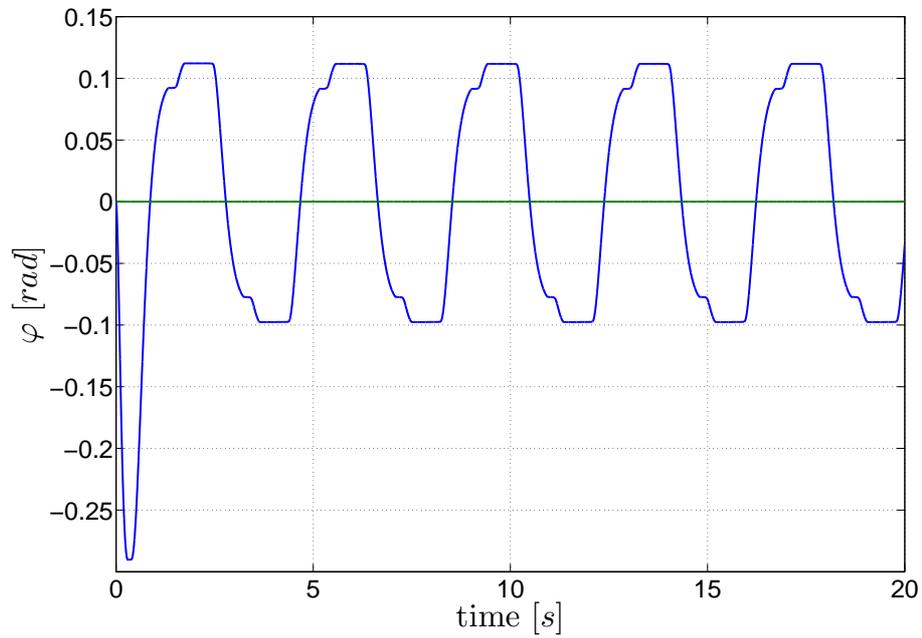


Figure 5.1: Simulated behavior of the arm angle φ without friction compensation for constant zero reference and state feedback.

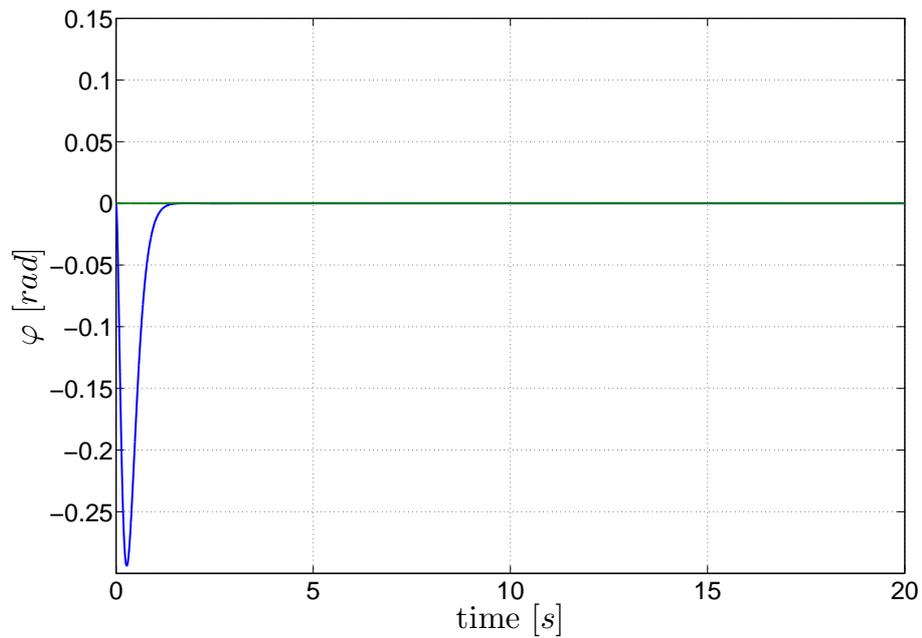


Figure 5.2: Simulated behavior of the arm angle φ with LuGre friction compensation for constant zero reference and state feedback.

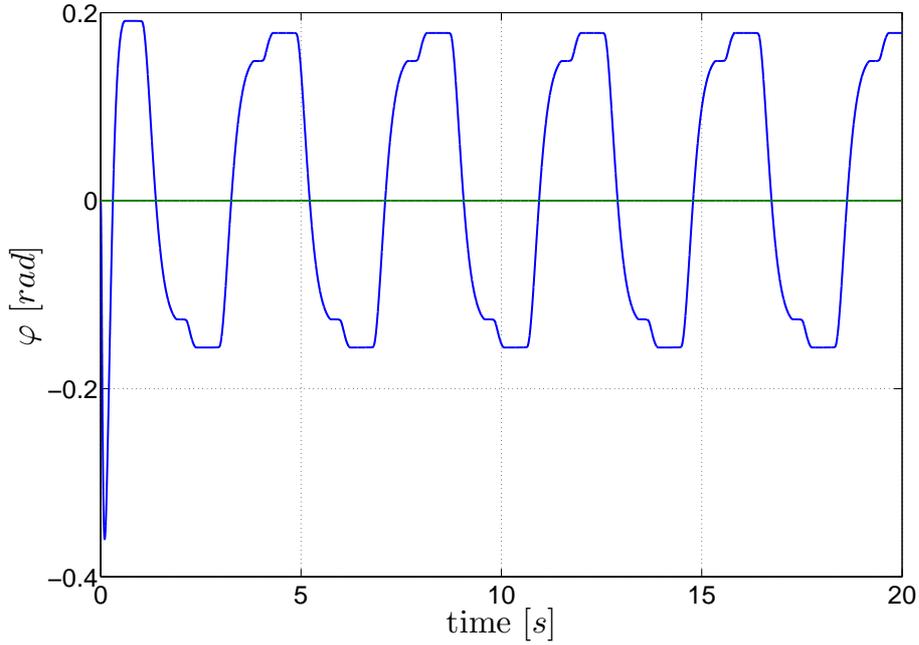


Figure 5.3: Simulated behavior of the arm angle φ without friction compensation for constant zero reference and output feedback.

Observer Feedback

To assess the influence of velocity estimation on the performance of the friction compensation the same simulations as in section 5.1.2 were run while using velocity reconstructions via high-gain observer.

Figures 5.3 and 5.4 are the to figures 5.1 and 5.2 corresponding figures, with state estimates from the high-gain observer. The initial deviation is bigger compared to the state feedback case mostly due to the initial state observation error.

The use of the observer has mostly deteriorating influence on the performance of the controller, since the amplitude of the limit cycle without friction compensation increased due to the use of the velocity estimates. The performance of the friction compensation is not significantly affected because of the use of the observer (compare figures 5.2 and 5.4).

Again the same statements apply for the use of other, not constant reference signals.

5.1.3 Closed-Loop LuGre Friction Observers

The state equation of the LuGre friction model can be augmented by a friction observer gain K :

$$\frac{dz}{dt} = \dot{\varphi} - \frac{|\dot{\varphi}|}{g(\dot{\varphi})}z + K \quad (5.1)$$

Thus the friction compensation using the LuGre model as presented above can be interpreted as an open-loop friction observer.

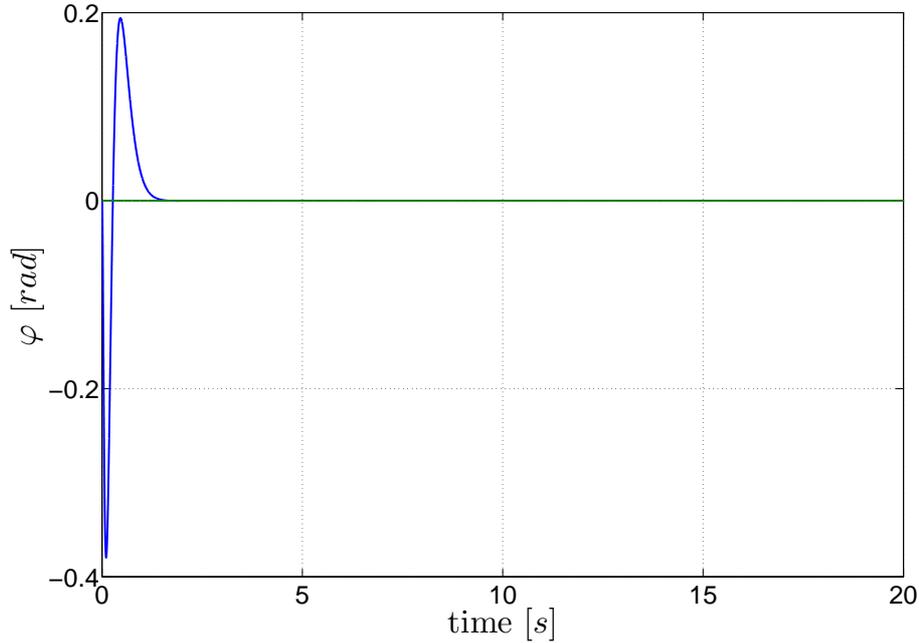


Figure 5.4: Simulated behavior of the arm angle φ with LuGre friction compensation for constant zero reference and output feedback.

Closed-Loop Friction Observer based on Shiriaev [4]

In Shiriaev [4] the following friction observer gain K is proposed:

$$K = -\frac{\sigma_0}{\rho} \left(1 + \sigma_1 \frac{|\dot{\varphi}|}{g(\dot{\varphi})} \right) y \quad (5.2)$$

with:

- ρ : Design constant of the friction observer.
- y : Output of the control plant. In the case of the Furuta pendulum $y = \varphi - \varphi_{ref}$ is the simplest choice.

For passive systems, on the assumption of perfect knowledge of the friction parameters and an assumed structure of the friction in the physical system according to the LuGre model (equations (1.1)-(1.4)), it is shown in Shiriaev [4] that the estimated friction state converges to the internal friction state of the control plant when the velocity $\dot{\varphi}$ is non-zero at at least one point in time, when K is chosen as in equation 5.2.

However the proof presented in Shiriaev [4] is not valid here, since the choice of $y = \varphi - \varphi_{ref}$ violates the assumption of zero-state detectability made in the paper. This problem arises due to the under-actuated nature of the Furuta pendulum. The plant has only one control input that is used to control the two minimal coordinates (φ and θ) that are needed to describe the kinematics of the pendulum.

This did not pose a problem in the example in Shiriaev [4] where the task was the stabilization of the limit cycle for a inertia wheel pendulum, since the interest lay only in the control of the pendulum angle. Therefore it was sufficient to show that the velocity of the inertia wheel is bounded.

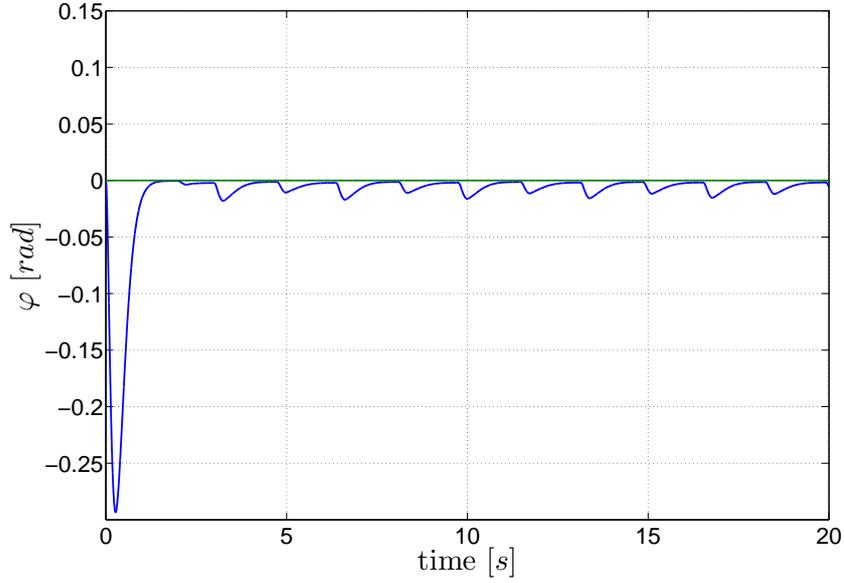


Figure 5.5: Simulated behavior of the Furuta pendulum and control signal with applied friction observer 1 for constant zero reference and output feedback.

For the Furuta pendulum the situation is different, because the task is to control the angle of the pendulum as well as the angle of the arm to a desired reference.

In the evaluation of the friction compensation the term “friction observer 1” will be used to refer to the friction observer gain given by equation (5.2). The parameter ρ was tuned by hand so the influence of the friction observer on the control performance becomes obvious.

Figure 5.5 shows the behavior of arm angle φ when LuGre friction observer 1 is used. The use of the observer worsens the situation. This behavior occurs because the output y used in the observer is not zero-state-detectable and is further discussed in chapter 6.2.2.

Closed-Loop Friction Observer based on Freidovich [2]

Freidovich [2] proposes an observer gain K as follows:

$$K = -\frac{\sigma_0}{\rho} \left(1 + \sigma_1 \frac{|\dot{\hat{\varphi}}|}{g(\dot{\hat{\varphi}})} \right) ((\varphi - \varphi_{ref}) + \rho_2(\dot{\varphi} - \dot{\varphi}_{ref})) \quad (5.3)$$

with:

- ρ, ρ_2 : Design constants of friction observer.
- $\dot{\hat{\varphi}}$: Estimate of the velocity $\dot{\varphi}$ of the arm.

The proof of convergence presented in Freidovich [2] is based on a particular controller design distinct from the LQ-controller used in this thesis and therefore not applicable in the given situation.

Experiments with the observer gain as in equation (5.3) will be made since the structure is similar to the approach of equation (5.2).

For the evaluation the term “friction observer 2” will be used to refer to the friction

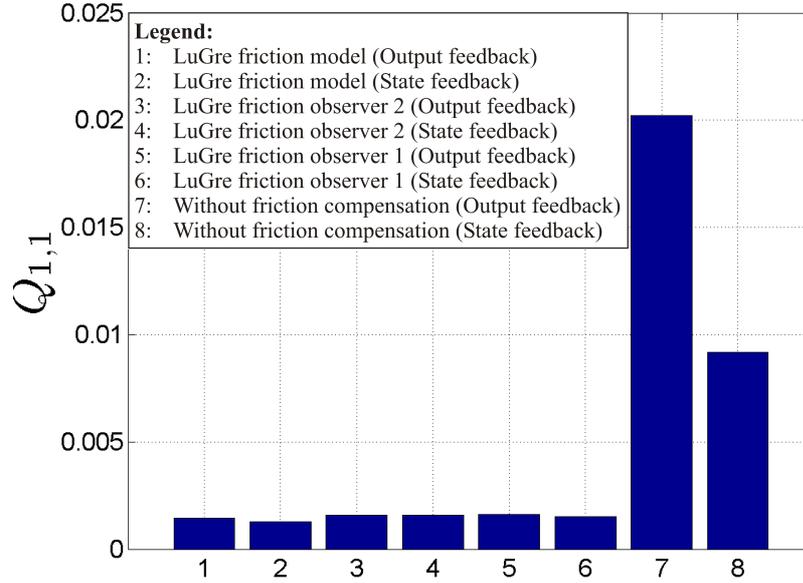


Figure 5.6: $Q_{1,1}$ -component of the error measure as defined in chapter 3.2.3 from simulation for constant zero reference using state feedback.

observer gain as in equation (5.3). The design parameters ρ and ρ_2 were tuned by hand.

Qualitatively the same behavior as in figure 5.5 can be observed with friction observer 2.

5.1.4 Quantitative Evaluation

Figure 5.6 shows the $Q_{1,1}$ -component of the performance index as defined in chapter 3.2.3. It can be seen that the error measure is significantly reduced through friction compensation.

The remaining values for bar 1 and 2 are mostly due the initial error of 0.1 rad for the pendulum angle θ .

The performance using state feedback is, as expected, better than using the observer. This is especially evident without friction compensation, since friction is not considered in the model of the plant implemented in the observer. Therefore the error introduced through observation in that case is mostly due to the mismatch between the model of the real plant comprising friction and the model in the observer without friction.

Only in case of friction observer 2 the control system using output feedback slightly surpasses the control system with state feedback. This is likely a result of the implementation of the friction observer being actually designed for a different kind of control system. No particular reason could be found for this phenomenon.

As expected considering figure 5.5 and the statements made above the performance indices using the closed-loop friction observers are higher than with open-loop friction compensation. The reasons for this is further discussed in the evaluation of the experiments in chapter 6.2.2.

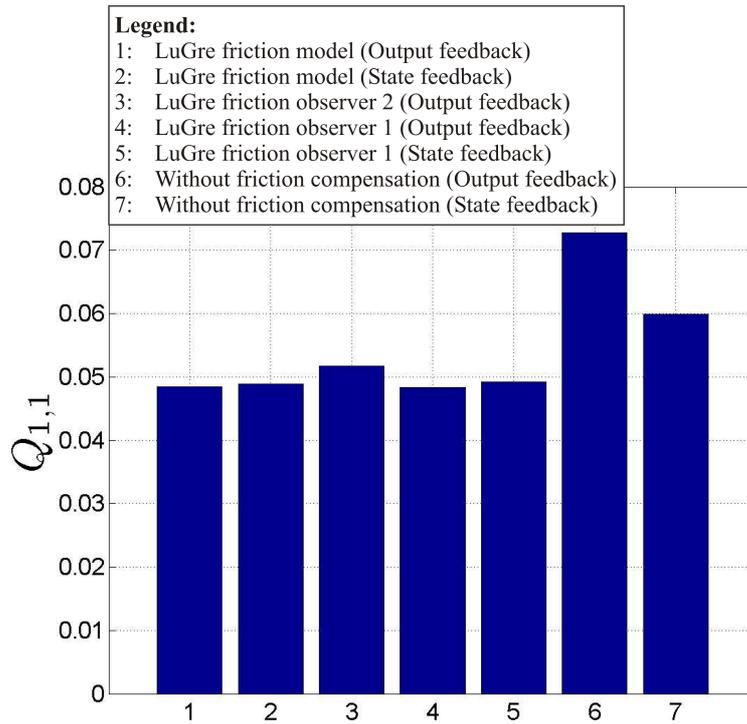


Figure 5.7: $Q_{1,1}$ -component of the error measure as defined in chapter 3.2.3 from simulation for step reference (see chapter 3.2) using state feedback.

Figures 5.7 and 5.8 are the to figure 5.6 corresponding plots for the step and the chirp reference signal.

The same statements as made above for the constant zero reference apply.

In these plots the performance indices for all tested friction compensation schemes are bigger due to the control errors that arise because the signals are not traceable. In figures 5.7 and 5.8 the bar for friction observer 2 with state feedback is missing since this setup with the parameters tuned in experiments resulted in instability in simulations when state feedback was used. No problems concerning stability arouse with all of the implemented compensator in experiments and when output feedback with high-gain observer was used in simulations.

Note that the performance with all tested friction compensators surpasses the performance achieved without friction compensation.

5.2 Influence of Velocity Dependent Damping

Concluding this chapter an interesting property of the LuGre model concerning the factor σ_1 is mentioned. The influence of the “damping” factor σ_1 is discussed further in chapter 6.1.5.

A friction model should be passive since it can be intuitively expected that friction dissipates energy. As proven on p.56f in Olsson [1] the state-equation of the LuGre

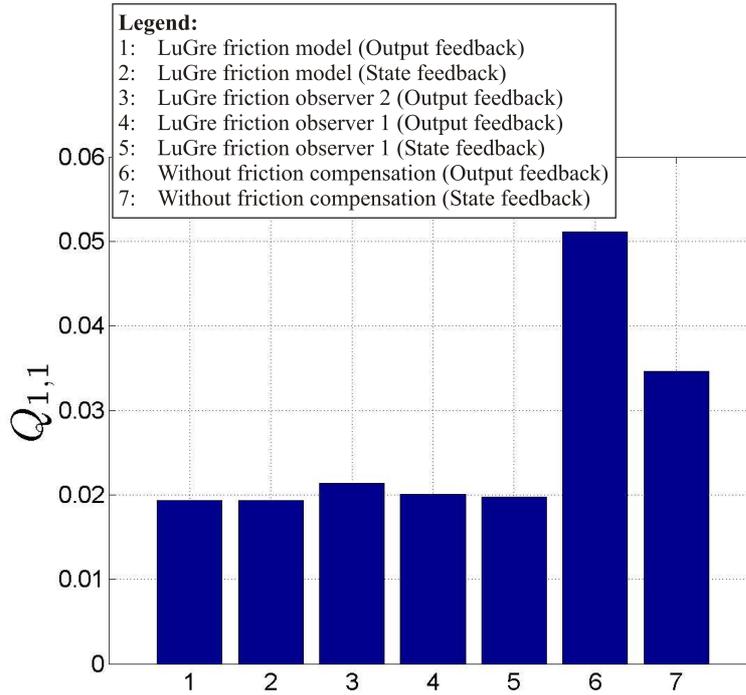


Figure 5.8: $Q_{1,1}$ -component of the error measure as defined in chapter 3.2.3 from simulation for chirp reference (see chapter 3.2) using state feedback.

model is dissipative if the damping $\sigma_1(v)$ fulfills the condition:

$$0 \leq \sigma_1(v) \leq \frac{4\sigma_0 g(v)}{|v|}.$$

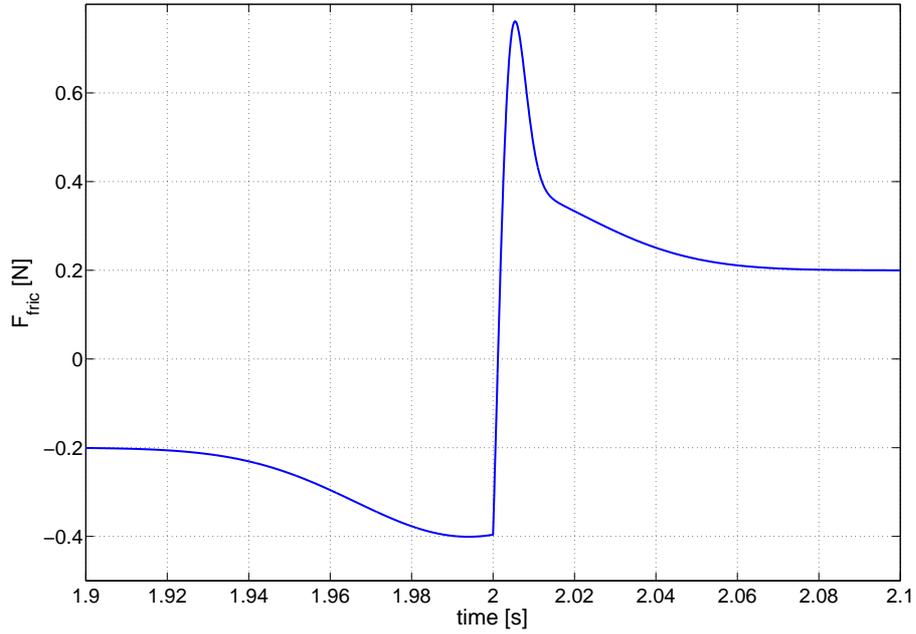
In order to be able to fulfill this condition for arbitrary velocities v a velocity variable damping $\sigma_1(v)$ was introduced. Olsson [1] suggests $\sigma_1(v) = \sigma_1 e^{-(v/v_d)^2}$. Another reason for the introduction of the velocity dependent damping as mentioned above is that, using constant σ_1 , over- and undershoots of the LuGre friction force can occur e.g. after break away and at velocity reversals that can be reduced by tuning the constant v_d . The cause of this over- and undershoots is the rapid change of the friction state z during break away and velocity reversals. Velocity dependent damping can elude this problem since the influence of the derivative $\frac{dz}{dt}$ on the friction force can be influenced by tuning the the parameter v_d .

However the introduction of a velocity dependent damping $\sigma_1(v)$ according to equation (1.4) as suggested in Olsson [1] can also have a deteriorating effect on the quality of the friction estimate. Figures 5.9, 5.10, 5.11 and 5.12 show the friction force that is produced by the LuGre model with variable damping according to equations (1.1) to (1.4) with the parameters shown in table 5.1 when the velocity input to the LuGre model is ramped up from $v = -0.5m/s$ with a slope of $a = 0.25m/s^2$ for different values of v_d .

When the parameter v_d is tuned that the friction force does not overshoot the desired maximum value of the friction force given by $F_s = 0.4N$ the friction force shows an undesired behavior, since it does not decline monotonous after the peak value is reached. This occurs because the contribution of the damping term $\sigma_1(v) \frac{dz}{dt}$

Table 5.1: Parameters of the LuGre model used to create figures 5.9, 5.10, 5.11 and 5.12.

<i>Parameter</i>	<i>Value</i>	<i>Unit</i>
σ_0	$1 \cdot 10^5$	Nm/m
σ_1	$2\sqrt{\sigma_0} \approx 632.46$	$Nm/(m/s)$
F_v	0	Ns/m
F_c	0.2	N
F_s	0.4	N
v_s	0.01	m/s
v_d	0.0015 to 2000	m/s

Figure 5.9: Friction force resulting from LuGre model with $v_d = 2000$.

to the friction force declines faster due to the fast decline of $\sigma_1(v)$ than the static part $\sigma_0 z$ increases to compensate for the decline in the contribution of the damping term. This becomes obvious by comparing figure 5.13, which shows the course of the static and damping term for $v_d = 2000$, with figure 5.14, which is the corresponding figure for $v_d = 0.15 \cdot v_s$.

The behavior described above can be influenced by changing equation (1.4), as already suggested in Olsson [1] to:

$$\sigma_1(v) = \sigma_1 e^{-(|v/v_d|)^{\delta_d}} \quad (5.4)$$

and tuning the parameter δ_d . But since the friction model is dynamic it remains questionable if the observed behavior can be eliminated for arbitrary slopes of the input velocity.

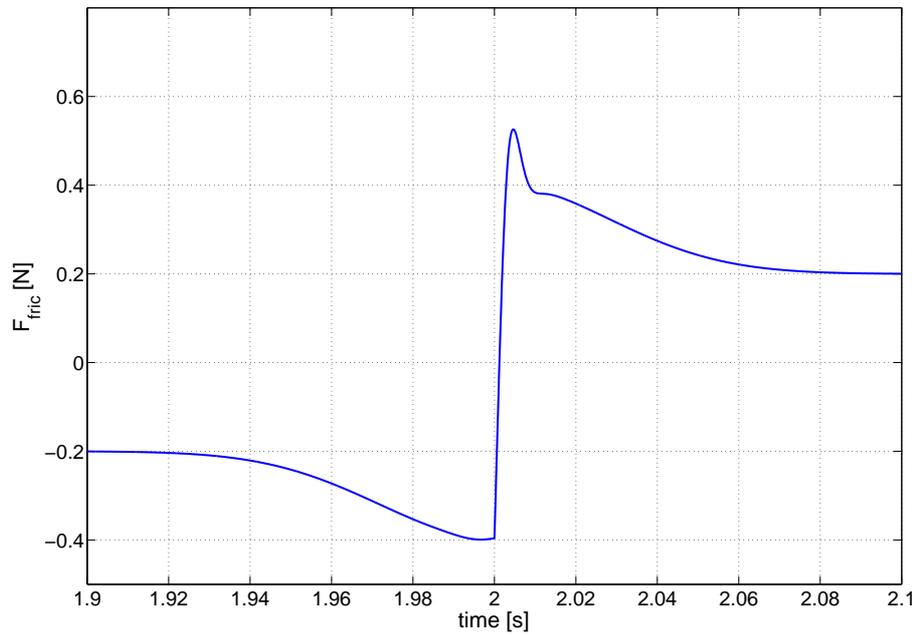


Figure 5.10: Friction force resulting from LuGre model with $v_d = 0.2 \cdot v_s$.

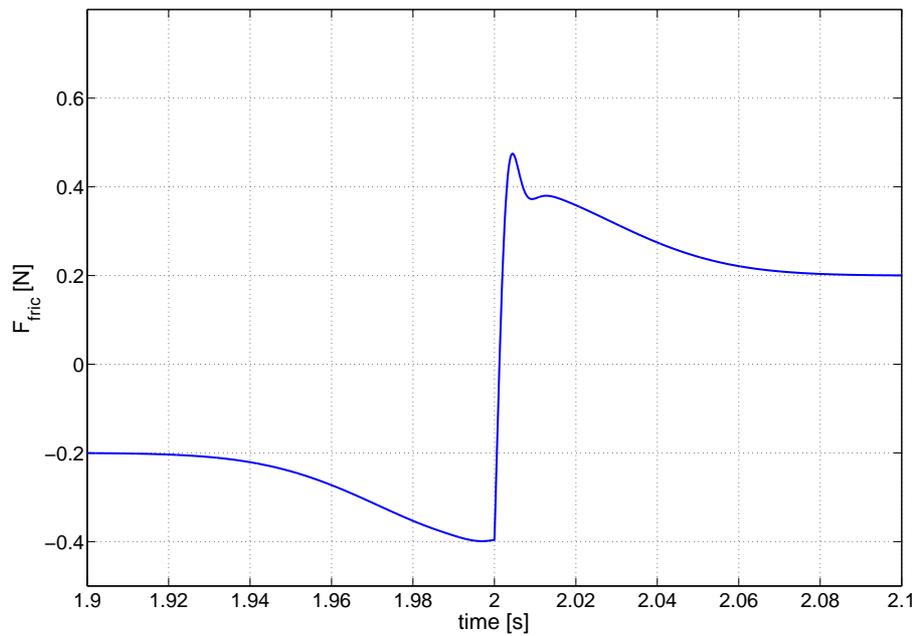
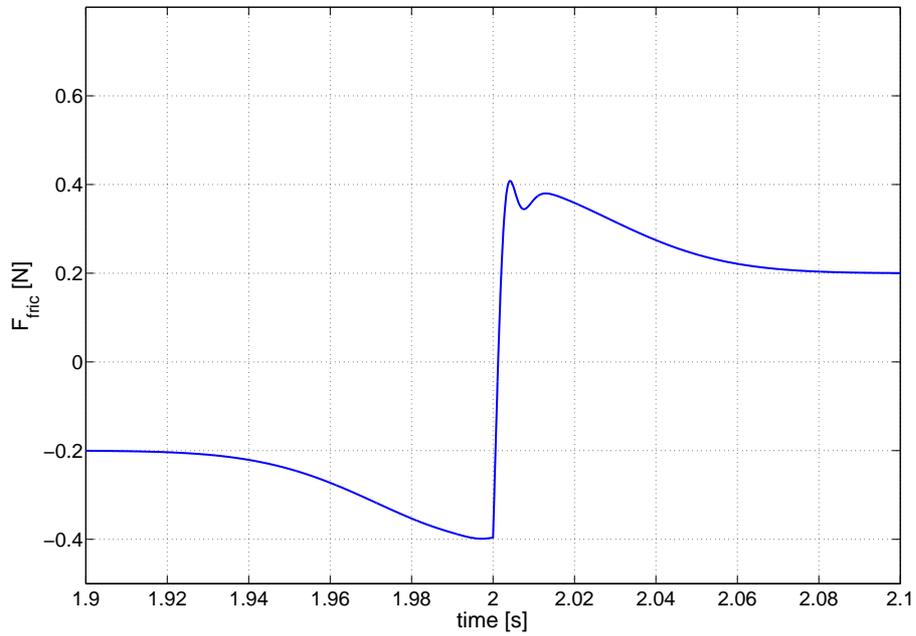
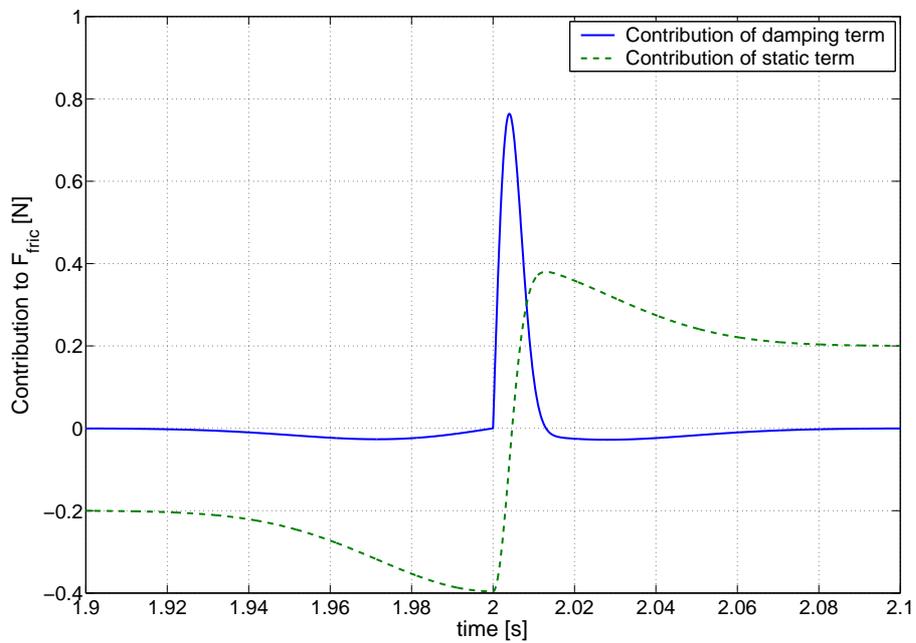


Figure 5.11: Friction force resulting from LuGre model with $v_d = 0.175 \cdot v_s$.

Figure 5.12: Friction force resulting from LuGre model with $v_d = 0.15 \cdot v_s$.Figure 5.13: Contribution of static term ($\sigma_0 z$) and damping term ($\sigma_1(v) \frac{dz}{dt}$) to friction force for $v_d = 2000$.

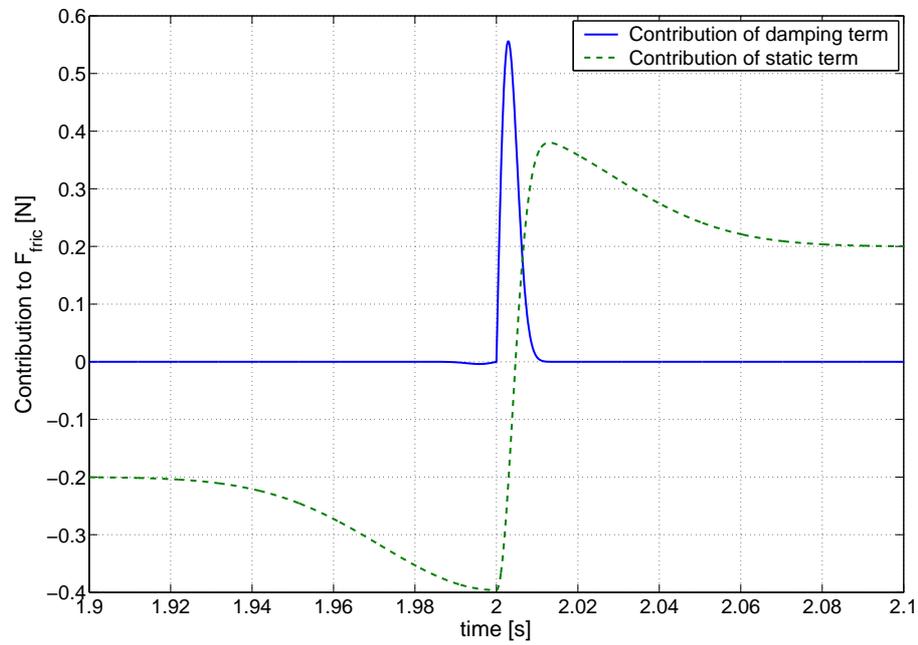


Figure 5.14: Contribution of static term ($\sigma_0 z$) and damping term ($\sigma_1(v) \frac{dz}{dt}$) to friction force for $v_d = 0.15 \cdot v_s$.

Chapter 6

Experiments with Friction Compensation

The following chapter documents the results obtained while experimenting with friction compensation with the Furuta pendulum. For the implementation of the friction compensation the model of the Furuta pendulum is removed from the Simulink model used for the simulations and replaced by analog input and output blocks from the dSPACE library in Simulink.

6.1 Influence of LuGre Friction Parameters on the Friction Compensation

This section documents the influence of the different parameters of the LuGre model on the performance of the friction compensation. The performance is assessed with hardware in the loop. For an examination of the influence of the parameters of the LuGre model in simulation the reader may refer to Olsson [1].

The experiments were carried out with the parameter settings as described in table C.2 in appendix C.2, unless other settings are indicated explicitly. For friction compensation a LuGre model as described by equations (3.12) to (3.15), discretized according to Freidovich [2] (see equations (3.16) and (3.17)), was used.

6.1.1 Influence of the Friction Forces

The friction forces F_c and F_s are the parameters with the biggest influence on the performance of the friction compensation.

Choosing the friction forces too big leads to overcompensation and finally to a situation where the controller loses the capability to stabilize the pendulum. Whereas the performance increase due to friction compensation is smaller if the friction forces are chosen too small.

Figure 6.1 shows the course of the arm position φ for a constant zero reference for three different settings of the friction forces. The first plot shows the behavior of φ when the nominal friction forces from the parameter identification are used (see table 4.3 on page 58). The second and third plots show the corresponding behavior when the friction forces are increased and decreased by 30% respectively, while the fourth plot is the corresponding figure without friction compensation.

The chosen reference is suitable for illustrating the influence of the friction forces since the limit cycle that occurs with constant zero reference causes frequent velocity reversals and therefore the influence of the stiction force F_s is visible. However a potential decrease in robustness can be observed better with bigger control errors and time varying references.

For smaller values of the friction forces the friction compensation works less efficient than for the nominal values, since the additional term of the friction compensation in the control signal does not suffice to compensate the friction effects. Further the frequency of the corresponding limit cycle is reduced.

For an increase of the friction forces the frequency of the limit cycle increases, while its amplitude remains the same or even decreases slightly. A reduction of the amplitude of the limit cycle due to an increase of the friction forces is possible due to two reasons. First the estimated friction forces are mean values for different positions of the arm and thus higher friction parameters can lead to performance improvements for some particular positions of the arm, while, using the same parameters, friction would already be overcompensated for other positions of the arm. Second the rate of increase of the moment used to identify the friction forces causes the state of the LuGre friction model not to reach steady-state. Since the break away forces are rate dependent this can lead to the estimation of friction forces that are lower than the actual values.

However care has to be taken when exploiting possible performance improvements due to higher friction forces than the estimated values, since higher friction forces can lead to overcompensation of friction and can thus reduce the stability margin of the system. Also the strong increase of the frequency for the increased friction force observed in the experiments can be seen as a sign of beginning overcompensation of the friction. Considering the variation of the friction forces due to the position of the arm and the operation conditions the used conservative approach seems appropriate to the author.

6.1.2 Influence of the Viscous Friction Coefficients

The viscous friction coefficient F_v influences the friction estimate only for nonzero velocities. Therefore the influence was assessed using non-constant reference signals, namely a sinusoidal signal.

An influence on the performance of the friction compensation when the viscous friction parameters deviate from their nominal values is not noticeable.

The main reason for this is that the viscous friction parameters determined for the Furuta pendulum are small compared to the friction forces F_c and F_s (see chapter 4.2.2).

Figure 6.2 shows the behavior of φ for different values of the viscous friction coefficients with a sinusoidal reference with amplitude 0.4 rad and frequency 0.2 Hz and a corresponding reference for the the speed of the arm, while the references for the pendulum remain zero ($\theta_{ref} = \dot{\theta}_{ref} = 0$). No significant differences are noticeable. The deviation from the desired reference occur mostly because zero references are used for the states of the pendulum and thus the used reference is not traceable without error.

Effects of overcompensation of the viscous friction are only visible if the viscous friction coefficients are increased by two orders of magnitude or more.

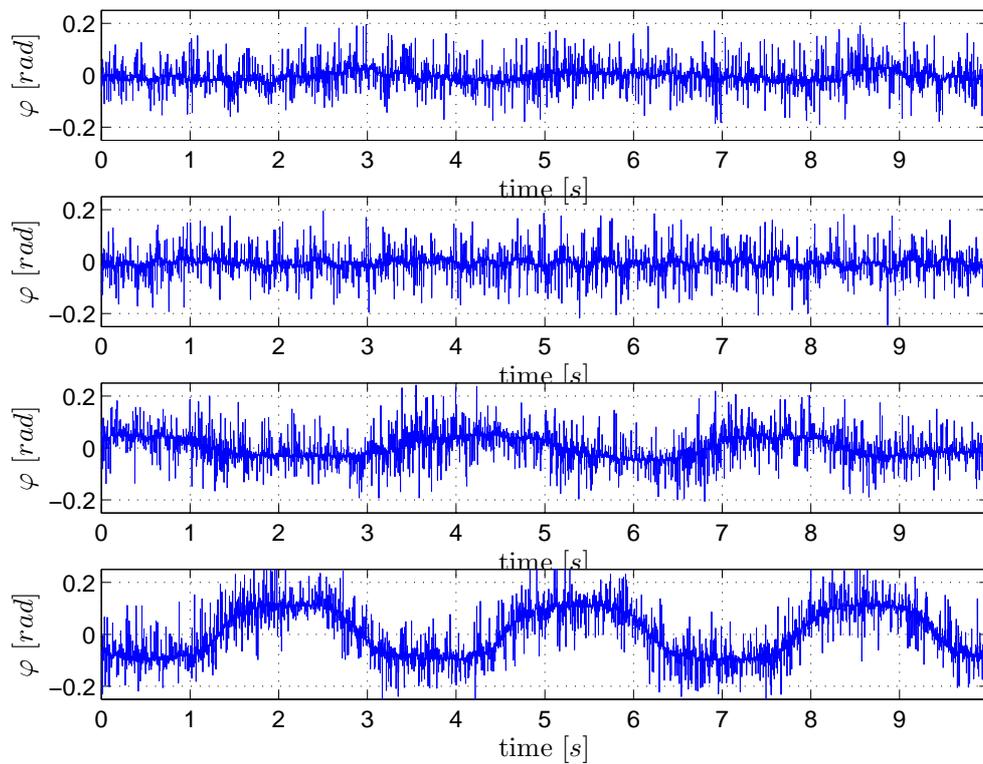


Figure 6.1: Behavior of the arm position φ with friction compensation with nominal parameter values (first plot), with 30% increased (second plot) and 30% decreased (third plot) parameter values. The fourth plot shows the behavior without friction compensation.

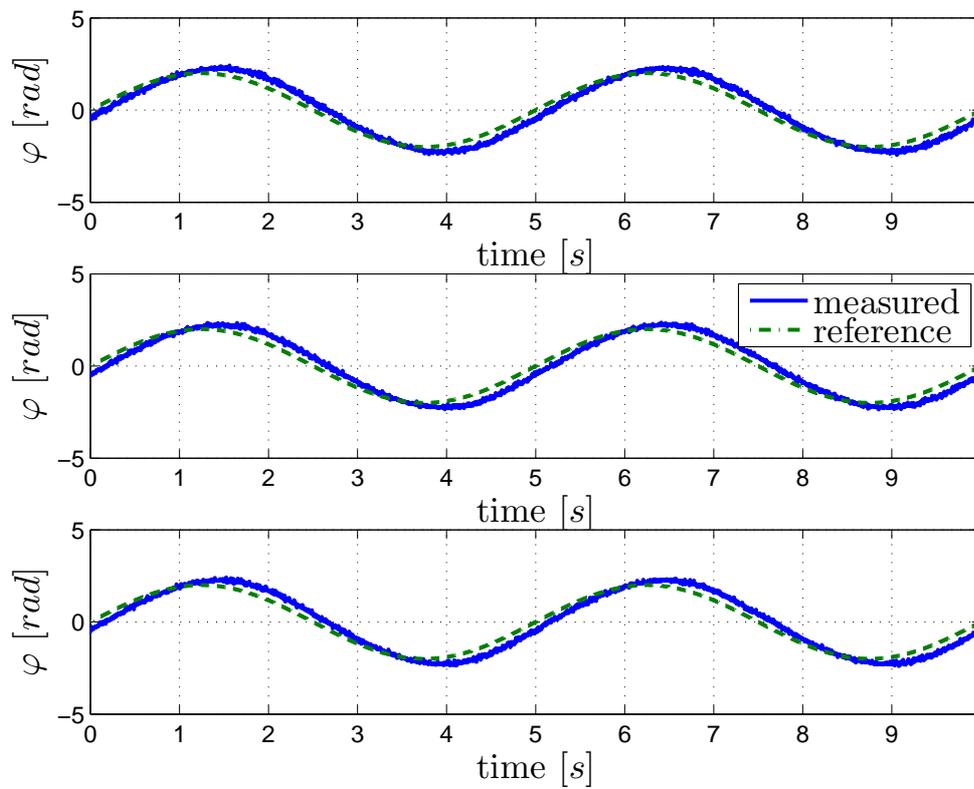


Figure 6.2: Behavior of the arm position φ following a sinusoidal reference with amplitude 2 rad and frequency 0.2 Hz for nominal values for F_v (first plot), 100% increased values for F_v (second plot) and without viscous friction (third plot).

6.1.3 Influence of the Stribeck Velocity v_s

For small Stribeck velocities ($v_s < o(10^{-2} \text{ m/s})$) the Stribeck effect is hardly visible in the friction estimation. This is due to the limited velocity resolution of the encoder and the high noise in the measurements of the arm angle φ and velocity $\dot{\varphi}$. The quantization of the velocity reconstructions for $\dot{\varphi}$ from the analog filter of the device due to the encoder is of $o(10^{-3} \text{ rad/s})$. Thus considering noise and quantization error a measurement accuracy of $o(10^{-2} \text{ m/s})$ or above seems reasonable. Due to this the behavior of the LuGre model for Stribeck velocities $v_s < 0.01 \text{ m/s}$ resembles the behavior of the Dahl model with additional viscous friction, if the damping σ_1 of the model is chosen small.

Figure 6.3 shows the behavior of the arm position for nominal (top), ten times increased and ten times decreased value of v_s . The influence of the Stribeck velocity on the performance of the friction compensation is small. The compensation reduces the limit cycle slightly better for a ten times increased v_s (this is hardly visible in figure 6.3 due to the high noise level).

However an increase of v_s to an order of magnitude higher than $o(10^{-2} \text{ m/s})$ causes audible noise from the actuator due to the sharper control signal and leads to overcompensation. This becomes obvious since values of v_s bigger than $o(10^{-2} \text{ m/s})$ tend to decrease the robustness of controllers with higher punishment of the control effort in comparison to the used controller. Thus the increase of v_s only works with fast controllers that possess the capability to catch the pendulum after the overcompensation due to the overestimated v_s . In this case the friction compensation can work better than with underestimated v_s , since the overcompensation helps to keep the state error in the states corresponding to the pendulum $(\theta, \dot{\theta})$ small.

This is risky since the overcompensation can reduce the robustness. Further the sharper control signal due to the higher propagation of noise resulting from a higher v_s ¹ causes more wear of the components of the device.

Smaller values for v_s slightly decrease the capability of the control system to suppress the limit cycles. This is because in this case the control signal has less punch to overcome static friction.

6.1.4 Influence of the Stiffness σ_0

The influence of the stiffness σ_0 on the friction compensation is limited. Figure 6.4 shows the resulting behavior of the arm for nominal (top), 10 times higher (middle) and 10 times lower (bottom) σ_0 .

The tracking of the constant zero reference tends to improve when σ_0 is increased. However the use of a higher stiffness σ_0 seems not reasonable, since the nominal value of σ_0 marks the upper limit of stiffnesses that are still measurable with the used sensor equipment.

6.1.5 Influence of the Damping $\sigma_1(\dot{\varphi})$

The damping $\sigma_1(\dot{\varphi})$ has a strong influence on the performance of the friction compensation.

According to Olsson [1], σ_1 was introduced to suppress high frequency oscillations in the system made up of the friction model and the model of the mechanical system.

¹The influence of the value of v_s on the noise propagation can be illustrated considering that when the friction model is at steady state v_s defines the interval around zero velocity in that the noise has to lie to be propagated into the friction estimate.

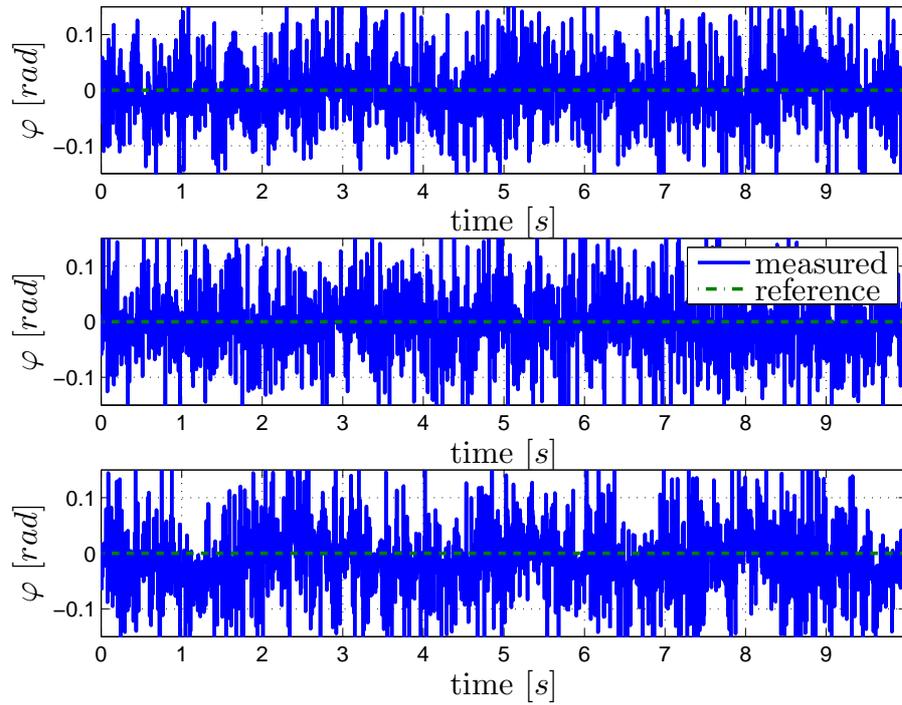


Figure 6.3: Behavior of the arm position φ for constant zero reference for nominal values of v_S (top), 10 times higher value of v_S (middle) and 10 times lower value of v_S (bottom).

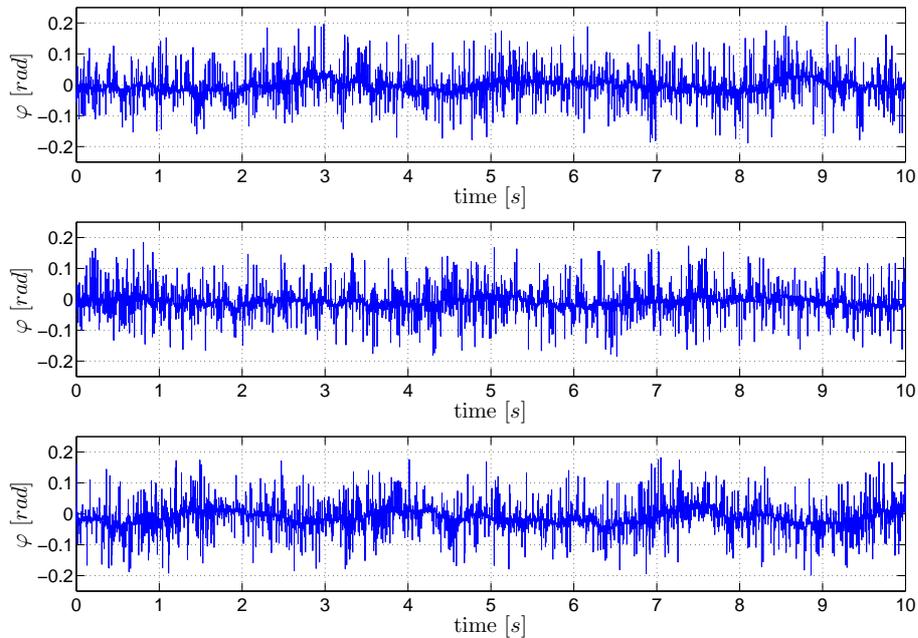


Figure 6.4: Behavior of the arm position φ for constant zero reference for nominal value of σ_0 (top), 10 higher value of σ_0 (middle) and 10 lower value of σ_0 (bottom).

In the experiments with the Furuta pendulum a need for the introduction of σ_1 could not be observed. It is possible to reduce the constant σ_1 to zero without any deteriorating effects.

On the other hand a nonzero σ_1 can have a negative influence on the performance of the friction compensation.

Since σ_1 adds an additional² direct term from the velocity estimate to the friction estimate a nonzero σ_1 increases the level of noise that is propagated from the velocity estimate to the friction estimate.

Further the high derivative of the friction state during velocity reversals leads to overshoots of the friction estimate over the stiction force F_s after velocity reversals when high values for σ_1 are used. This problem and to cause the state equation of the LuGre model to be dissipative for arbitrary high velocities (see Olsson [1] p.56) lead to the introduction of the velocity dependent damping $\sigma_1(v)$. However the overshoots in the friction estimate can even appear when $\sigma_1(v)$ is used. If a constant σ_1 is used the overshoots can reach such high values that the overload protection of the internal current controller of the Furuta pendulum activates the emergency stop of the device.

Even when the control signal is applicable for the plant the overshoots cause peaks in the demanded control signal that increase the wear in the actuators and the control plant and have a negative influence on the control performance.

Figure 6.5 shows the increased noise propagation and tendency for overshoots depending on the value of σ_1 . The uppermost plot shows a friction estimate resulting for the nominal values $\sigma_1 = 1 [Nm/(m/s)]$, $v_d = 0.006 m/s$. The plot in the middle shows a sample of a friction estimate when the σ_1 is 10 times increased, while the plot of the bottom is a corresponding plot when the σ_1 is set to zero.

The influence of the parameter v_d on the friction estimate is similar to the influence of σ_1 . An increase of v_d prolongs the decrease of the “damping” $\sigma_1(v)$ in dependence of velocity and thus causes similar effects as an increase in σ_1 .

Summing up the introduction of the direct term $\sigma_1(v)$ seems not necessary from a practical point of view. If the term is kept for reasons of the model structure it should be kept as small as possible and should be decreasing with velocity.

Further, for small values of σ_1 , the passivity condition derived by Barabanov and Ortega [5] (see equation (1.5)) is fulfilled for a broader range of the remaining LuGre friction parameters.

6.2 Experimental Evaluation of Friction Compensation

6.2.1 Performance Improvement through Friction Compensation

Also in the experiment the limit cycles that can be observed with the Furuta pendulum without friction compensation can be reduced significantly through friction compensation.

Figure 6.6 shows the limit cycle of the arm with the LQ-controller with velocity reconstructions from the analog filter of the device when no friction compensation

²In addition to F_v .

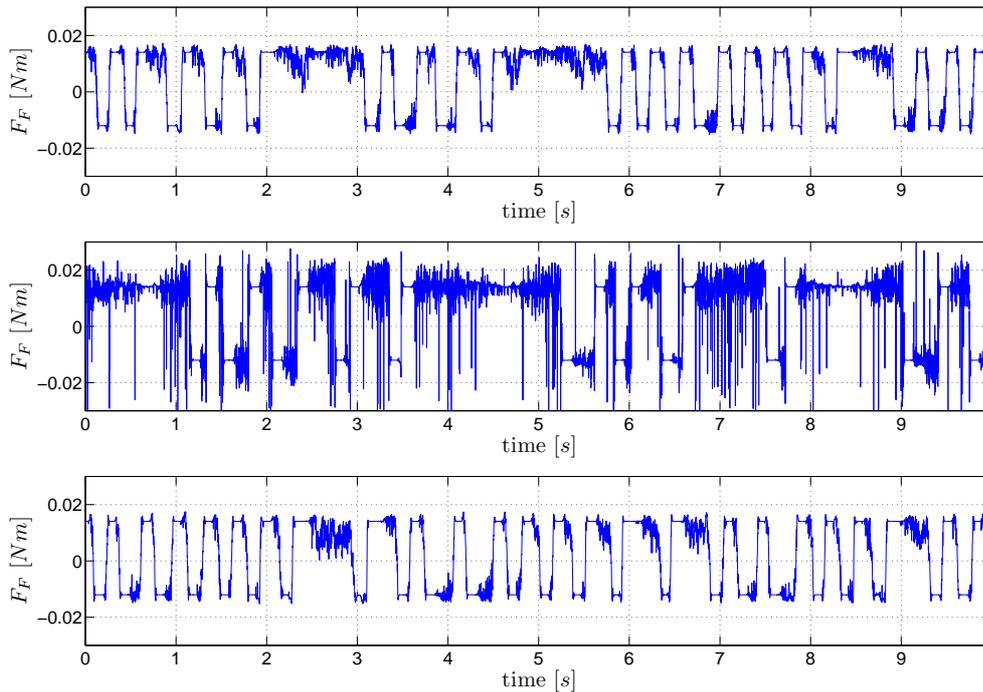


Figure 6.5: LuGre friction estimate for constant zero reference for nominal value of σ_1 (top), 10 higher value of σ_1 (middle) and $\sigma_1 = 0$ (bottom).

is applied. Figure 6.7 is the corresponding plot when the friction estimate obtained by the LuGre model is added to the control signal.

To evaluate the performance improvement due to friction compensation quantitatively, ten measurements are taken with zero reference and five with the other two test cycles defined in chapter 3.2.2. The mean value of the error matrices (see chapter 3.2.3) from these measurements is calculated and used for evaluation. For the evaluation presented below the velocity reconstructions from the analog filter of the Furuta pendulum were used. For a complete listing of the used parameters please refer to appendix C.2.

Figure 6.8 shows a bar plot depicting the mean value of the $Q_{1,1}$ -component of the error matrices of the single measurements computed as in equation (3.20) in chapter 3.2.3 for constant zero reference. Figure 6.9 shows the corresponding sample standard deviations (see equation (3.21) in chapter 3.2.3).

The average least square control error in φ ($Q_{1,1}$ -component) is clearly reduced through all the applied friction compensation schemes. The differences between the different friction compensation schemes are small.

The sample standard deviation of all performance indices is smaller than of order $o(10^{-3})$. Thus the differences in the performance indices between the different friction compensation schemes in figure 6.8 lie just on the borderline of being significant.

The close results are backed by the impression from observing the performance of the friction compensation. None of the tested friction compensation schemes yields an improvement in reducing of the limit in comparison to other compensation schemes that is noticeable while observing the experiment.

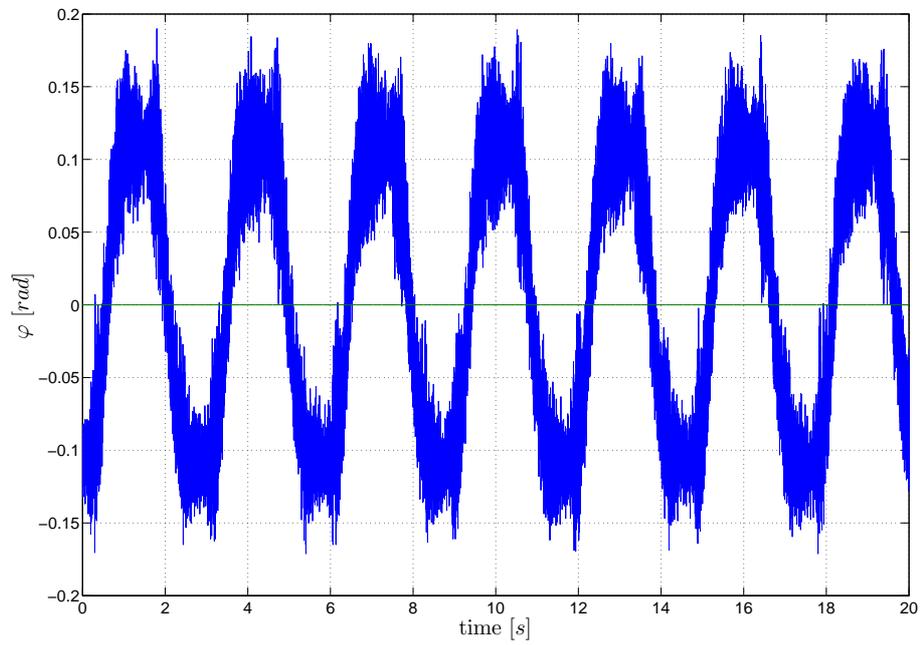


Figure 6.6: Resulting limit cycle of the arm of the pendulum without friction compensation using velocity reconstructions from the analog filter of the device.

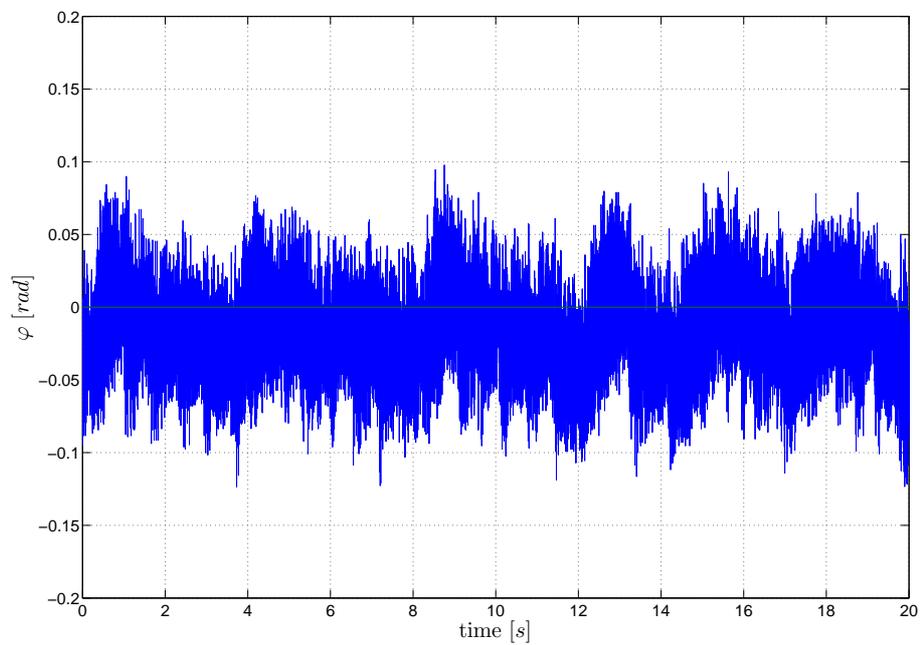


Figure 6.7: Resulting behavior of the arm of the pendulum with friction compensation through the LuGre model using velocity reconstructions from the analog filter of the device.

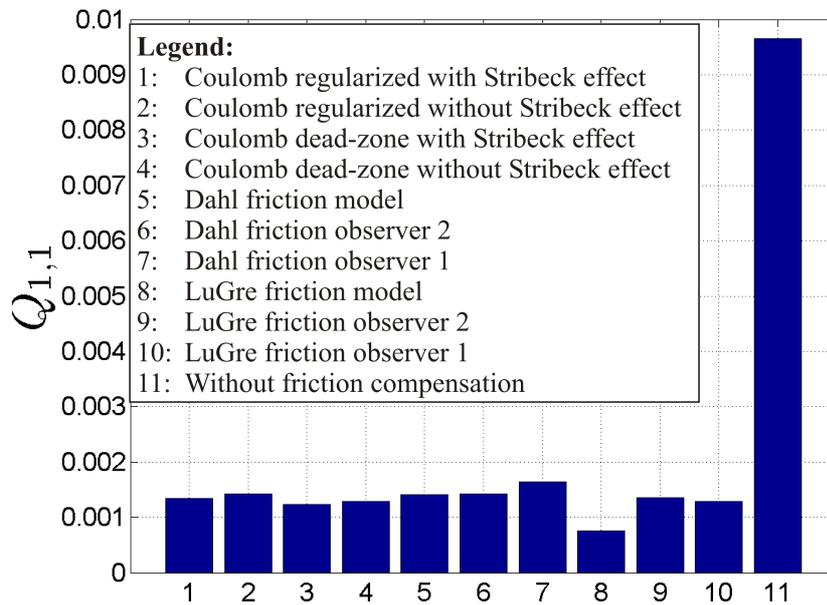


Figure 6.8: Mean value of least squares deviation of φ for zero reference with velocity reconstructions from the pendulum.

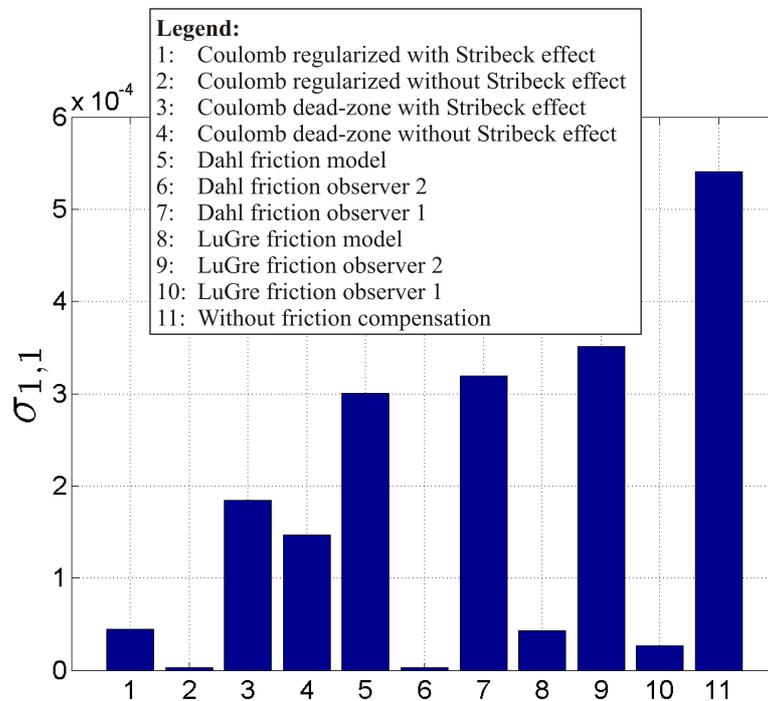


Figure 6.9: Sample standard deviation of least squares deviation of φ for zero reference with velocity reconstructions from the pendulum.

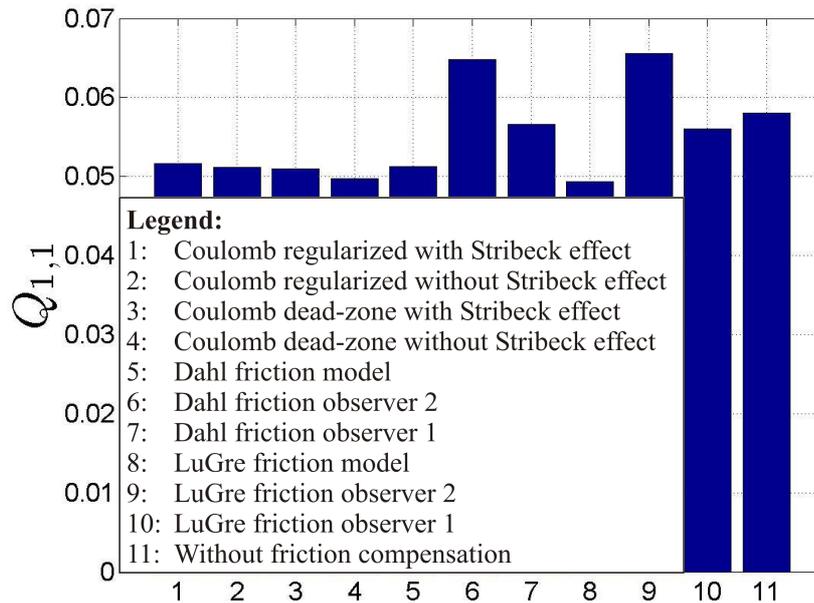


Figure 6.10: Mean value of least squares deviation of φ for step reference with velocity reconstructions from the pendulum.

Figure 6.10 shows the least square error of the angle φ corresponding to figure 6.8, but for the step signal (see chapter 3.2.2) as reference. The corresponding values of the sample standard deviation are depicted in figure 6.11.

The error measures are higher than for zero reference and the differences between the bars with and without friction compensation are less pronounced. This is due to that the major part of the error measure is accumulated during the transient phase after a step in the reference signal occurred.

Again the best results are achieved with the open-loop LuGre model friction compensation, however the differences are small. The closed-loop friction observers produce significantly higher error measures than the remaining friction compensation schemes. In the case of observer 1 the error measures are even higher than the errors that result without friction compensation. The possible reasons for this behavior are addressed in section 6.2.2.

The differences between the open-loop friction compensation schemes are of the same order of magnitude as in for zero reference and thus, as expected, there are no significant differences in the speed of the step responses of the different open-loop friction compensation schemes.

The same statements that were made for the error measures using the step reference apply for the error measures resulting when the chirp signal is used (see figures 6.12 and 6.13). The higher error measures when using the closed-loop friction observers are even more obvious when using this reference signal.

The differences in the performance indices for the open-loop friction compensation schemes are smaller than with the step or constant zero reference. This becomes clear considering that the constant movement of the pendulum with the chirp signal produces less velocity reversals than with the other control signals. Since the friction

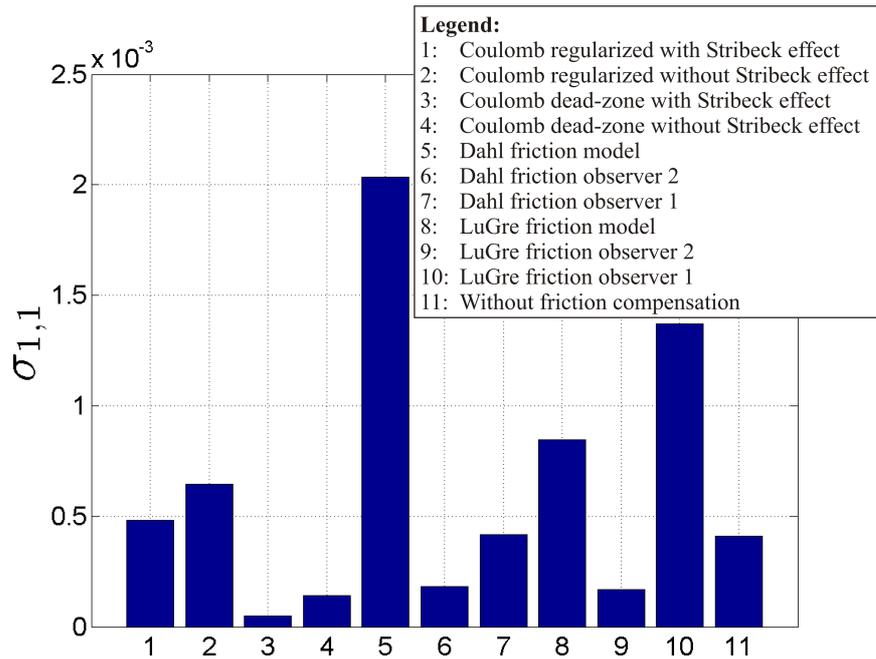


Figure 6.11: Sample standard deviation of least square deviation of φ for step reference with velocity reconstructions from the pendulum.

estimates yielded by the different friction models are almost identical for high relative velocities the resulting error measures are also expected to have similar values.

Examination of other components of the error matrix Q did not yield remarkable results.

The following conclusions are drawn from the analysis presented above:

- For all three reference signals the open-loop LuGre friction compensation yields a small performance improvement in comparison to all other friction compensation schemes.
- The differences between the remaining open-loop friction compensation schemes are small and not significant considering the scattering of the evaluation results.
- The closed-loop friction observation schemes produce worse results when compared to the open-loop LuGre friction compensation, especially for transient reference signals.

6.2.2 Closed-Loop Friction Observers

In figure 6.10 it can be noticed that the closed-loop friction observers produce higher error measures even compared to error measures from experiments without friction compensation. If the transient responses of the friction compensation schemes with and without friction observer are compared the origin of these high error measures becomes obvious.

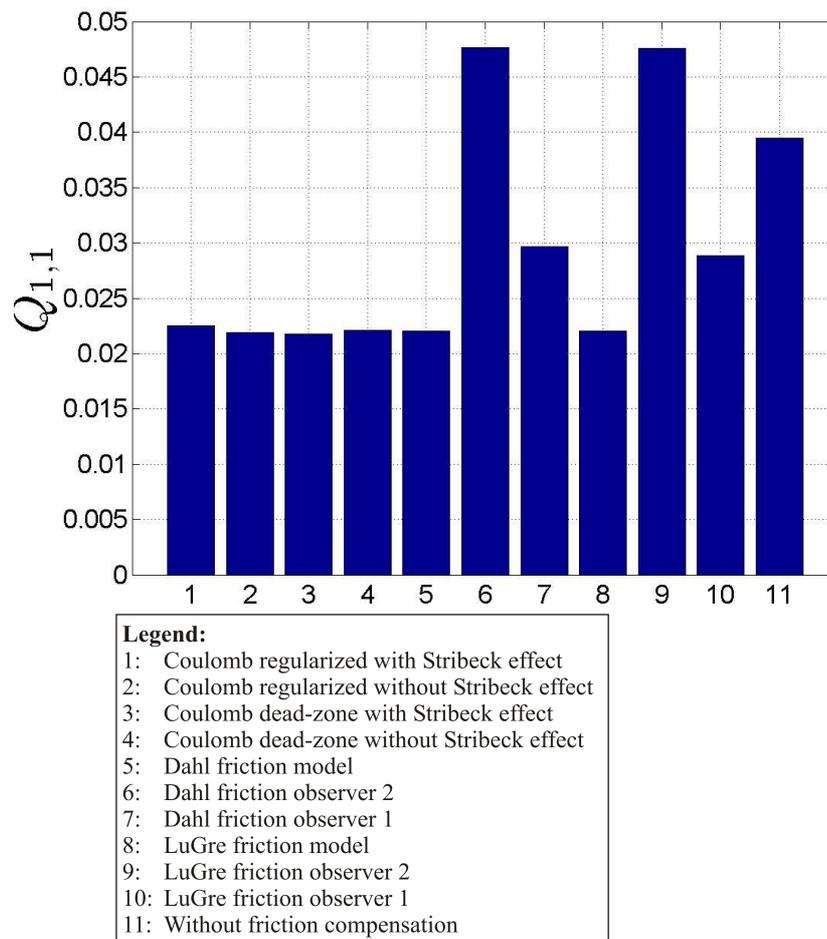


Figure 6.12: Mean value of least squares deviation of φ for chirp reference with velocity reconstructions from the pendulum.

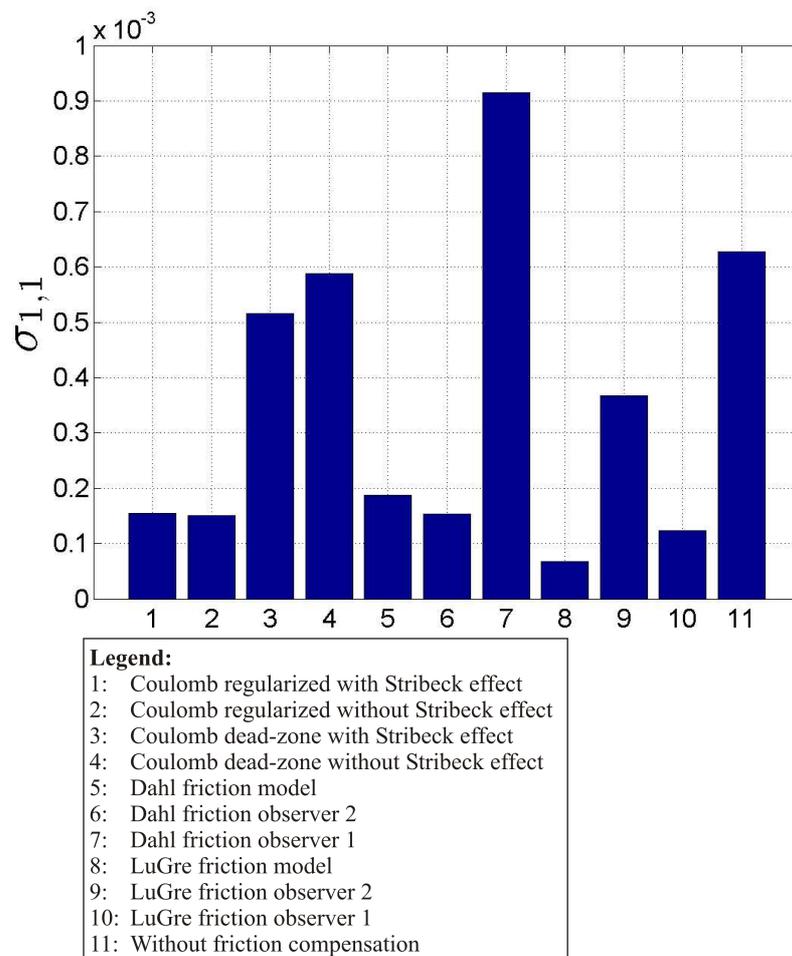


Figure 6.13: Sample standard deviation of least squares deviation of φ for chirp reference with velocity reconstructions from the pendulum.

Figure 6.14 compares the transient behavior of the arm angle φ after a step in the reference signal occurred with open-loop and closed-loop LuGre friction compensation. The time needed to reach the new reference is longer when closed-loop friction compensation is applied³.

The reason for this behavior is that the friction observer carries the control error in φ that arises after the step in the reference signal into the friction estimate. The Observer thus interprets the control error as an error in the friction estimate, since perfect parameter knowledge was assumed during the design of the friction observer. The friction observer tends to correct the control error ($\varphi_{ref} - \varphi$) by manipulation of the friction estimate, e.g. a positive control error leads to an increase in the friction estimate. However the friction observer has no information about the state of the pendulum attached to at the tip of the arm, since the chosen input to the observer does not fulfill the condition of zero-state detectability. Thus by trying to force the arm to the desired reference position by increasing the absolute value of the friction estimate and thus of the control signal the angle of the pendulum is decreased. Since the angle of the pendulum is related to the acceleration of the arm that is possible without loosing control of the arm⁴ this behavior is counterproductive to reaching the new reference quickly, since the decreased angle of the pendulum forces the LQ-controller, that primarily controls with attention to the pendulum angle, to slow down the movement. Therefore during the transient the LQ-controller and the friction compensation produce control signals that cancel each other partly out, slowing down the transient behavior of the system.

As mentioned before the step reference is not a reasonable reference signal for the control of the pendulum. However it is used here to illustrate a problem arising with the friction observer because the plant has fewer control inputs than the number of minimal coordinates that is needed to describe its kinematics. The step in the reference signal could be interpreted as a control error. Then the transient response of the system characterizes the ability of the system to reduce control errors.

6.2.3 Interplay of Velocity Estimation and Friction Compensation

When the velocities reconstructed by the high-gain observer are used for the friction compensation additional problems arise.

An important role plays the trade-off between the speed of the observer and the level of noise in the state estimates. On the one hand the observer has to be fast enough to exploit the description of the fast friction dynamics in the stiction regime of the LuGre model. On the other hand fast observers propagate more noise into the velocity estimates produced by the observer. This noise is propagated through the friction estimate into the control signal.

However if the direct term σ_1 in the LuGre model is reduced to a small value or set to zero the noise propagation is less dramatic. In this case the only remaining direct term from the velocity estimate to the friction estimate and therefore to the control signal is the viscous friction. As indicated in chapter 4.2.2 the viscous friction plays a negligibly small role for the friction behavior of the device.

³Figure 6.14 depicts a situation where the initial position of the arm is even more favorable in the plot were the closed-loop friction observer was used. This emphasizes the statements made above. Differences in the starting positions occur due to the remaining limit cycle when friction compensation is enabled.

⁴An inclination of the pendulum is required to accelerate or decelerate.

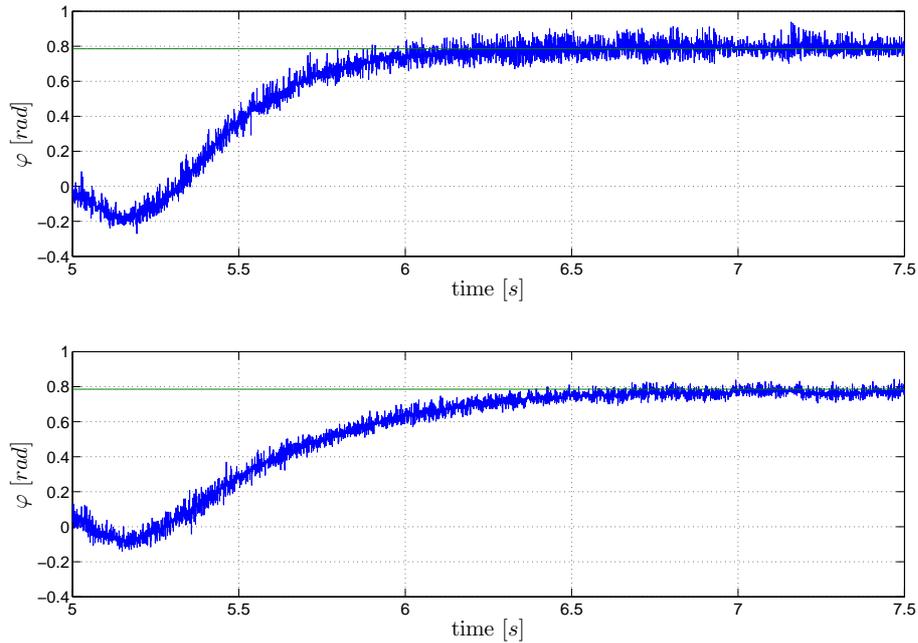


Figure 6.14: Comparison of transient response after step in reference signal with open-loop LuGre friction compensation (top) and closed-loop LuGre friction observer type 2 (see chapter 5.1.3) (bottom).

In the present application a rather fast observer was chosen, since the direct term σ_1 was set to a small value, because it did not yield an improvement in the friction compensation behavior (see section 6.1.5) and the viscous friction is negligible. The performance of the control system increases in comparison to slower observers, also if no friction compensation is used. If the observer gain is increased further the noise level in the friction estimated exceeds a level where the controller loses the capability of stabilizing the pendulum in the upright position (see chapter 5.1.1 for the chosen parameters of the high-gain observer).

The control performance achieved with the velocity reconstructions from the Furuta pendulum could not be completely recovered when using a state observer - without and with friction compensation. The control system with velocities from the high-gain observer tends to exhibit additional oscillatory behavior with a frequency above the frequency of the limit cycle due to friction that was observed with the velocity reconstructions from the analog filter. These oscillations can be best observed in the measurements of the pendulum angle θ (see figure 6.15) since the amplitude of the noise in those measurements is smaller.

Reasons for this behavior could be the delays introduced by the observer and inaccuracies in the model used in the observer, e.g. the influence of not compensated friction and high-frequency dynamics.

An alternative observer approach described in Erlic and Lu [11] was examined at the department by Francesco Pierri, but no significant improvement in comparison with the used high gain observer was achieved. No further investigation was carried out since the design of state observers does not lie within the main scope of this thesis.

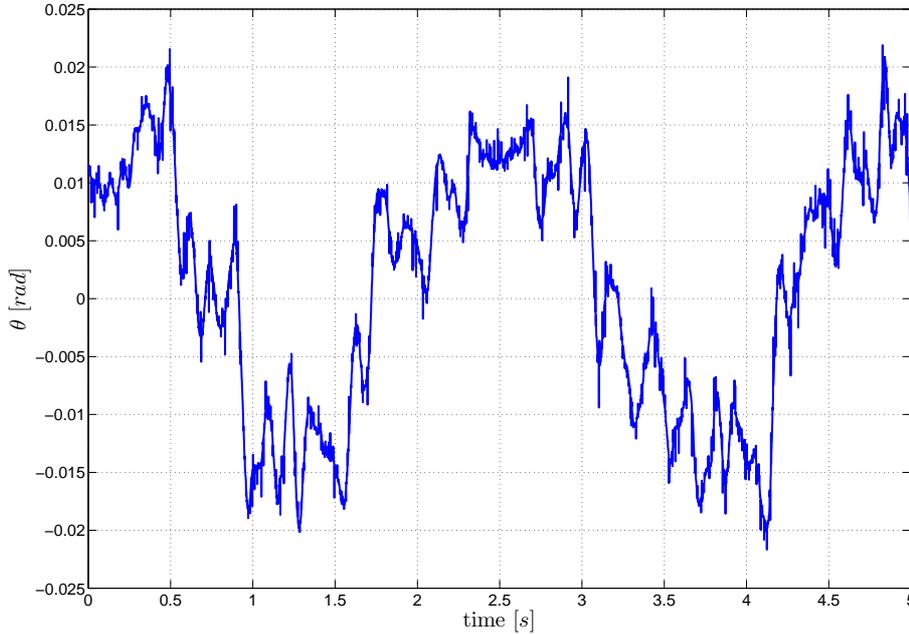


Figure 6.15: Oscillations due to the use of the high-gain observer in the pendulum angle θ .

The same parameter values as for the evaluation with velocity reconstructions from the pendulum (see appendix C.2) were used for the evaluation of the performance using the high-gain observer. Since the goal is only to validate that the results using the velocity reconstructions from the pendulum do also apply when the high-gain observer is used only three measurements for each of the reference signals were taken.

Figure 6.16 shows the $Q_{1,1}$ -component of the error matrix (see chapter 3.2.3) using the high-gain observer and a constant zero reference. The achieved results resemble the results achieved with the analog velocity reconstructions. Again the performance of the open-loop friction compensation using the LuGre model is slightly better than performance achieved with the remaining friction compensation schemes. With the use of the high-gain observer the accumulated error without friction compensation is smaller in comparison to the case with velocity reconstructions from the analog filter. A reason therefore could be that the estimated angular velocities are bigger than the reconstructions with the analog filter from the Furuta pendulum. The reason for this difference are inaccuracies in the model of the plant that is used in the observer⁵. These can lead to bigger control errors in the states corresponding to the angular velocities of the pendulum and thus to larger control effort and a reduction of the accumulated error in the arm position.

The plots for other reference signals corroborate the statements made for the use of the velocities from the analog filter. The following conclusions are made:

- The same statements about the effect of friction compensation apply when the high-gain observer is used instead of the velocity reconstructions from the pendulum.
- High frequency oscillations of the pendulum arm arises when the high-gain observer is used. This behavior also appears without friction compensation

⁵E.g. the model in the observer does not comprise friction.

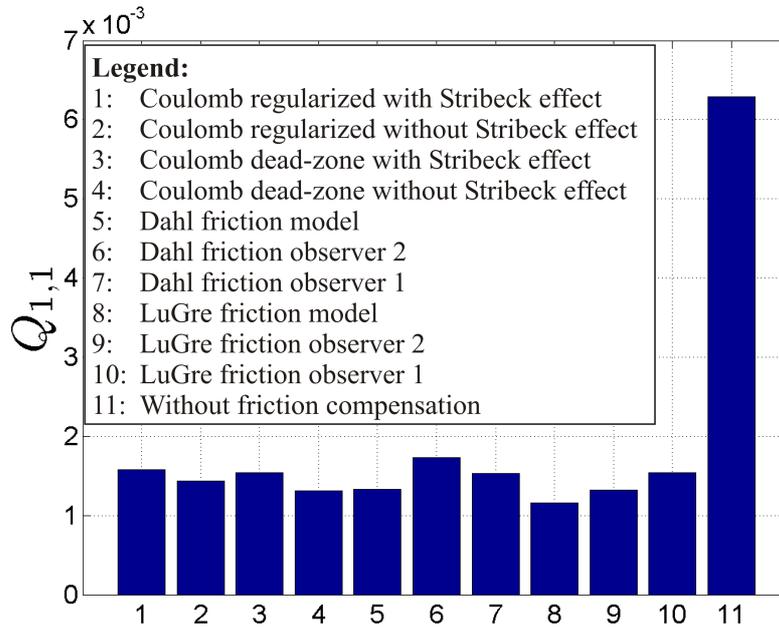


Figure 6.16: Mean value of least square deviation of φ for zero reference with velocity reconstructions using the high-gain observer.

and is thus due to the state observer and not due to the friction compensation schemes. However this performance degradation does not clearly appear in the used error, since the error measure is least squares error from the desired reference.

6.2.4 Qualitative Assessment of Friction Compensation Schemes

In addition to the mostly quantitative analysis presented in section 6.2.1 some qualitative aspects of the different friction compensation schemes and observations that were made while running experiments are mentioned in this section.

Smoothness of Control Signal

In contrary to the static coulomb friction compensation, the dynamic friction models ensure that no discontinuities are introduced to the control signal by the friction compensation. However this problem for using the static friction compensation schemes can be eluded by regularizing the Coulomb model (see chapter 3.1.5).

Noise Suppression through Integration

In dynamic friction models the velocity estimates supplied to the friction model are integrated before entering the friction estimate. Only the viscous friction and σ_1 carry the velocity estimate directly into the friction estimate.

However for the Furuta pendulum viscous friction is negligible (see chapter 4.2.2). Further viscous friction can be compensated more easily by the state controller since the friction dynamics are much slower than the friction dynamics for sticking behavior.

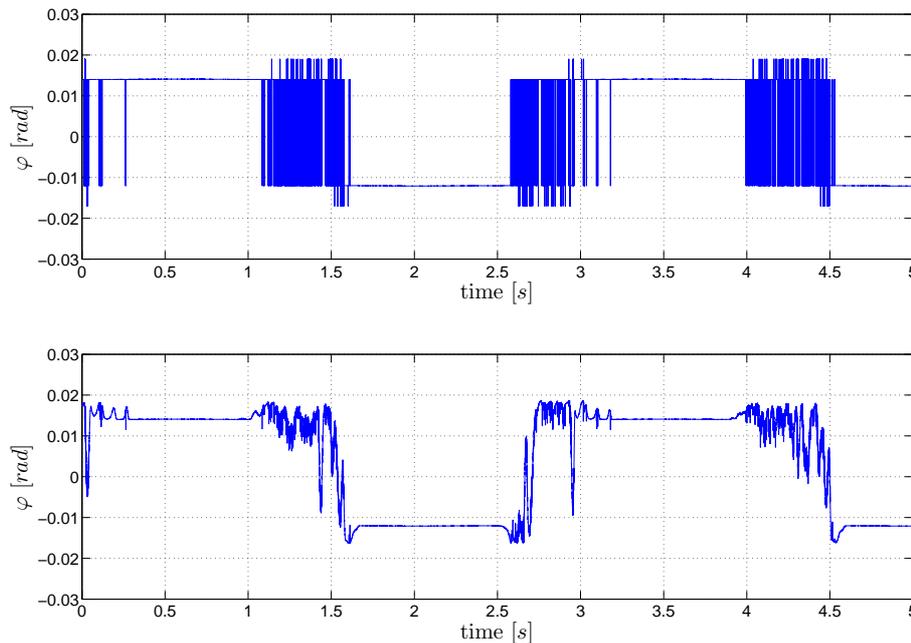


Figure 6.17: Comparison of resulting friction estimate with Coulomb friction estimation without Stribeck effect (top) and open-loop LuGre friction compensation (bottom) when no friction compensation is applied to the system.

The direct term σ_1 was chosen small in the current application, since no beneficial, but only deteriorating effects on the friction estimation were noticeable (see section 6.1.5).

Thus in the present case there is almost no direct term bypassing the integration.

Because of the dynamic friction compensation schemes integrate the velocity estimate the noise in the friction estimate and thus in the control signal, especially at velocity reversals, is lower in comparison with static friction compensation schemes. For static friction compensation schemes the friction estimate may switch frequently for noisy velocity estimates. The tendency to do so can be reduced by regularizing the compensation schemes. However static models with big intervals of regularization do not capture the typical stiction behavior since the regularization introduces drift for infinitely small velocities.

Figure 6.17 compares friction estimates resulting with Coulomb (top) and LuGre (bottom) friction compensation. The Coulomb friction estimate switches excessively at velocity reversals, while the LuGre friction estimate is smoother. The difference can also be witnessed when examining the fft of the two signals. The power spectrum of the coulomb friction estimate shows constantly higher values for frequencies above 40 Hz (see figure 6.18)

This switching of the friction estimate and therefore of the control signal is noticeable when running experiments since it causes audible noise in the motor. Further the unsteady signal can cause higher wear of the motor and mechanic components of the device.

Thus the dynamic friction compensation schemes offer the advantage of smoother control signals without introducing the permanent drift as with regularized Coulomb friction models.

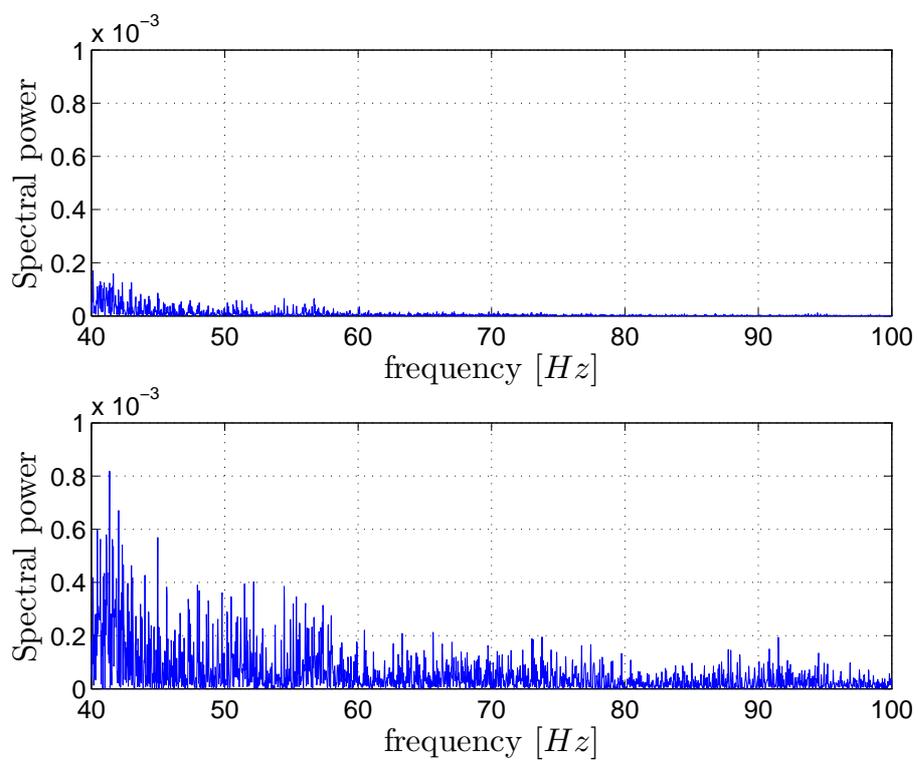


Figure 6.18: Power spectrum of the friction estimate as in figure 6.17 with LuGre model (top) and Coulomb friction model without Stribeck effect (bottom).

When considering the influence of noise on friction estimation the following remark seems appropriate here. Noise in the control signal can also have a beneficial influence on friction compensation, since the resulting vibrations create peaks in the applied control moment that change at a high rate and can therefore be helpful to overcome static friction and reduce stick-slip behavior. A similar technique is sometimes applied to overcome static friction in airplane rudders, where a high-frequency oscillation is added to the control signal to reduce the effects of stiction. However care has to be taken that the actuators and mechanical parts of the system are not harmed by the resulting control signal.

6.2.5 Comparison of Simulation and Experiment

The evaluation of the experiments is concluded with the comparison of results from the simulation with the experimental data.

Figures 6.19 to 6.22 show a comparison of the limit cycles of the real plant and the simulated limit cycle for constant zero reference. Figure 6.23 shows the comparison of the corresponding control signals.

The simulated limit cycle was obtained by running a model of the plant and a continuous time LuGre model implementation solved with variable step size solver. The parameters of the LuGre model were set to the parameters determined in the parameter identification in chapter 4 (see table 4.3 on page 58). The initial states for the simulation were obtained from plots from the measurements from the pendulum and the velocity reconstructions by the analog filter.

Figure 6.19 shows that the period time of the simulated limit cycle is about 27% longer than the period time of the measured limit cycle, while the amplitude is slightly smaller.

A reason for this could be an error in the friction parameters. Simulation shows that an increase in the friction forces leads to an increase in the period time. However also the amplitude of the limit cycle increases.

Another reason for the differences are structural differences of the friction behavior of the LuGre model from the friction behavior of the Furuta pendulum.

From figure 6.20 it becomes obvious that the sticking behavior is more pronounced in the simulation than in the measurements. The small hump in the angular velocity of the simulation data interrupting the sticking is due to that the controller does not manage to catch the pendulum with the first effort before sticking. This can be seen in figure 6.21 since the angle θ hits zero in the simulation data at the same time the hump in $\dot{\varphi}$ occurs, while it does not in the data from the experiment.

In the oscillations for the pendulum angle θ the first maximum, starting from $\theta = 0$ has approximately the same absolute value as measured. After the first maximum the angle of the arm in the simulation decreases to zero forcing the controller to do additional control effort. This causes the absolute value of the second peak to be higher than than the measured value.

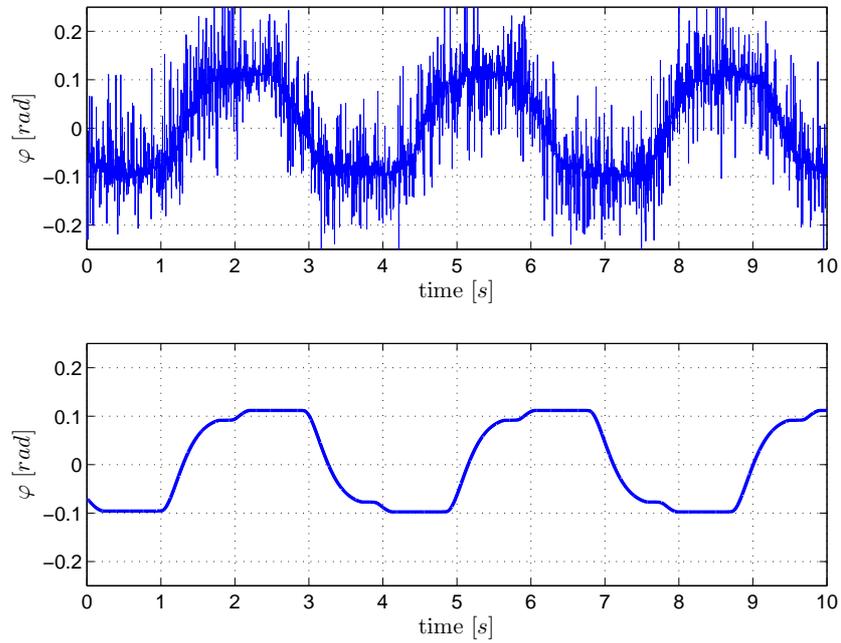


Figure 6.19: Comparison of measured (top) and simulated (bottom) behavior of φ for constant zero reference.

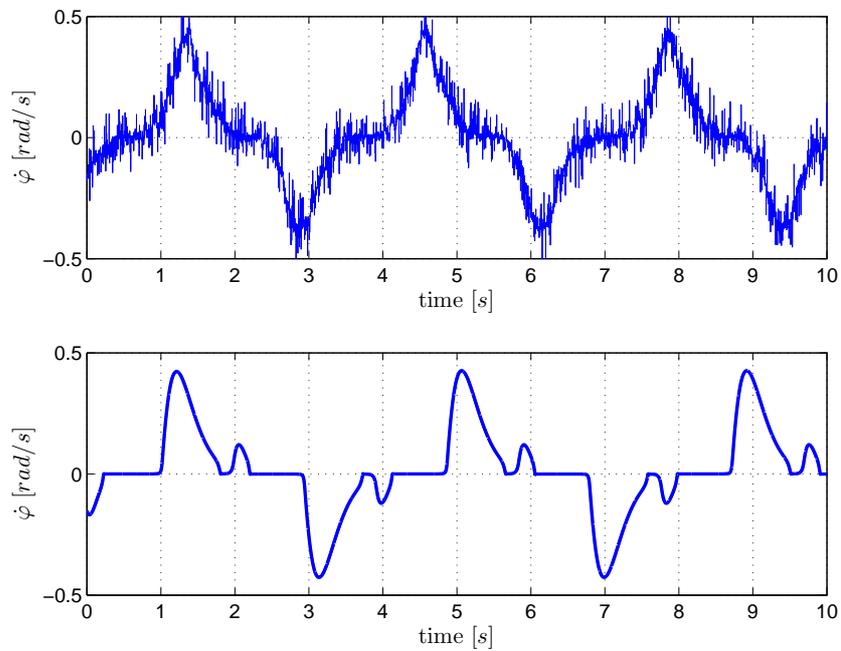


Figure 6.20: Comparison of measured (top) and simulated (bottom) behavior of $\dot{\varphi}$ for constant zero reference.

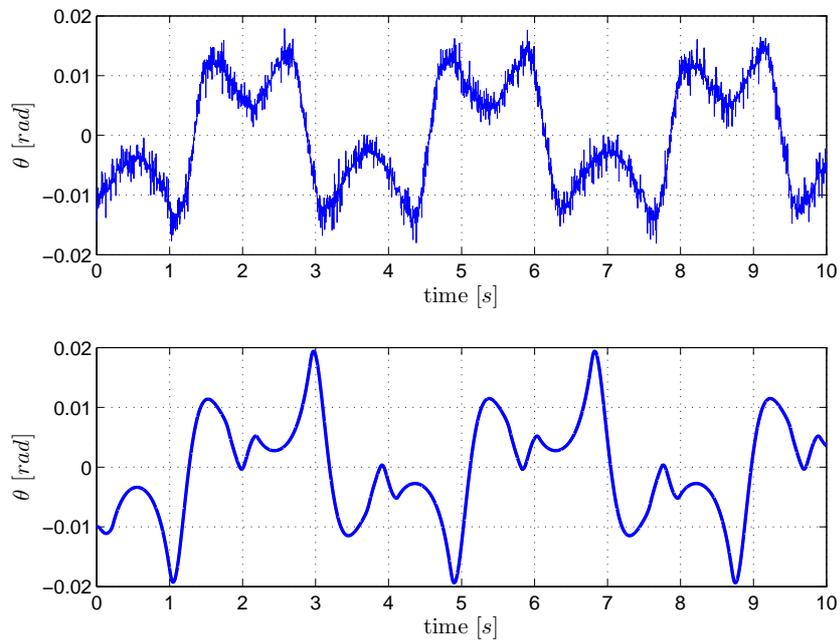


Figure 6.21: Comparison of measured (top) and simulated (bottom) behavior of θ for constant zero reference.

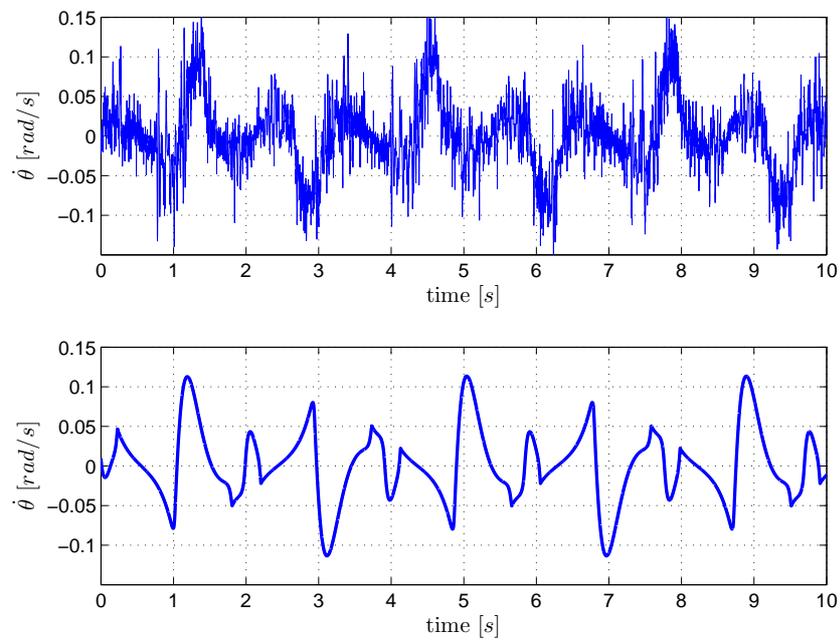


Figure 6.22: Comparison of measured (top) and simulated (bottom) behavior of $\dot{\theta}$ for constant zero reference.

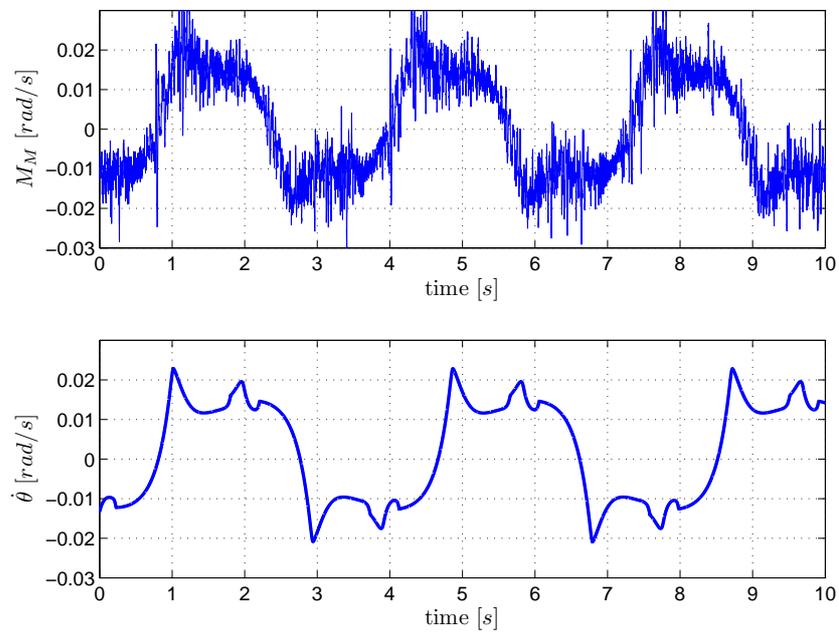


Figure 6.23: Comparison of measured (top) and simulated (bottom) control signal for constant zero reference.

Chapter 7

Conclusions and Outlook

7.1 Conclusions

The following conclusions are drawn from the analysis presented beforehand:

7.1.1 Friction Compensation

- Friction compensation reduces the limit cycles of the Furuta pendulum substantially.
- The differences between the different friction compensation schemes are marginal.
- Open-loop LuGre friction compensation produces slightly better results than other friction compensation schemes.
- The resolution and quality of the position measurements of the arm conceal the subtleties of the dynamic friction models in describing friction behavior. The main advantage of the dynamic friction models presented lies in the accurate description of friction behavior, in particular in the presliding regime. However the high noise level in and the relatively coarse quantization of the velocity and position measurements provided by the pendulum cause that the control systems using the dynamic friction compensation cannot completely exploit these subtleties. This statement is corroborated considering that important LuGre friction parameters, that govern the friction behavior in the presliding and the transition between presliding and sliding regime, namely the stiffness σ_0 and the Stribeck velocity v_s , cannot be estimated using the measurements from the Furuta pendulum.

Due to the fast dynamics of friction these parameters are hard to measure - independent of the used device. However the author holds the opinion that this is not a shortcoming of the friction models, since the corresponding fast dynamics of friction can be witnessed in experiments where high precision sensors are used and have to be captured by friction models aiming to describe the phenomenon of friction accurately.

- The under-actuated nature of the Furuta pendulum poses difficulties for the implementation of closed-loop friction observers. The proposed observation schemes have to be modified for the situation where the number of minimal coordinates of the system surpasses the number of control inputs.

- Friction compensation using the LuGre model offers the following main advantages:
 - Smooth control signal, especially no abrupt changes in the control signal.
 - Noise reduction through integration of the velocity estimate before entering the friction estimate and thus the control signal.
 - Best friction compensation performance for all tested friction compensation schemes.
 - Capturing of Stribeck effect, presliding behavior and frictional lag. However this advantage cannot be fully exploited for the given setup.
- The main disadvantages using the LuGre friction model for friction compensation are:
 - Implementation of dynamic model poses higher demands on hardware.
 - Tuning of relatively many, sometimes difficult measurable parameters necessary¹.

7.1.2 Friction Parameters

- The measurable friction parameters of the Furuta pendulum depend on the position of the arm and the operating conditions.
- Crucial parameters of the LuGre friction model, namely the stiffness σ_0 of the LuGre model and the Stribeck velocity v_S , are not measurable with the current sensor equipment of the device.
- Friction forces F_c and F_s have the largest influence on the performance of the friction compensation.
- The achieved performance of the friction compensation is best for small values of σ_1 .
- Viscous friction is negligible for the Furuta pendulum.
- The influence of the other LuGre friction parameters is relatively small.

7.1.3 LuGre Friction Model

- The LuGre friction model is suitable for friction compensation.
- The discretization according to Freidovich [2] works in practice, produces good and stable results and eludes the problems when discretizing the LuGre model via Euler discretization for the setup presented here.
- The direct term $\sigma_1(v)$ is not needed for the application of the LuGre model for the Furuta pendulum. Further nonzero $\sigma_1(v)$ increases the level of noise in the friction estimate and therefore in the control signal and at velocity reversals it can result in overshoots of the friction estimate over the stiction force F_s . Especially with constant $\sigma_1(v) = \sigma_1$ these peaks in the friction estimate can reach intensities that cause the resulting control signal to be inapplicable to the plant.
Further for small values of σ_1 the LuGre model fulfills the passivity condition for a wider range of values of the remaining friction parameters.

¹This is a general disadvantage of accurate friction compensation.

7.2 Outlook and Recommendations

- An assessment of the LuGre friction compensation with high-precision devices like machine tools would be interesting. These devices provide position measurements with higher quality and therefore allow for velocity reconstructions with higher quality. Further high-precision mechanical parts cause less dependency of the friction parameters on position and operation conditions. The finesse of the dynamic friction models especially in describing the pre-sliding behavior that was shown in simulations (see e.g. Olsson [1], Canudas de Wit et al. [3]) could be exploited and assessed better using high precision machinery.
- Attempts to improve the signal quality of the signals from the Furuta pendulum through signal filtering and/or improved velocity observation could lead to improvements of the control and friction compensation performance. However the statements made for the resolution of the encoder for the measurement of φ remain valid. Another attempt to improve the signal quality could be to read the signals directly from the encoder of the device. Until now an internal analog electronics integrates and evaluates the measurements from the encoder and provides a voltage that is proportional to the determined angular position. The encoder signals could be read directly with the encoder interface of the dSPACE board and evaluated on the board.
- An estimation of friction parameters by adaptation could prove to be beneficial for the control performance. Especially on-line tuning of the friction forces that appeared to be the friction parameters with the highest influence on the control performance (see chapter 6.1.1) appears to be interesting. However adaptation of the parameters that could not be estimated from the measurements, namely v_s and σ_0 , appears, due to the limited quality of the measurements, to be hardly feasible.

Appendix A

Task Description

Title: Friction Compensation for the Furuta Pendulum using the LuGre Model

Background:

The deteriorating effects of friction on the control of mechanical systems is a major problem in a multitude of applications such as high-performance robotics and pointing systems.

Problem Description:

This thesis aims at improving control by using a nonlinear friction observer to detect friction in the system and use this information to modify the control input. Simulations and experiments are to be made using the unstable Furuta pendulum and the efficiency of the observer approach should be compared to other standard methods for friction compensation. Methods:

- LuGre friction model
- High gain observer for reconstruction of velocity
- Furuta Pendulum with dSPACE equipment

Expected Results/ work steps:

- Acquisition of knowledge about friction compensation in general and the LuGre Friction Model in particular.
- Implementation and Simulation of friction observer in Matlab Simulink.
- Connecting and initial operation of dSPACE equipment.
- Implementation of friction compensation including observer for velocity for Furuta Pendulum with special attention on the discretization of the friction model.
- Carrying out of experiments and evaluation of experimental results from different approaches.
- Compensation of Friction effects in experiments and in a simulation environment.
- Detailed documentation of all work steps.

References LuGre friction model:

- H. Olsson. Control Systems with Friction. Department of Automatic Control, Lund Institute of Technology. Lund, 1996.
- A. Shiriaev, A. Robertsson, and R. Johansson. Friction Compensation for Passive Systems based on the LuGre Model. In Proc. 2nd IFAC Workshop on Lagrangian and Hamiltonian Methods for Nonlinear Control, pp. 183-188. Seville, Spain, 2003

Supervision: Prof. R. Johansson, Dept. Automatic Control, Lund University

Start: 13.03.2006

End: 21.07.2006

Appendix B

Setup and Operation of the dSPACE System

B.1 Instructions for the Use of the dSPACE System

This document aims to give a short introduction into working with the dSPACE system. It summarizes the knowledge that the author gained during the setup of the dSPACE equipment. This document claims on no account to be complete nor to be a replacement for the dSPACE documentation.

B.1.1 General Setup and Nomenclature

The dSPACE system consists of three physical parts:

1. *The dSPACE board in the extension box:*
A gray box, approx. 10cm x 15cm x 50cm (height x width x depth) with a fan on the front side (see figure 3.1 on page 30). The extension box contains the dSPACE board (Type: 1103) on which the controller code is executed in real time.
2. *The dSPACE connection panel:*
The dSPACE connection panel provides an interface between the extension box and the pendulum (see figure 3.1 on page 30).
3. *The host computer:*
The host computer is the computer attached to the extension box. This computer is used to manipulate the Simulink models, to create and download code to the extension box, to control the execution of applications on the dSPACE board and to visualize and save data from the experiments.

B.1.2 Important Instructions

- Ensure that the extension box is always switched on when the host computer or the pendulum are switched on! I.e. Switch on the extension box before switching on the pendulum and the host PC and leave the extension box switched on as long as the host computer or the pendulum are switched on!
- Ensure that extension box and host computer are turned off when connecting devices to the connection panel!

B.1.3 Getting Started

Switching On the dSPACE System

Perform the following steps in the indicated order:

1. Ensure that all devices are disconnected from the power supply.
2. Set up all physical connections, i.e. between extension box and host PC and between connection panel and pendulum.
3. Connect pendulum, extension box and host PC to power supply.
4. Switch on the dSPACE Box.
5. Switch on the pendulum; ensure that the emergency stop button is pushed.
6. Switch on the host PC.

Remark:

Never switch on the host PC or the pendulum while the extension box is switched off. Ensure that the extension box is always switched on while the host PC or the pendulum are switched on.

Switching Off the dSPACE System

Perform the following steps in the indicated order:

1. Switch off the host PC.
2. Switch off the pendulum; ensure that the emergency stop button is pushed.
3. Switch off the dSPACE Box.
4. Disconnect all devices from the power supply.
5. Disconnect the physical connections between the devices.

Remark:

Never switch off the extension box while the host PC or the pendulum is switched on. Ensure that the extension box is always switched on while the host PC or the pendulum are switched on.

B.1.4 Brief Overview of the Used Connectors and how to Access them in Simulink

The used analog in- and outputs of the dSPACE system and the encoder inputs are arranged as follows:

- There are 16 analog inputs using BNC connectors named “ADHC 1-16”. These analog inputs can be accessed by using the block “Mux ADC” in Simulink (*rtlib1103/DS1103 MASTER PPC/DS1103MUX_ADC_CON1*).
- There are 4 analog inputs named “ADHC 17-20” using BNC connectors that can be accessed using the Simulink block “ADC” (*rtlib1103/DS1103 MASTER PPC/DS1103ADC_C17*).
- The 8 analog outputs using BNC that are named “DAHC 1-8” can be accessed by the Simulink block “DAC” (*rtlib1103/DS1103 MASTER PPC/DS1103DAC_C1*).

- Further the system possesses digital encoder interfaces (Labeled: “Inc 1-7”). These can be accessed using the encoder position block (*rtlib1103/DS1103 MASTER PPC/DS1103ENC_POS_C1*). To use the encoder interfaces also an encoder master setup block has to be inserted into the model (*rtlib1103/DS1103 MASTER PPC/DS1103ENC_SETUP*).

For all the analog in- and outputs the voltage range is -10V...+10V. A voltage of +10V corresponds to a signal value of 1 from/to the corresponding Simulink block. I.e. if the controller is tuned to deliver the voltage that is to be delivered to the system the controller output has to be divided by 10 before guiding the signal to the DAC block of the model. Analogous the input from a Simulink block corresponding to an analog digital converter has to be multiplied by 10 to retrieve the voltage values that were delivered to the dSPACE system.

B.1.5 General Tips for Working with the dSPACE System

- dSPACE asks to change the default simulation settings in Simulink when starting MATLAB for the first time after installation of dSPACE. It is recommendable to agree. However care has to be taken since from now on the default solver in Simulink will be the Euler approximation (ode1) with fixed step size. Further the default end time of simulations will be infinity.
- Change of rti platform: type: rtixxxx (replace xxxx with platform number) in Matlab command window.

B.2 Manual for Running the Friction Compensation Experiment

B.2.1 Setting Up the Experiment

1. Check that all devices (host computer, dSPACE board and pendulum) are switched off and disconnected from the power supply!
2. Connect computer with dSPACE extension box and dSPACE connection panel with pendulum (see appendix B.2.4).
3. Connect the devices to their power supply.
4. Switch on the dSPACE board (switch at the back of extension box).
5. Switch on the Furuta pendulum.
6. Switch on the host computer (Login: Username and password: dspace).
7. Start Matlab 7.1 SP3.
8. Check that dSPACE software correctly installed (messages during initialization of Matlab).
9. Insert dSPACE license dongle.
10. Start dSPACE ControlDesk.
11. In dSPACE ControlDesk click: File → Open experiment: Open experiment: *[thesis_root]/Matlab/Controller_dSPACE/Stabilization of Furuta Pendulum.cde*.
12. In Matlab run m-file: *[thesis_root]/Matlab/Controller_dSPACE/para_control_fric_comp_furuta.m*.

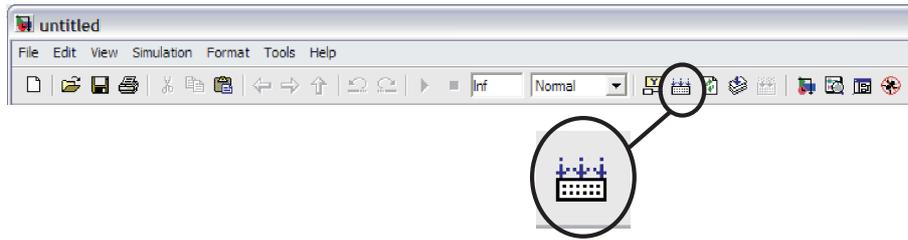


Figure B.1: “Incremental build” button in the menu bar of Simulink.

13. Open Simulink: Open model:
 $[thesis_root]/Matlab/Controller_dSPACE/fur_try.mdl$.
14. Check that the working directory is: $[thesis_root]/Matlab/Controller_dSPACE$.
15. Compile the model by pushing the button “incremental build” in Simulink (see figure B.1).
16. Wait until build procedure is finished (MATLAB is not busy anymore).
17. Switch to dSPACE ControlDesk and use the experiment (for further information on the use of dSPACE ControlDesk please refer to the “ControlDesk Experiment Guide”).

B.2.2 Shutting Down the Experiment

1. Stop the experiment by clicking “Off” in the layout of the experiment (see number 1 in figure B.2).
2. End all programs running on the host computer.
3. Shut down the host computer.
4. Switch off the pendulum.
5. Switch off the dSPACE system using the switch at the back of the extension box.
6. Disconnect the devices from the power supply
7. Disassemble the connections between the devices.

Remark:

The pendulum and the host computer must not be switched on while the dSPACE system is switched off, i.e. always switch on the pendulum and the host computer after the dSPACE system and always switch off the pendulum and the host computer before the dSPACE system! Otherwise uncontrolled and possibly harmful behavior of the pendulum will be the result.

B.2.3 Using the Experiment

The Layout as depicted in figure B.2 is used for the control of the experiment. The different buttons, their use and function is described below. For information concerning the use of “dSPACE ControlDesk” please refer to the “ControlDesk Experiment Guide” delivered with the dSPACE system.

On/Off Button (number 1 in figure B.2)

As long as the on/off button is set to “Off” (the LED to the right is black) the control voltage delivered to the pendulum is zero. The initial state of the on/off button is off. If the emergency stop of the pendulum is disabled and the pendulum is reset the experiment can be started by clicking on the button “On” (the LED to the right turns red).

Friction Compensation Settings (number 2 in figure B.2)

- With the radio button on the left side of the panel the friction compensation can be enabled and disabled.
- The friction model that is to be used for compensation can be chosen with the upper pull down menu.
- The second, lower pull down menu is used for the choice of the friction observer gain to be used. The choice does only affect the friction estimate when a dynamic friction model is chosen.
- The numeric inputs below the pull down menus define the design parameters of the friction observer gains.
- The radio button to the right determines whether the same state as used for the controller or the measured state is used for friction compensation.

Friction Parameters (number 3 in figure B.2)

The numeric input panels can be used to modify the friction parameters for the LuGre and the Dahl friction model. The Coulomb friction models use the same friction forces and Stribeck velocity as the LuGre friction model.

Measurement Settings (number 4 in figure B.2)

- The used observer is chosen with the pull down menu at the top.
- The four radio buttons below allow to chose for each of the four state variables if the estimate from the observer or the measurement from the device is used.
- The radio button on the right of the pull down menu is for choosing if the friction estimate is to be used in the control input to the observer¹.
- The radio button below allows to chose whether the friction estimate is to be used in the model of the plant implemented in the high-gain observer or not.
- With the pull down menus on the right it can be chosen which measurement for θ is used. Either always the measurement from the 360 degree potentiometer, or always the measurement from the potentiometer for positions close to the upright position, or a measurement that is automatically switched (default) can be used.

¹It makes only sense to use the friction estimate in the control signal delivered to the observer if it is also used in the model of the plant implemented in the observer. In this case the friction estimate in the control signal and in the model of the plant in the observer cancel each other out.

Settings for the Controller (number 5 in figure B.2)

- The radio button is used to choose if the controller only for stabilization or the swing-up controller with switching to the stabilizing controller is used (the swing-up controller does not work properly due to a discontinuity in the measured signal and due to structural oscillations.).
- The slider bar below is used to choose the reference energy level of the (energy based) swing-up controller.
- With the radio button below the additional minimum variance controller can be activated.

Settings for the Reference Signal (number 6 in figure B.2)

- The radio button on the left allows to choose the used reference signal. Either zero reference (default), sinusoidal reference or one of the test runs defined in chapter 3.2.2 can be chosen.
- The first slider gain on the right side is used to choose the reference angle φ for constant zero reference.
- The two sliders below are used to tune the frequency and amplitude of the sinusoidal signal.
- The radio button below is used to choose one of the test cycles (zero reference, step reference or chirp reference.)
- With the push button on the right from the radio button the test cycle can be started.
- The big slider gain on the bottom is used to set the slope of a ramp signal that is added to the φ reference if the radio button on the left is set to the corresponding position.

Settings for Signal Filtering (number 7 in figure B.2)

The controls here are used to enable and to tune several low pass filters implemented in the model. Each of the blocks has a radio button to enable or disable the filter, a slider to tune the cut-off frequency (upper slider) and a slider to tune the static gain (lower slider).

- The uppermost filter is for filtering the control signal to prevent excitation of unmodeled high frequency dynamics (default: on).
- The second filter is for filtering the angular velocity of the pendulum (default: off).
- The third filter is for filtering the angular position and velocity of the arm (default: off).

Control of Recorder Settings (number 8 in figure B.2)

Control of the settings for recording data. For further information please refer to the “ControlDesk Experiment Guide”. Basic functions:

- Setting of record length (How long it will be recorded).
- Setting of downsampling (For a downsampling factor n only every n^{th} measured point is saved).

- Auto repeat (If enabled a new measurement is started immediately after the subsequent measurement is finished. The data of the subsequent measurement is discarded).

Plotter Array (number 9 in figure B.2)

The following data is displayed in the plots:

1. plot: Applied control signal (zero if on/off switch is set to “Off”) and computed control signal.
2. plot: Friction estimate.
3. plot: Measured and estimated value of arm angle φ .
4. plot: Measured and estimated value of pendulum angle θ .
5. plot: Measured and estimated value of arm velocity $\dot{\varphi}$.
6. plot: Measured and estimated value of pendulum velocity $\dot{\theta}$.
7. plot: Reference signals.
8. plot: Control signal before and after filtering with low-pass filter.

B.2.4 Additional Information

Signal Connections

Connect the connectors of the dSPACE connection panel to the pendulum as follows:

- ADCH 1: Arm angle
- ADCH 2: Arm velocity
- ADCH 5: Pendulum angle 360
- ADCH 6: Pendulum velocity 360 (not needed)
- ADCH 7: Pendulum angle top
- ADCH 8: Pendulum velocity top
- DACH 1: In 1 (motor voltage)

Connect the plus pole (red pole, center pin of BNC connector on connection panel) to the corresponding socket and the minus pole (black pole, outer ring of BNC connector on connection panel) to the ground socket of the motor.

Access of Measured Data

If measurement data was saved using the filename “[*Filename*]”, using the button “save” in the plotter settings (number 8 in figure B.2), it can be accessed in Matlab after loading the corresponding .mat file as follows:

- [*Filename*].*X.Data*: Time values.
- [*Filename*].*Y.Name*: Path of the recorded signals in the Simulink model (the name of the corresponding Simulink block is listed before the last slash in the pathname).
- [*Filename*].*Y(i).Data*: Data values from the signal and block as described in [*Filename*].*Y(i).Name*.

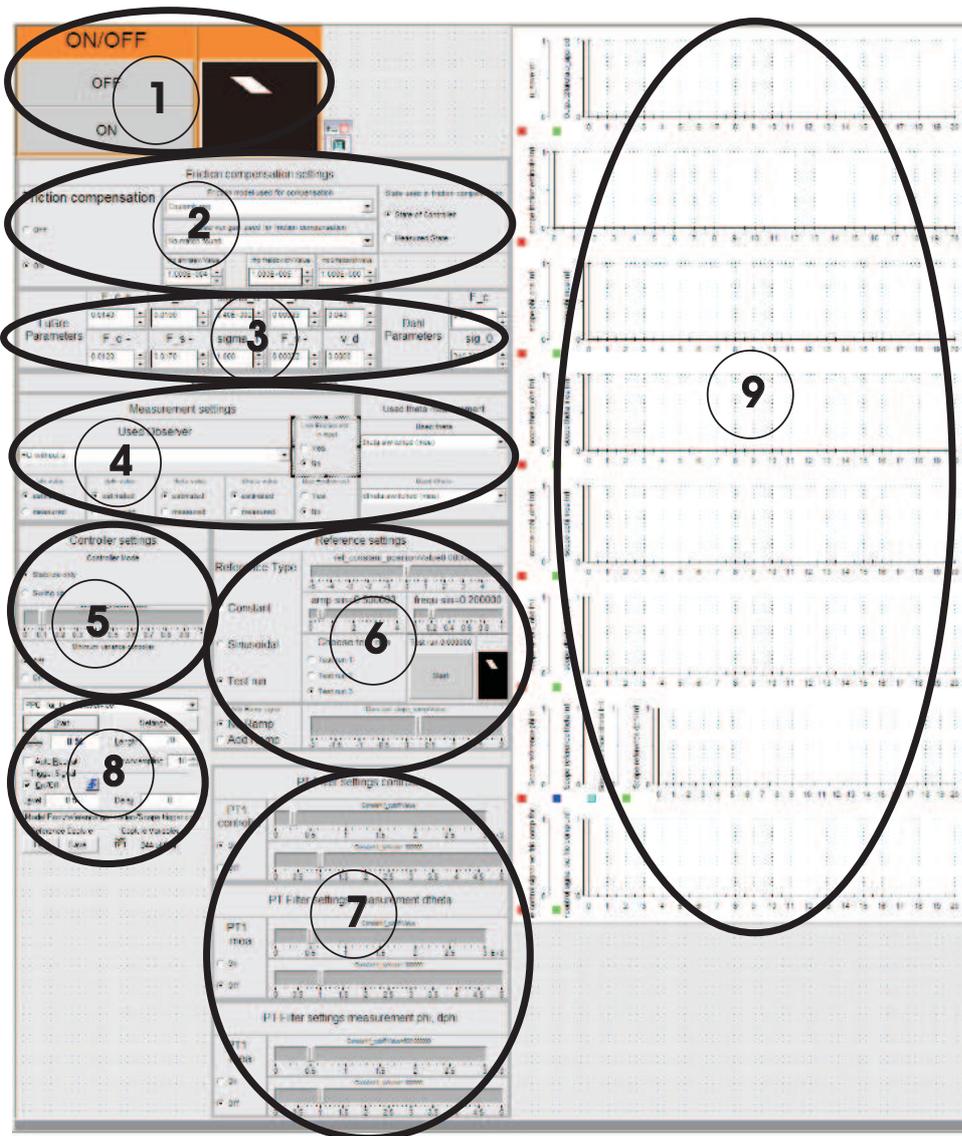


Figure B.2: Picture showing the layout used for the experiments annotated with numbers indicating groups of instruments.

Legend

[thesis_root]: root directory of the thesis

Appendix C

Parameter Values

C.1 Explanation of Parameters

Table C.1: Explanation of parameters

	<i>Parameter</i>	<i>Explanation</i>
Simulation parameters	T_sample_discrete	Fundamental sampling time that is used during the execution of the system.
	k_u	Output factor for the conversion of the moment computed by the controller into control voltage that is applied to the system.
System parameters	m_a_est	Mass of the arm of the pendulum.
	l_a_est	Length of the arm of the Furuta pendulum.
	l_a_inert_est	Distance of the cog of the arm from its axis of rotation.
	J_m_est	Moment of inertial of the motor shaft around its axis of rotation.
	m_2_est	Mass of the pendulum rod.
	m_p_est	Mass of the weight attached to the top of the pendulum.
	l_2_est	Distance of the cog of the pendulum rod from the joint connecting pendulum and arm.
	l_p_est	Distance of the weight attached to the top of the pendulum and the joint connecting pendulum and arm.
Friction Compensation Parameters	F_c_p_est_p_f	Coulomb friction of the arm for positive velocities (see F_c in equation (1.3)).
	F_c_p_est_n_f	Coulomb friction of the arm for negative velocities (see F_c in equation (1.3)).
	F_s_p_est_p_f	Stiction force of the arm for transfer from stiction to friction in positive turning direction (see F_s in equation (1.3)).
	F_s_p_est_n_f	Stiction force of the arm for transfer from stiction to friction in negative turning direction (see F_s in equation (1.3)).
	v_s_est_f	Stribeck velocity (see v_s in equation (1.3)).
	sig_0_est_f	Stiffness of the LuGre model (see σ_1 equations (1.1) to (1.4)).

	sig_1_est_f	“Damping” of the LuGre model (see σ_0 in equations (1.1) to (1.4)).
	v_d_est_f	Parameter that controls the speed of decrease of the damping rate with increasing velocity for the LuGre model with velocity dependent damping (see v_d in equation (1.4)).
	F_v_est_p_f	Viscous friction parameter for positive velocities (see F_v in equation (1.2)).
	F_v_est_n_f	Viscous friction parameter for negative velocities (see F_v in equation (1.2)).
	F_c_est_dahl	Coulomb friction for the Dahl model.
	sig_0_est_dahl	Stiffness of the Dahl model.
	exp_dahl	Exponent used in the Dahl model.
	thres_coul_vel	Half width of the dead-zone for velocities in the static coulomb map, to prevent excessive switching of the friction estimate (Velocities that have a smaller absolute value than this threshold are assumed to be zero).
	thres_coul_cont	Half width of the dead-zone for the control signal in the static coulomb map, to prevent excessive switching of the friction estimate (Control signals that have a smaller absolute value than this threshold are assumed to be zero).
	$\rho_{fricobs1}$	Parameter ρ of friction observer as in chapter 5.1.3.
	$\rho_{1,fricobs2}$	Parameter ρ_1 of friction observer as in chapter 5.1.3.
	$\rho_{2,fricobs2}$	Parameter ρ_1 of friction observer as in chapter 5.1.3.
Controller parameters	R_l	Punishment for control effort for discrete time LQ-controller design.
	Q_l	Punishment for control error for discrete time LQ-controller design.
	Controller type	Type of the controller used (discrete time/continuous time).
Observer parameters	roots_factors_1/2	Roots that are used for the computation of the high-gain observer for the integrator chain for the arm (index 1) and the pendulum (index 2) respectively.
	eps_hg_1/2	Observer gain of the high-gain observer for the integrator chain for the arm (index 1) and the pendulum (index 2) respectively.

C.2 Basic Parameter Setup

Table C.2: Parameters for Observation of Resonance Behavior

	<i>Parameter</i>	<i>Value</i>	<i>Unit</i>
Simulation parameters	T_sample_discrete	0.1	[ms]
	k_u	10.96	[V/Nm]

System parameters	m_a_est	0.165	[kg]
	l_a_est	0.254	[m]
	l_a_inert_est	0.044	[kg]
	J_m_est	$0.381 \cdot 10^{-4}$	[kg m ²]
	m_2_est	0.02	[kg]
	l_p_est	0.421	[m]
	l_2_est	=l_p_est/2 = 0.2105	[m]
	m_p_est	0.015	[kg]
Friction Compensation Parameters	F_c_p_est_p_f	0.014	[Nm]
	F_c_p_est_n_f	0.012	[Nm]
	F_s_p_est_p_f	0.019	[Nm]
	F_s_p_est_n_f	0.017	[Nm]
	v_s_est_f	0.04	[m/s]
	sig_0_est_f	$3.4 \cdot 10^2$	[Nm/m]
	sig_1_est_f	1	[Nm s/m]
	v_d_est_f	0.006	[m/s]
	F_v_est_p_f	0.00023	[Nm s/m]
	F_v_est_n_f	0.00022	[Nm s/m]
	F_c_est_dahl	=F_c_p_est_p_f	[Nm]
	sig_0_est_dahl	=sig_0_est_f	[Nm/m]
	exp_dahl	1	[-]
	thres_coul_vel	$1 \cdot 10^{-4}$	[m/s]
	thres_coul_cont	$1 \cdot 10^{-4}$	[Nm]
	$\rho_{fricobs1}$	$1 \cdot 10^4$	[-]
	$\rho_{1,fricobs2}$	$1 \cdot 10^5$	[-]
$\rho_{2,fricobs2}$	2	[1/s]	
Controller parameters	R_1	5000	[-]
	Q_1	$\begin{pmatrix} 1/0.1^2 & 0 & 0 & 0 \\ 0 & 1/1^2 & 0 & 0 \\ 0 & 0 & 1/0.3^2 & 0 \\ 0 & 0 & 0 & 1/2^2 \end{pmatrix}$	[-]
	Controller type	discrete LQ	-
Observer parameters	roots_factors_1/2	[-1, -1]	[-]
	eps_hg_1/2	$1 \cdot 10^{-2}$	[-]

C.3 Gain values for Estimation of Voltage Constant

Table C.3: Used gain values and initial amplitudes for estimation of the voltage constant k_u (see chapter 4.1).

<i>Measurement No.</i>	<i>Used initial amplitude</i>	<i>Used gain K_p</i>
1-3	0.5 rad	0.518 V/rad
4-6	1.5 rad	0.280 V/rad
7-9	1 rad	0.350 V/rad

Remark: The values for K_p also comprise the initial estimate for the voltage constant ($k_u = 1.4 \text{ V}/(\text{Nm})$) and the transformation from values in the Simulink model to the output voltage of the dSPACE board (1 in model corresponds to 10V on the board).

Bibliography

- [1] H. OLSSON: *Control Systems with Friction*. Department of Automatic Control, Lund Institute of Technology. Lund, 1996.
- [2] L. FREIDOVICH, A. ROBERTSSON, A. SHIRIAEV, R. JOHANSSON: *Friction Compensation Based on LuGre Model*. Preprint submitted to 45th Conference on Decision and Control, 2006.
- [3] C. CANUDAS DE WIT, H. OLSSON, K. J. ÅSTRÖM, P. LISCHINSKY: *A New Model for Control of Systems with Friction*. IEEE Transactions on Automatic Control, Vol. 40, No. 3, March 1995.
- [4] A. SHIRIAEV, A. ROBERTSSON, R. JOHANSSON: *Friction Compensation for Passive Systems based on the LuGre Model*. 2nd IFAC Workshop on Lagrangian and Hamiltonian Methods for Nonlinear Control, Seville 2003.
- [5] N. BARABANOV, R. ORTEGA: *Necessary and Sufficient Conditions for Passivity of the LuGre Friction Model*. 14th World Congress of IFAC, Beijing, 1999.
- [6] J. SWEVERS, F. AL-BENDER, C. G. GANSEMAN, T. PRAJOGO: *An Integrated Friction Model Structure with Improved Pre-sliding Behavior for Accurate Friction Compensation*. IEEE Transactions on Automatic Control, Vol. 45, No. 4, April 2000.
- [7] V. LAMPAERT, J. SWEVERS, F. AL-BENDER: *Modification of the Leuven Integrated Friction Model Structure*. IEEE Transactions on Automatic Control, Vol. 47, No. 4, April 2002.
- [8] K. J. ÅSTRÖM, K. FURUTA: *Swinging Up a Pendulum by Energy Control*. 13th IFAC World Congress, San Francisco, CA, 1996.
- [9] H. P. GEERING: *Regelungstechnik: Mathematische Grundlagen, Entwurfsmethoden, Beispiele*. Springer Verlag, Fünfte Auflage, 2001.
- [10] H. K. KHALIL: *Nonlinear Systems*. Prentice Hall, Third Edition, 2002.
- [11] M. ERLIC, W.S. LU: *A Reduced-Order Adaptive Velocity Observer for Manipulator Control*. IEEE Transactions on Robotics and Automation, Vol. 11, No. 2, April 1995.

